NUMERICAL INVESTIGATION OF FLUID FLOW AND HEAT TRANSFER IN A LOUVER-FIN RADIATOR

WINIT JAIBOON

A THESIS SUBMITTED IN PARTIAL FULFILLMENT

OF THE REQUIREMENT FOR THE DEGREE OF

MASTER OF ENGINEERING IN AUTOMOTIVE ENGINEERING

(INTERNATIONAL PROGRAM)

INTERNATIONAL COLLEGE

KING MONGKUT'S INSTITUTE OF TECHNOLOGY LADKRABANG

2012

KMITL-2011-IC-M-004-008

Thesis Title	Numerical Investigation of Fluid Flow and Heat Transfer in a Louver-Fin Radiator
Radiator	
Student	Mr. Winit Jaiboon
Student ID.	50061907
Degree	Master of Engineering
Program	Automotive Engineering (International Program)
Year	2012
Thesis Advisor	Assoc. Prof. Dr. Jarruwat Charoensuk
	Assoc. Prof. Dr. Seiji Okawa

ABSTRACT

The objective of this study is to explore the effects of geometric parameters on heat transfer and friction loss in automotive radiator louver fins, Station number and friction factor are used as a performance indicator and are obtained at various Reynolds numbers. The numerical technique known as finite volume method is used. Simulations are performed for different geometries with various louver pitch, louver angle, fin pitch, tube pitch, fin thickness and different Reynolds number within the range of 100 to 4000. Firstly the models' parameters will be calibrated against the reliable experimental results of similar geometry. A three-dimensional model is constructed with the smallest fluid cell size next to the wall being smaller than the fin's thickness and conjugate heat transfer as suggested by Patankar, 1960 and RNG k-epsilon turbulent model with enhanced wall treatment are used for the modeling of heat transfer at the fluid domain and the solid-fluid interface, respectively. The simulations are validated against well-known empirical results proposed by Achaichia and Cowell, 1988. The predictive quality of the selected model is good in general with the maximum deviation in heat transfer of ±15%. As far as friction factor is concerned, the maximum deviation is ±15%. The heat transfer characteristics of louvered plate fin are discussed in relation with flow aerodynamic and the distribution of pressure and temperature.

ACKNOWLEDGEMENT

This thesis could not be completed without the assistance of many persons to whom I would like to express my sincere appreciation.

First, I would like to sincerely thank my advisor, Assoc. Prof. Dr. Jarruwat Charoensuk for his support, guidance and assistance throughout the research project. Without his support, this research could not have been finished.

I would also like to thank Mr. Niwat Phoocharoen for well suggestion in using software and Systems Laboratory, National Metal and Materials Technology Center for the software package used in this research.

Moreover, I would like to show gratitude to CH. Watanayont and CH. Auto Parts .Co. Ltd. for providing the high performance computer as well as financial supporting.

Finally, I am very grateful to my family for all love, caring, understanding and motivation throughout my life.

Winit Jaiboon

CONTANTS

CONTANTS (CONT.)

Page

CONTANTS (CONT.)

Page

LIST OF TABLE

LIST OF FIGURE

LIST OF FIGURE (CONT.)

Figure Page

NOMENCLTURE

A	Total heat transfer area	[mm^2]
A_c	Minimum flow area	[mm^2]
A_k	Cross section area of fin heat transfer	[mm^2]
$A_{k,x}$	Cross section area at x direction	[mm^2]
C	Heat capacity rate	[W/K]
c_p	Specific heat	[J/kg K]
d_h	Hydraulic diameter	[mm]
F_p	Fin pitch	[mm]
F_t	Fin thickness	[mm]
F_h	Fin height	[mm]
f	Friction factor	
G	Mass flux of air based on minimum flow area	[kg m^2/s]
h	Heat-transfer coefficient	[W/m^2 K]
j	Colburn factor: $Nu/RePr^{1/3}$	
k	Thermal conductivity	[W/m^{2}K]
L_l	Louver length	[mm]
L_p	Louver pitch	[mm]
n	Number of tube row	
$\dot{m}$	Mass flow rate	[kg/s]
ΔP	Pressure drop	[Pa]
q	Heat-transfer rate	[W]
Re_d	Reynolds number best on hydraulic diameter	
Re_{L_p}	Reynolds number best on fin length	
T	Temperature	[K]
U	Air velocity	[m/s]

Greek Letters

δ	Tube wall thickness [m]
ε	Effectiveness
η	Fin efficiency
η_o	Surface effectiveness
μ	Dynamic viscosity [kg/ms]
ρ	Density [kg/m^3]

Subscripts

a	Air side
avg	Average value
i	inlet
in	Inlet
f	Fin surface
m	Mean value
min	Minimum value
max	Maximum value
o	Outlet
w	Wall of tube
0	Base surface

CHAPTER 1

INTRODUCTION

1.1 Background and Problems

Louver fin geometry **Figure 1.1** is used widely for industrial heat exchangers, air conditioning as well as automotive radiator, heater, oil coolers, and condenser. The outstanding characteristic of complex flow associated with this configuration has a high heat transfer effect thus inevitably creates high pressure drop. Both performance aspects are higher than the conventional louver plate fin. It is essential to find the reliable method to indentify the heat transfer and pressure performance of louver fin. Computational Fluid Dynamic has been widely used and has been a successful tool for understanding the flow and heat phenomena in many heat transfer devices. The underlying behavior of air flow through louvered fin array as well as its associated pressure distribution to reflects the heat transfer and the overall pressure drop. These parameters can be obtained from the experiment related with the geometric parameters of louver and fin.

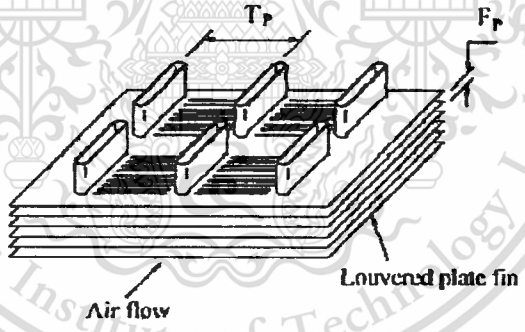

Figure 1.1 Flat-side tube and louver fin heat exchanger [24]

Nowadays, the design process of louver fin heat exchanger usually starts from the empirical calculations and can be obtained from extensive comparisons of the existing products, followed by the saving cost of manufacturing. However, the important obstacle is the building of the heat exchange louver on the fin. Tooling has a very high cost for full side radiator production, not to mention the making, testing of the new design's performance. Moreover, building of the testing facility and conducting of measurement was developed prototype to consume using a long period of time and large investment budget.

The mechanism was very important because the air flow through the louver fins exchanger and to emphasize on experimental method with expensive instrument of the wind tunnel. The complex characteristics of flow pattern will be used the great tool for accuracy.

1.2 Previous Research

1.2.1 Experimental Approach

A study on air flow through louver fin is essential to understand heat transfer mechanism. In the past, the experimental method using the wind tunnel was emphasized and was involved expensive instrument and tools. The complexity in shape of the air flow was studied. During the past two decades, many researchers had taken extensive studies on this problem.

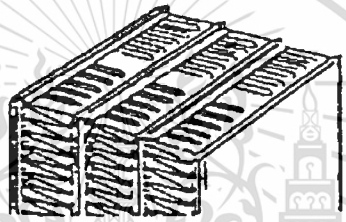

Figure 1.2 Flat tube and louvered corrugated heat exchangers [5]

Davenport [5] reported a comprehensive study of a non-standard variant of the flat tube and louvered corrugated heat exchangers. Totally, 32 samples of louver fin were tested. The fin geometry tested by Davenport is shown in **Figure 1.2**. In their studies the louver fin is triangular shaped channel. They use the different flow within the range of Reynolds Number 300< Re_{Lp} <4000. The air-side performances were analyzed using the effectiveness-NTU method. They proposed a correlation for geometry in their studies. Up to 95% of the experimental cases were success fully correlated by the j factors, with data had been correlated within ±6% of accuracy. The final correlation was as follows:

$$j = 0.249\,\mathrm{Re}_{Lp}^{-0.42}\,L_h^{0.33}\left[\frac{L_h}{F_l}\right]^{1.1} F_l^{0.26} \tag{1.1}$$

In Equation 1.1, F_l is the fin length, L_h is the louver height. The remaining variables have similar meaning as in the current study.

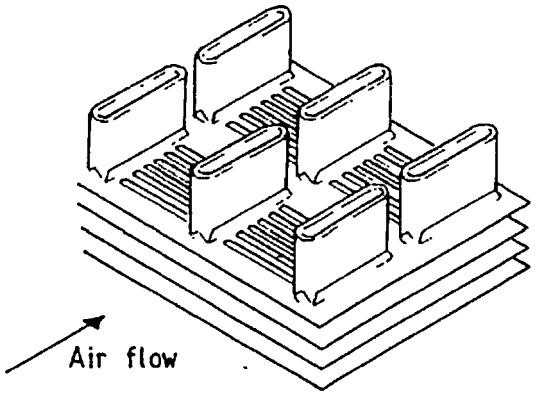

Figure1.3 Flat-sided tube and louvered plate fin heat transfer surface [1]

Achaichia and Cowell [1] were the first researchers who presented the performance data for flat tube and louvered plate fin surfaces (**Figure 1.3**). They had verified the flattening characteristics of the Stanton number and friction factors at low Reynolds number previously observed by Davenport (1983). They had explained the flattening characteristics as the effective heat transfer configuration changes from flat plate to duct flow. A total of 15 samples were tested in their study. They presented a correlation of Stanton number data for $\mathrm{Re}_{Lp} > 75$ to be within ±10%. The final correlation was as follows:

$$St = 1.554\frac{\left(0.936 - \frac{243}{\mathrm{Re}_{LP}} - 1.76\frac{F_p}{L_p} + 0.995\theta\right)}{\theta} \times \mathrm{Re}_{Lp}^{-0.59}\left(\frac{T_p}{L_p}\right)^{-0.09}\left(\frac{F_p}{L_p}\right)^{-0.04} \tag{1.2}$$

Moreover they predicted the friction factors to within ±10% for value of Reynolds number between 150 and 3000.

$$f = 0.895 f_A^{1.07} F_p^{-0.22} L_p^{0.25} T_p^{0.26} H^{0.33} \tag{1.3}$$

where Louver height is $H = L_p \sin\theta$, the value of f_A can be calculated from the value of Re_{Lp} as follow:

$$f_A = 596\,\mathrm{Re}_{LP}^{(0.318\log \mathrm{Re}_{LP} - 2.25)} \tag{1.4}$$

In Equation 1.2 through 1.4, F_p is the fin pitch, T_d is the tube depth, L_p is the louver pitch, T_p is the tube pitch, θ is the angle of louver fin. The remaining variables have the same meaning as in the current study.

Webb and Jung -[16] presented experimental data for six brazed aluminum heat exchangers. The fin geometry of their brazed aluminum heat exchangers includes three standard corrugated and three splitter fin geometry. The brazed aluminum heat exchanger is made of multi-louver fins brazed to a flat, extruded tube, with a cross section of several independent passages. They found that the standard corrugated brazed aluminum flat tube design gives a 90% higher heat transfer coefficient for only 25% higher pressure drop compared with the round tube plain plate fin design.

Rugh et al. -[12] provided data on a high fin density louvered surface. Data were presented against Reynolds number based on Hydraulic diameter (D_h) in the range of 150 to 3000. The heat exchanger was corrugated louver fin with a splitter plate. Comparisons were drawn relative to the plain fin, and they reported that the louver fins produce an approximately 25% increase in heat transfer coefficient and 110% increase in pressure drop.

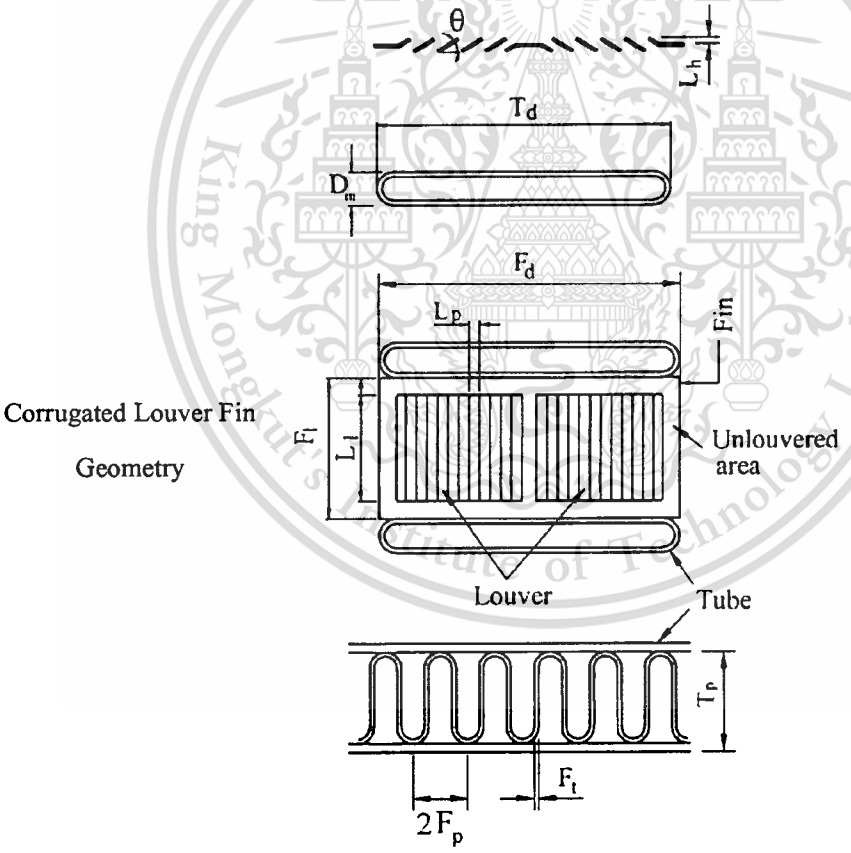

Corrugated Louver Fin Geometry

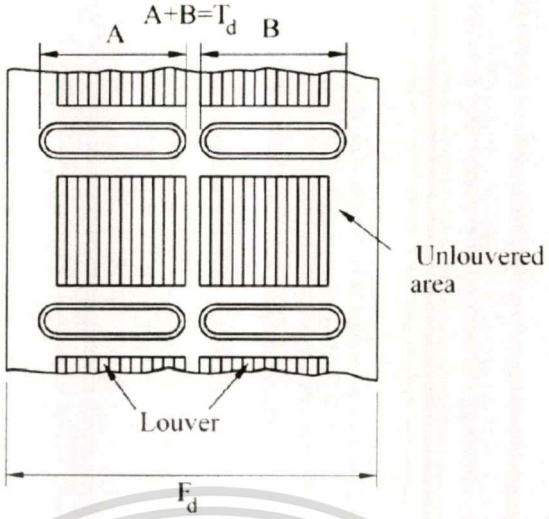

Figure 1.4 Definitions of various geometric parameters [24]

Chang and Wang [24] presented the heat transfer correlation for louver fin geometry based on 91 louvered fin heat exchangers with different geometrical parameter (**Figure 1.4**), including louver angle, tube width, louver length, louver pitch, fin length and fin pitch. They derived the correlation data from the data of Davenport[5], Achaichia and Cowell [1], Webb and Jung [16], and Rugh et al. [12]. They had developed the heat transfer correlations for louvered fin heat exchangers and presented the correlation that had 89.3% of the louvered fin data explained within 15% of accuracy with mean deviation of ±7.55%. The final correlation as follows,

$$j = \mathrm{Re}_{Lp}^{-0.49}\left(\frac{\theta}{90}\right)^{0.27}\left(\frac{F_p}{L_p}\right)^{-0.14}\left(\frac{F_l}{L_p}\right)^{-0.29}\left(\frac{T_d}{L_p}\right)^{-0.23}\left(\frac{L_l}{L_p}\right)^{0.68}\left(\frac{T_p}{L_p}\right)^{-0.28}\left(\frac{\delta_f}{L_p}\right)^{-0.05} \quad (1.5)$$

In Equation 1.5, T_d is tube depth, L_l is louver length and δ_f is fin thickness. The remaining variables have similar meaning as in this study.

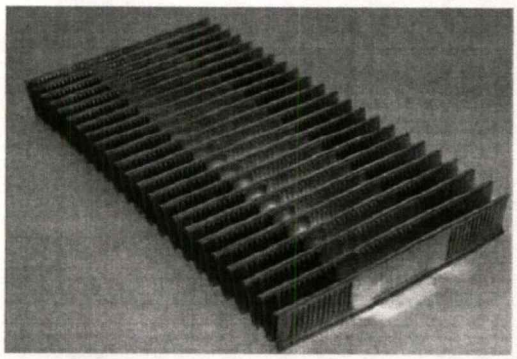

Figure 1.5 Multi-louver fins [11]

Dong et al. [11] presented the experimental studies on the air-side heat transfer and pressure drop characteristics for 20 types of multi-louvered fin and flat tube heat exchanger (**Figure 1.5**). The Reynolds Number using the range from 200 to 2500 based on louver pitch with difference geometrical of louver fin at constrain tube side flow rate of 2.8 m^3/h. The air-side performances were analyzed using the effectiveness-NTU method. Characteristics of the heat transfer and pressure drop were reported in terms of Colburn *j*-factor and Fanning factor as a function Reynolds Number (Re_{Lp}). They proposed the correlation for geometry in their studies with the errors of ±10% and ±12%, and the mean deviations are 4.1% and 5.6% respectively. The final correlation as follows;

$$j = 0.26712 \mathrm{Re}_{Lp}^{-0.1944} \left(\frac{L_a}{90}\right)^{0.257} \left(\frac{F_p}{L_p}\right)^{-0.5177} \left(\frac{F_h}{L_p}\right)^{-1.9045} \left(\frac{L_h}{L_p}\right)^{1.7159} \left(\frac{L_d}{L_p}\right)^{-0.2147} \left(\frac{\delta}{L_p}\right)^{-0.05} \quad (1.6)$$

and

$$f = 0.54486 \mathrm{Re}_{Lp}^{-0.3068} \left(\frac{L_a}{90}\right)^{0.444} \left(\frac{F_p}{L_p}\right)^{-0.9925} \left(\frac{F_h}{L_p}\right)^{0.5458} \left(\frac{L_h}{L_p}\right)^{-0.2003} \left(\frac{L_d}{L_p}\right)^{0.0688} \quad (1.7)$$

1.2.2 Numerical Approach

Leu et al. [13] performed a numerical investigation of the airside performance for fin-and tube heat exchanger having circular and oval configuration. The numerical simulations are performed for different geometries with various louver angles, louver pitches, and louvered lengths. In their studies Phoemics, Version 3.1 software was used with SIMPLEST algorithms. The model was fixed louver length (6.25 mm.) and louver angle (14°). The simulation result was 14% decreasing in heat transfer performance and 41% decreasing in pressure drop.

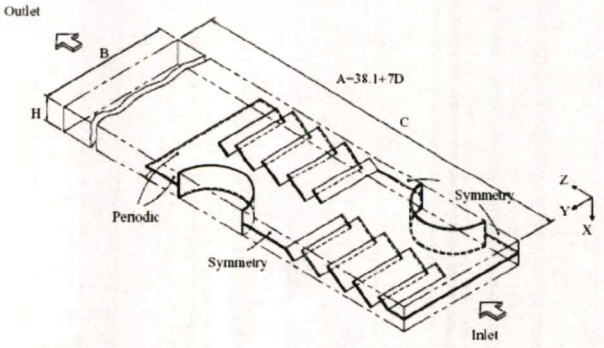

Figure 1.6 Computation domain of Circular tube heat exchanger [13]

Hansen [4] has been studied the heat transfer and pressure drop characteristics of compact tube and fin heat exchanger. The unit was investigated for Reynolds numbers ranging from 330 to 7000.

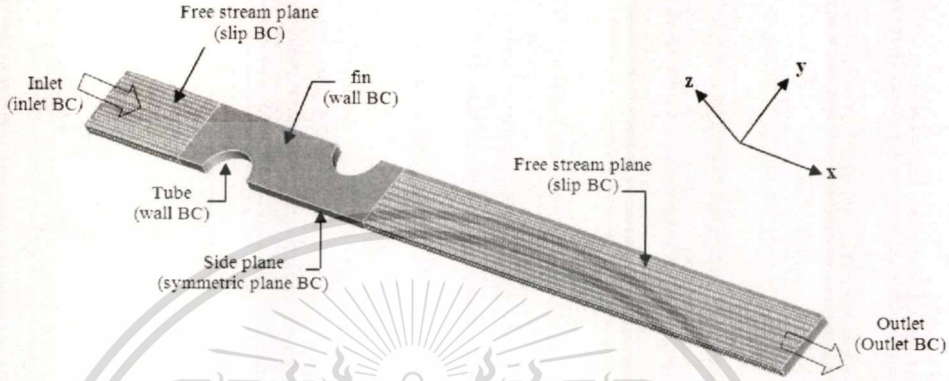

Figure 1.7 Computation domains and boundary condition of tube and fin heat exchangers [4]

The model geometry was created (**Figure 1.7**) and meshed using the hexagonal mesh (**Figure 1.8**).His work, the mesh was chosen approximately 50,000 cells.

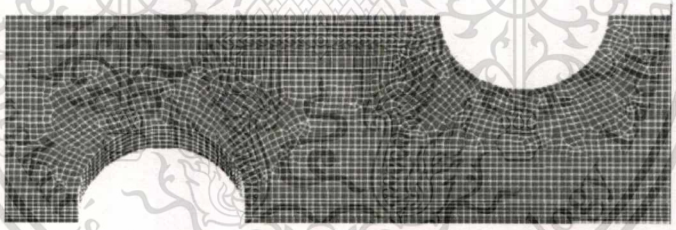

Figure 1.8 Computational meshes [4]

The result of simulated case in term of friction factor *f* and Colburn factor *j* were compared with experimental results from the literature. The steady-state solver was used for numerical simulation of laminar and turbulent flow models (*k-epsilon*, an SST *k-omega)* to estimate the heat transfer and pressure drop characteristics, flow and temperature fields.

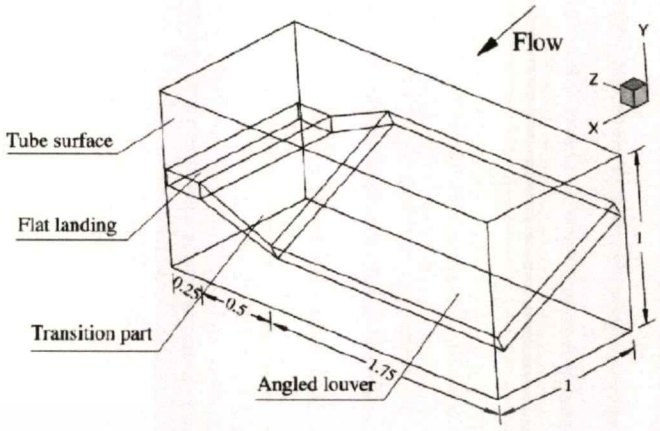

Figure 1.9 The computational domain [10]

Cui and Tafti, [9] they present the computational result in complex three-dimensional louver fin geometry (**Figure 1.9**), the result show that Re_b=110. Their computational mesh an infinite array of louver put together in the streamwise and cross-stream direction (**Figure 1.10**) for study the characteristic of transition region of louver fin by a swept leading edge and decreasing flow area between louvers. The result of overall heat transfer coefficient is small because of the small spatial extent of the transition region.

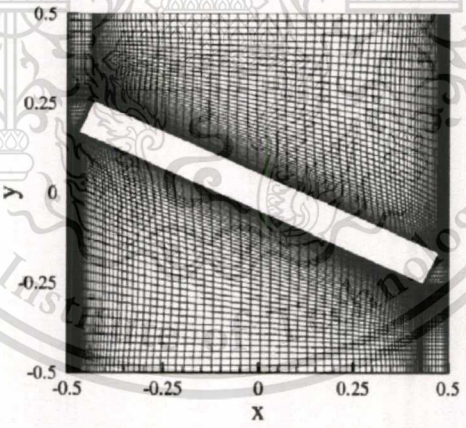

Figure 1.10 The computational mesh in a Z-plain [10]

Lyman et al. [3] conducted the experimental of six scaled up louvered fin geometry compared with two-dimensional CFD to improve the heat transfer performance of compact heat exchanger, and is show in the **Figure 1.11**.

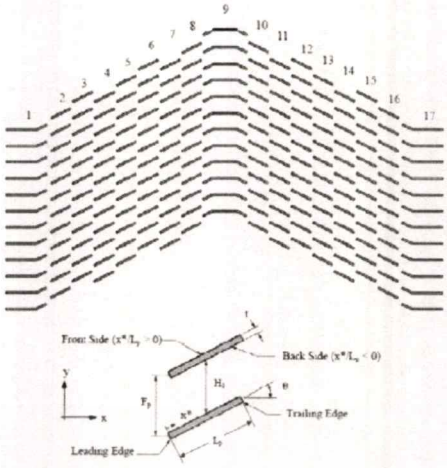

Figure 1.11 Computation domains [3]

The computation mesh model with triangular meshed and controlled fine calls around the louvered as show in **Figure 1.12**. Experiments were conducted in a number of large-scale louver models with varied fin pitch and louver angle within the commercial CFD package Fluent 5.5 software. The CFD prediction was carried out by solving the momentum and energy equations and using second-order discretization, laminar flow models with steady-state solvers to calculate pressure drop flow and temperature fields.

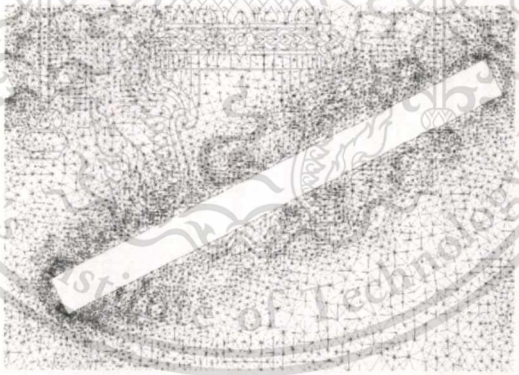

Figure 1.12 Portion of CFD mesh used for predict flow boundary [3]

Perrotin and Clodic [18] used the two and three-dimensional CFD simulation to investigate a one-row automotive condenser for Reynolds numbers ranging from 40 to 1200. CFD simulations are compared with experimental results and the correlation from the literature by Zhang and Tafti [22]. They presents the 2D and 3D mesh with quadrilateral cells and controlled three cells around the louver zone (equal to the fin thickness 0.1 mm, half the fin thickness and one-quarter the fin thickness). CFD simulations with using STAR-CD V3.15 software was done in their study. They assumed the flow model to be laminar at Re_{LP} range from 40 to 1200 for 3D model, but for 2D

model the simulation had been performed with the low Reynolds k-ε turbulence model. The heat transfer results in these cases of 58% higher than those without turbulence model. The result of 2D model with constant wall temperature over predicted the heat transfer coefficient for up to 80% compared with experimental data. The 3D models with constant wall temperature (**Figure 1.13**) predicted the heat transfer coefficients are closer to the experimental data. Moreover, the results are still over predicted and are 13% higher than the experiment data.

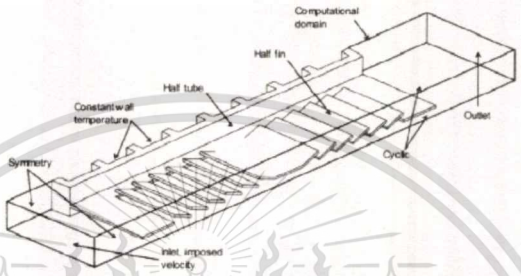

Figure 1.13 Computational domain and boundary condition [18]

Hsieh and Jang [6] they presented the five difference cases of successively increased or decreased louver angle +2, +4, 2, 4, and uniform angle 20 patterns(**Figure 1.14**) and designate the physical model and computation domain for the louvered fin heat exchanger (**Figure 1.15**).

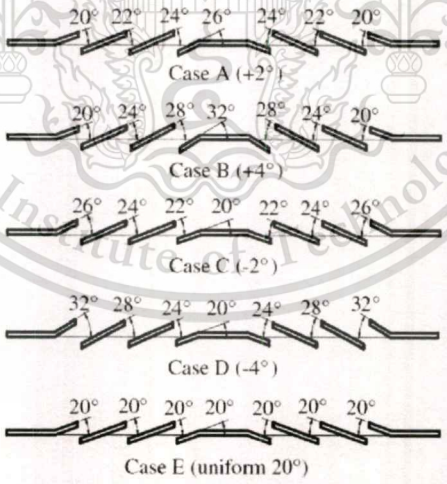

Figure 1.14 Five different cases of successively increased or decreased louver angle [6]

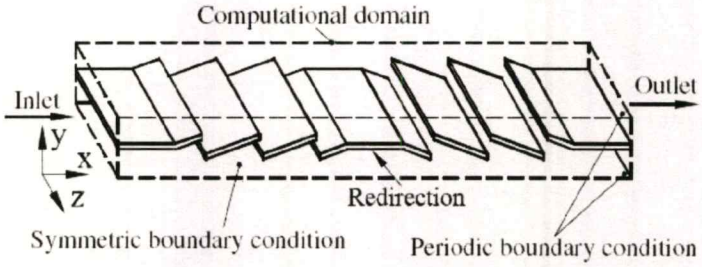

Figure 1.15 The computational domain [6]

CFD simulation with third-order upwind scheme is used to model the convective terms of governing equations. Second-order central difference schemes are used for the viscous and source terms. A pressure based predictor/multi-corrector solution procedure is employed to enhance velocity–pressure coupling and continuity-satisfied flow filed. The numerical mesh with cells parallels the louvered fin (**Figure 1.16**). The considered the fluid as incompressible with constant properties and the flow was assumed to be turbulent.

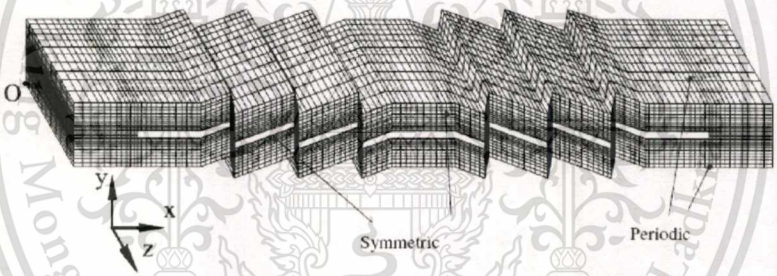

Figure 1.16 Computational grid system [6]

Their result of Nusselt number and pressure drop coefficient for successively variable louver angles (cases A–D) were higher than the uniform louver angle (case E) and the maximum area reduction for case B (+4) can reach up to 25.5%.

Malapure et al. [20] studied the three-dimensional CFD simulation of flat-sided tube and louvered plate fin heat exchanger (**Figure 1.17**) for Reynolds Number ranging from 400 to 4000. The results were satisfactorily compared with Stanton number and Friction factor given as a Function of Reynolds number of Achaichia and Cowell (1988).

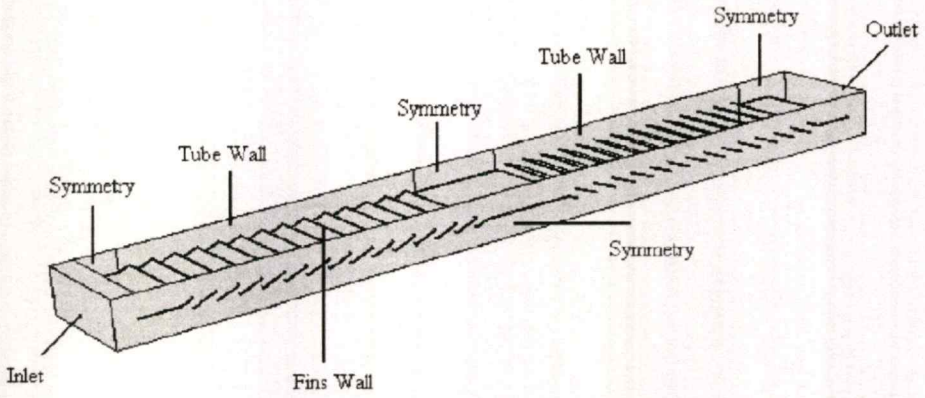

Figure 1.17 Computational domain and boundary condition [20]

CFD simulation was performed with commercial code FLUENT 6.1 software. Hex/Wedge mesh using GAMBIT to generate the cell size equal to or half of the fin thickness. The three-dimensional model with SIMPLE algorithm, pressure, velocity coupling and second-order upwind scheme for space discretization of momentum with RNG k-epsilon turbulence model to estimate the heat transfer and pressure drop characteristics and to verify the local turbulence behavior of the flow field. They calculated the heat transfer coefficient in term of the logarithmic mean temperature difference (*LMTD*) with ΔT_i is the temperature difference between fin area weighted average and air temperature at the inlet plane, $\Delta T_i = T_{f,i}^{aw} - T_{a,i}$ and the outlet plane, $\Delta T_o = T_{f,o}^{aw} - T_{a,o}$. The heat transfer results were found to be 6-7% higher than those without turbulence model.

Problem Formulation

Several years ago, many researchers had taken extensive studies on this problem. Cui and Tafti, [9] they present the computational mesh an infinite array of louver put together in the streamwise and cross-stream direction for study the characteristic of transition region of louver fin by a swept leading edge and decreasing flow area between louvers. Perrotin and Clodic, [18] presents the 2D and 3D mesh with quadrilateral cells and controlled three cells around the louver zone (equal to the fin thickness 0.1mm, half the fin thickness and one-quarter the fin thickness). Hsieh and Jang, [6] they present the numerical mesh with cells parallel the louvered fin. Malapure et al., [20] they presented the Hex/Wedge mesh using GAMBIT to generate the cell size equal to or half of the fin thickness. In this research, a three-dimensional model was constructed with the smallest fluid cell size next to the wall being smaller than the fin's thickness. Additionally, our modeling method has controlled the near-wall mesh to be fine enough so that the first nodes at the boundary cells are placed at $Y^+ \leq 5$ for all cases.

Perrotin and Clodic, [18] assumed the flow model to be laminar at Re_{LP} range from 40 to 1200 for 3D model, but for 2D model the simulation had been performed with the low Reynolds k-ε turbulence model. The heat transfer results in these cases were 58% higher than those without turbulence model. The result of 2D model with constant wall temperature over predicted the heat transfer coefficient for up to 80% compared with experimental data. The 3D models with constant wall temperature predicted the heat transfer coefficients are closer to the experimental data. Nevertheless, the results are still over predicted and are 13% higher than the experiment data. Hsieh and Jang, [6] considered the fluid as incompressible with constant properties and the flow was assumed to be turbulent. Malapure et al., [20] presented a study on three dimensional simulations with RNG k-epsilon turbulence model to estimate the heat transfer and pressure drop characteristics and to verify the local turbulence behavior of the flow field. The heat transfer results were found to be 6-7% higher than those without turbulence model. In this study we had adopted RNG k-epsilon turbulent model with enhanced wall treatment modeling applied at the first cell next to the boundary. The nodes of these cells are controlled in Laminar Sub layer with $Y^{+} \leq 5$.

Malapure et al., [20] they presented the heat transfer coefficient in term of the logarithmic mean temperature difference (*LMTD*) with ΔT_i is the temperature difference between fin area weighted average and air temperature at the inlet plane, $\Delta T_i = T_{f,i}^{aw} - T_{a,i}$ and the outlet plane $\Delta T_o = T_{f,o}^{aw} - T_{a,o}$. Theoretically speaking, the logarithmic mean temperature difference of cross-flow heat exchange is computed by the temperature difference between hot and cold fluid. Therefore, in this study we computed the heat transfer coefficient using log-mean-temperature difference between the coolant and the air at the inlet and outlet.

For this research, an extensive numerical investigation of flow and heat transfer in louver fin radiator was presented using FLUENT software to perform for fifteen cases in which containing seven sub-cases of simulations with different geometrical parameters of fin pitch, louver pitch, louver angle and different Reynolds number within the range from 400 to 4000. The simulations were validated by the empirical result against well-known by Achaichia and Cowell, [1] with Stanton number parameter (Equation 1.2) and Friction factor parameter (Equation 1.3).

1.3 Objectives

The main objective of this research is introduced the simulation technique as an alternative for cost reduction of new product design and development cycle. The numerical technique is called finite volume method is used in this study to investigate the effects of geometric parameters on heat transfer and fiction factor of louvered fin radiator.

1.3.1 To explore the validity of the computational modeling techniques and the models of momentum, mass and heat transfer among the air, solid and water domains encountered in the louvered fin radiator against the similar experimental results.

1.3.2 To apply the technique and model investigates the effects of geometric parameters of heat transfer and friction factor of corrugated louver fin radiator.

1.4 Scope of Research

1.4.1 To study on the effects of geometric parameters of heat transfer and friction loss of louver plate fins in terms of Stanton number and friction factor within the range of Reynolds number 400 to 4000.

1.4.2 To analyses the effects of fin characteristics on performance of louver fin heat transfer.

1.5 Research Methodology

1.5.1 To survey general requirement of automotive radiator.

1.5.2 To study the related theory to specify the scope of work and mathematical model to be used.

1.5.3 To select the geometrical parameters to investigate their effects on the performance of Louver Fin.

1.5.4 Simulation and collection data for all of the conditions.

1.5.5 To calculate of heat transfer performance and pressure drop.

1.5.6 To comparison of the empirical equation of Achaichia and Cowell and evaluate the predictive quality of the technique within the specified range of operating conditions and geometries.

CHAPTER 2

THEORY

2.1 Heat Transfer and Efficiency

Heat transfer is thermal energy due to a temperature difference. The mechanisms of heat transfer have three types' conduction, convection, and radiation heat transfer. For this study, the heat exchanger using two modes of heat transfer are conduction and convection which are focused in this chapter.

2.1.1 Conduction Heat Transfer

In heat transfer, conduction or heat conduction is the transfer of thermal energy between neighboring molecules in substance due to a temperature gradient. It always takes place from a region of high temperature to a region of low temperature and acts to equalize temperature differences. The heat transfer rate per unit area perpendicular to the direction of transfer, and it is proportional to the temperature gradient, in this direction. The proportionality constraint is a transport property known as the thermal conductivity and is a characteristic of the direction of decreasing temperature.

The basic equation for the analysis of heat conduction is *Fourier's law,* which is based on experimental observations, can be defined as:

$$q_{cond} = -kA\frac{dT}{dx} \tag{2.1}$$

where the conduction *heat flux* q is the heat transfer rate in the x direction per unit area perpendicular to the direction of transfer and dT/dx. It is the *temperature gradient* in this direction. The proportionality constant k is a transport property known as the *thermal conductivity* and is a characteristic of the wall material.

2.1.2 Convection Heat Transfer

When, fluid flow through and become to contact with the surface of the material that has a difference in the temperature of fluid. The heat will transfer between the fluid and solid. The heat transfer rate will depend on the difference between the temperature of fluid and solid as well as the convection heat transfer coefficient of fluid that flows through the surface of the material.

Newton's Law of cooling has presented the relation of heat transfer by the convection. It can be defined as;

$$q_{conv} = hA(T_s - T_\infty) \tag{2.2}$$

where the convection *heat flux* q_{conv} is proportional to the difference between the surface and fluid temperatures, T_s and T_∞ respectively. The proportionality constant h is termed the *convection heat transfer coefficient.* It depends on conductions in the boundary layer, which are influenced by surface geometry, the nature of the fluid motion, and an assortment of fluid thermodynamic and transport properties.

2.1.3 Fin Heat Transfer

The heat transfer analysis of simple fin is simplified with certain assumptions are made.

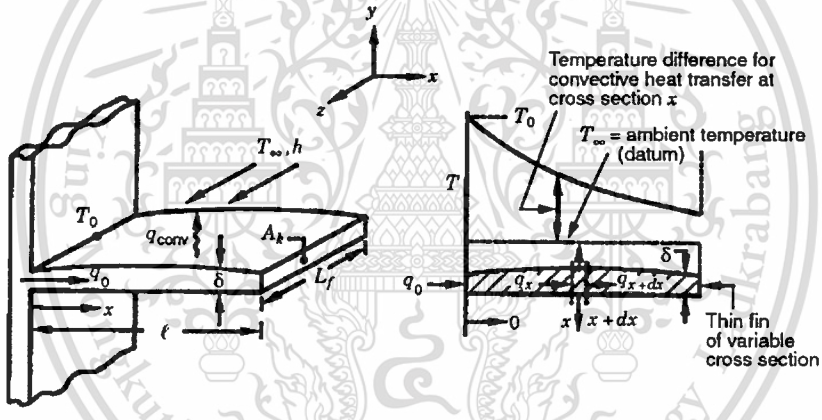

Figure 2.1 Thin fin of a variable cross section [15]

Shah and Sekulic, [15] they chose to assume one-dimensional conduction conditions in the longitudinal (x) direction. Steady-state conditions are considered constant thermal conductivity by assumption. Thermal radiation from the surface was negligible, heat generation effects were absent, and the convection heat transfer coefficient h was uniform over the surface. Applying the conservation of energy requirement from **Figure 2.1**, this can be defined as:

$$q_x - q_{x+dx} - dq_{conv} = 0 \tag{2.3}$$

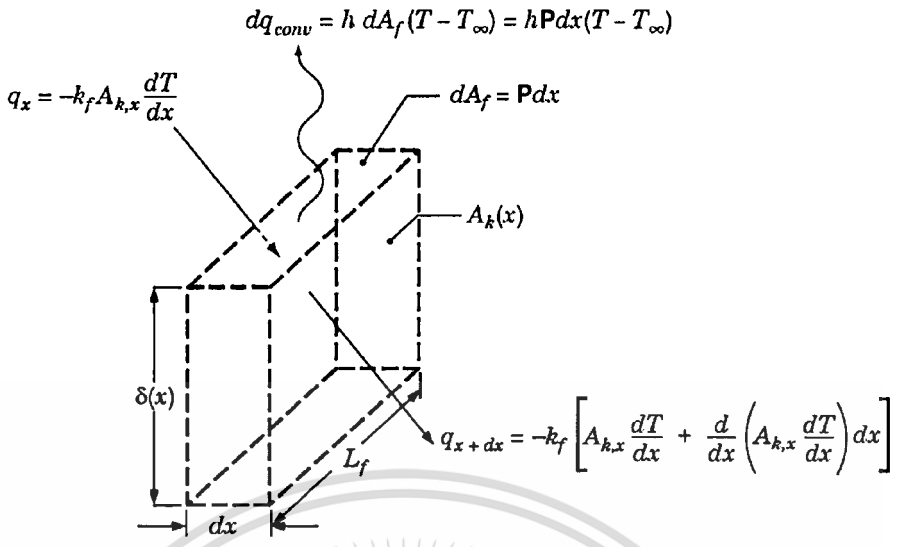

Figure 2.2 Energy terms associated with the differential element of the fin [15]

The energy balance on an element between x and $x+dx$ of **Figure 2.1** is show in **Figure 2.2.** Heats enter this element by conduction at x direction, part of this heat leaves the cross section at $x+dx$ and the rest leaves by convection through its surface area (dA_f).

From *Fourier's law* we know that

$$q_x = -k_f A_{k,x}\frac{dT}{dx} \tag{2.4}$$

where q_x is the conduction heat transfer rate, $A_{k,x}$ is the cross-section area in x direction and the conduction heat transfer rate at $x+dx$ can be defined as:

$$q_{x+dx} = q_x + \frac{dq_x}{dx}dx \tag{2.5}$$

Follows that

$$q_{x+dx} = -k_f A_{k,x}\frac{dT}{dx} - k_f\frac{d}{dx}\left(\frac{A_{k,x}dT}{dx}\right)dx \tag{2.6}$$

or

$$q_{x+dx} = -k_f\left[A_{k,x}\frac{dT}{dx} + \frac{d}{dx}\left(A_{k,x}\frac{dT}{dx}\right)dx\right] \tag{2.7}$$

where the heat convection through surface area $dA_f = Pdx$, the convection heat transfer rate can be defined as:

$$dq_{conv} = hdA_f(T - T_\infty) = h(Pdx)(T - T_\infty) \tag{2.8}$$

Then the conservation of energy requirement from Equation 2.3, it can be followed that

$$k_f \frac{d}{dx}(\frac{A_{k,x}dT}{dx})dx - h(Pdx)(T - T_\infty) = 0 \tag{2.9}$$

where differentiation and rewriting.

$$\frac{d^2T}{dx^2} + (\frac{1}{A_{k,x}}\frac{dA_{k,x}}{dx})\frac{dT}{dx} - \frac{hP}{k_f A_{k,x}}(T - T_\infty) = 0 \tag{2.10}$$

or

$$\frac{d^2T}{dx^2} + d(\frac{\ln A_{k,x}}{dx})\frac{dT}{dx} - m^2(T - T_\infty) = 0 \tag{2.11}$$

where

$$m^2 = \frac{hP}{k_f A_{k,x}} \tag{2.12}$$

where surface convection is $P(x) = 2\left(L_f + \delta(x)\right)$ and cross sectional area for heat conduction is $A_k(x) = L_f\delta(x)$. Equation 2.12 can be rewrite:

$$m^2 = \frac{2h(L_f + \delta)}{k_f L_f \delta} \approx \frac{2h}{k_f \delta} \tag{2.13}$$

To simplify the form of this equation, transform the dependent variable by defining an excess temperature $\theta(x)$ as:

$$\theta(x) = T(x) - T_\infty \tag{2.14}$$

where assume that ambient temperature T_∞ is a constant, so that $d\theta / dx = dT / dx$ then equation 2.11 can be defined as:

$$\frac{d^2\theta}{dx^2} + d(\frac{\ln A_{k,x}}{dx})\frac{d\theta}{dx} - m^2\theta = 0 \tag{2.15}$$

for $L_f >> \delta$. Since $A_{k,x}$ is constant, $d(\ln A_{k,x})/dx = 0$ and m^2 is constant. Equation 2.15 can be reduces to:

$$\frac{d^2\theta}{dx^2} - m^2\theta = 0 \tag{2.16}$$

From equation 2.16 is a linear, homogeneous, second-order differential equation with constant coefficients. Its general solution will be:

$$\theta = C_1 e^{-mx} + C_2 e^{mx} \tag{2.17}$$

For the second-order differential equation condition Equation 2.16 specified at the fin tip $x = 0$ and $T = T_0$ can be define as:

$$\theta(0) = T_0 - T_\infty = \theta_0 \tag{2.18}$$

From this study the temperature distribution at the fin surface enter from both sides of the tube wall then the temperature difference very small. The heat transfer rate through the fin tip is zero.

$$q_l = -k_f A_x \left.\frac{dT}{dx}\right|_{x=l} = -k_f A_x \left.\frac{d\theta}{dx}\right|_{x=l} = 0 \tag{2.19}$$

$$\left.\frac{d\theta}{dx}\right|_{x=l} = 0 \tag{2.20}$$

Substituting from Equation 2.17 and 2.18 to solve for C_1 and C_2 we than obtain.

$$C_1 + C_2 = \theta_0 \tag{2.21}$$

$$-mC_1 e^{-ml} + mC_2 e^{ml} = 0 \tag{2.22}$$

Using this expression with Equation 2.17 can be defined as:

$$\frac{\theta}{\theta_0} = \frac{\cosh m(l-x)}{\cosh(ml)} \tag{2.23}$$

and from Equations 2.19 and 2.23, the fin heat transfer rate to the base is obtained

$$q_0 = \frac{hP}{m}\theta_0 \tanh ml \tag{2.24}$$

2.1.4 Fin Efficiency

Another measure of fin thermal performance is provided by the *fin efficiency* η_f. The maximum driving potential for convection is the temperature difference between the base $(x=0)$ and the fluid, $\theta_0 = T_0 - T_\infty$. Hence the maximum rate at which a fin could dissipate energy is the rate would exist if the entire fin surface were at the base temperature. However, since any fin is characterized by a finite conduction resistance, temperature gradient must exist along the fin and the above condition is an idealization. A logical definition of fin efficiency is therefore:

$$\eta_f = \frac{q_0}{q_{\max}} \tag{2.25}$$

From Equation 2.24

$$q_0 = \frac{hP}{m}\theta_0 \tanh ml \tag{2.26}$$

and maximum heat transfer rate can be defend from Equation as:

$$q_{\max} = hPl(T_0 - T_\infty) = hPl\theta_0 \tag{2.27}$$

then fin efficiency can be defined as:

$$\eta_f = \frac{hP\theta \tanh(ml)}{mhPl\theta} = \frac{\tanh(ml)}{ml} \tag{2.28}$$

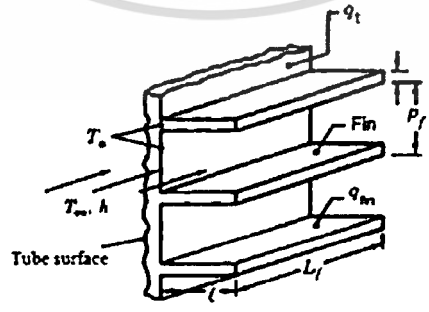

Figure 2.3 Plate fin surface heat exchanger [15]

Plate fin surface has fins attach to the tube surface by brazing, soldering, welding fit the plate fins heat exchanger show in **Figure 2.3**. Then the heat transfer performance of this heat exchanger was measured by overall surface efficiency (η_o), can be defined as:

$$\eta_o = \frac{q_{Total}}{q_{\max}} = \frac{q_t + q_f}{h(A_t + A_f)(T_0 - T_\infty)} \tag{2.29}$$

where q_t is heat transfer rate of tube surface, q_f is heat transfer rate of fin surface, A_t is tube area and A_f is fin area, q_{Total} from Equation 2.28 can define as:

$$q_{Total} = q_t + q_f = hA_t(T_0 - T_\infty) + hA_f\eta_f(T_0 - T_\infty) = h(A_t + \eta_f A_f)(T_0 - T_\infty) \tag{2.30}$$

from Equation 2.28 and 2.29 when $A = A_t + A_f$ can be rewrite:

$$\eta_o = 1 - \frac{A_f}{A}(1 - \eta_f) \tag{2.31}$$

2.1.5 Heat Exchange Analysis

When we design or predict the heat transfer of a heat exchanger, it is necessary to relate the total heat transfer rate to quantities of inlet and outlet fluid temperature, overall heat transfer coefficient and total surface area for heat transfer. This project concentrates on the heat transfer rate. There for, calculation is based on the heat transfer balance at the inlet and outlet on the air side. The heat transfer rate equation can be defined as:

$$q = h_c A\Delta T_m = \dot{m}c_p(T_{a,o} - T_{a,i}) = \rho U A_c c_p(T_{a,o} - T_{a,i}) \tag{2.32}$$

where mass flow rate is $\dot{m} = \rho A_c U$, A (m^2) is the total heat transfer area, A_c is the cross sectional minimum flow area, h_c is the heat transfer coefficient for design of heat exchangers and ΔT_m is the log mean temperatures difference (*LMTD*) defined as:

$$LMTD = \Delta T_m = \frac{\Delta T_o - \Delta T_i}{\ln(\Delta T_o / \Delta T_i)} \tag{2.33}$$

where ΔT_i is the temperature difference between coolant and air at the inlet plane, $\Delta T_i = T_w - T_{a,i}$, ΔT_o is the temperature difference between coolant and air at the outlet plane, $\Delta T_o = T_w - T_{a,o}$. It is assumed that there is a small difference in coolant and tube temperature thus T_w is equal to the temperature of tube wall. Therefore the heat transfer coefficient can be rewrite as:

$$h_c = \rho U c_p \frac{A_c}{A} \frac{(T_{a,o} - T_{a,i})}{LMTD} \tag{2.34}$$

2.2 Dimensionless Group

Heat transfer characteristics of a heat exchanger can be presented in terms of the Nusselt number, Stanton number, or Colburn factor versus the Reynolds number. Flow friction characteristics are presented in terms of the Fanning friction factor versus the Reynolds number. These and other important dimensionless groups used in heat exchanger design and internal flow forced convection.

2.2.1 Fluid Flow

2.2.1.1 *Reynolds Number*

The Reynolds Number (Re_d) is a ratio of flow momentum rate to viscous force, and thus it is a flow modulus. It should be added, though, that the physical interpretation of the Reynolds number as the ratio of inertia force to viscous force.

$$\mathrm{Re}_d = \frac{\rho U d_h}{\mu} \tag{2.35}$$

where ρ is the density of fluid flow, U is the mean velocity through the minimum flow area, d_h is the pipe inside diameter and μ is the dynamic viscosity.

2.2.1.2 *Hydraulic diameter*

The Hydraulic diameter (d_h) is consideration to internal flow of *non-circular tube* cross section area. We well be used the *hydraulic diameter* in calculating parameter of Reynolds number.

$$d_h = \frac{4 A_c L_s}{A} \tag{2.36}$$

where A_c is the minimum flow area, A is the total heat transfer area and L_s is the fin length of heat exchange.

2.2.1.3 *Friction Factor*

Friction Factor is the ratio of wall shear stress (τ_w) to the flow kinematic energy per unit volume $\rho U^2 / 2$, can be defined as:

$$f = \frac{\tau_w}{\rho U^2 / 2} \tag{2.37}$$

In a steady-state isothermal fully developed flow in a constant-cross-sectional geometry, the momentum rate at any cross section is constant. The pressure drop is then a result of the wall friction. In the absence of core entrance and exit losses, from the application of Newton's second law of motion the pressure drop in dimensionless can be define as:

$$\Delta P = f\frac{4L}{D_h}\frac{\rho U^2}{2} \tag{2.38}$$

from Equation 2.36 hydraulic diameter $d_h = 4A_cL_s/A$, Friction Factor can be rewrite as:

$$f = \frac{\Delta P}{\frac{\rho U^2}{2}\frac{A}{A_c}} \tag{2.39}$$

2.2.2 Heat Transfer

2.2.2.1 *Stanton number*

The Stanton number is dimensionless representation of the heat transfer coefficient. In this project St is the ratio of convection heat transfer to the enthalpy rate change of the fluid reaching the wall temperature per unit of flow cross-sectional areas, Single-phase heat transfer from the wall to the fluid is related to enthalpy rate change. The Stanton number is also directly related to the number of heat transfer units on one fluid side of the exchanger can be defining as:

$$St = \frac{h}{Gc_p} = \frac{h}{\rho U c_p} \tag{2.40}$$

where G is the fluid mass flux based on the minimum free area $\dot{m}/A_c$, from Equation 2.33 of heat transfer coefficient is $h_c = \rho U c_p \frac{A_c}{A}\frac{(T_{a,o}-T_{a,i})}{LMTD}$ then Stanton number can be rewrite as:

$$St = \frac{Ac}{A}\frac{(T_{a,o}-T_{a,i})}{LMTD} \tag{2.41}$$

2.2.2.2 *Nusselt number*

The Nusselt number is one of the dimensionless representations of the heat transfer coefficient. It is defined for a external flow as the ratio of the convective conductance h to the pure molecular thermal conductance k/L. The Nusselt number calculated using parameters as follows:

$$Nu = \frac{hL}{k} = \frac{qL}{k(T_w - T_b)} \tag{2.42}$$

where L is fluid flow length, T_w is wall temperature and T_b is fluid bulk temperature

CHAPTER 3

NUMERICAL TECHNIQUE

3.1 Computational Fluid Dynamics

Computational fluid dynamics or CFD is the analysis of system for fluid flow, heat transfer and related phenomena such as chemical reactions by means of computer-based simulation (In this project used CFD for analysis of flow and heat transfer not for comical reaction). The technique is very powerful and spans a wide range of industrial and non-industrial application area. Examples application areas are: aerodynamic of aircraft and vehicles lift and drag, hydrodynamics of ships, power plant combustion in IC engine and gas turbines, turbo machinery of flows inside rotating passages electrical, chemical processes and biomedical of blood flows through arteries etc. From 1960, CFD techniques are used to the design, R&D and manufacture of aircraft and jet engines, internal combustion engines, combustion chamber of gas turbines and furnaces, as well as industrial products and process.

The advantage to use CFD over traditional experimental-based analyses, since substation reduction of lead times and costs of new design, ability to study systems where controlled experiments are difficult or impossible to perform limits etc, unlike with CFD, where large amounts of results can be produced at practically no added expense. In this way, parametric studies to optimise equipment are very inexpensive with CFD when compared to experiments.

The purpose of this project is to introduce a simulation technique as an alternative for cost reduction of new product design and development cycle. The numerical technique called finite volume method is used in this study to investigate the effects of geometric parameters on heat transfer and fiction factor of louvered fin radiator and validate the simulation result with actual experimental results from the literature. Different solvers and turbulence models are used to try to determine the most accurate CFD method for predicting pressure loss and heat transfer in this type of louver plate fin Radiator.

3.2 Governing equations

The numerical simulation of flow passing through the louver fin heat exchanger was performed by the numerical technique called computational Fluid Dynamics. It was assumed the air is

incompressible, constrained boundary, steady-state flow type of Newtonian fluid, and three dimensional. The distributions of the velocity, pressure, and temperature in the flow fields were governed by Navier-Stokes and energy equations.

3.2.1 Mass Conservation

$$\frac{\partial}{\partial x_j}(\rho u_j) = 0 \tag{3.1}$$

3.2.2 Momentum Conservation

$$\frac{\partial}{\partial x_j}(\rho u_j u_i - \tau_{ij}) = -\frac{\partial p}{\partial x_i} \tag{3.2}$$

where, τ_{ij} is the viscous stress tensor components defined as:

$$\tau_{ij} = 2\mu S_{ij} - \frac{2}{3}\mu \frac{\partial u_k}{\partial x_k}\delta_{ij} \tag{3.3}$$

and δ_{ij} is the kronecker delta and S_{ij} is the rate of strain tensor defined as:

$$S_{ij} = \frac{1}{2}\left(\frac{\partial u_i}{\partial x_j} + \frac{\partial u_j}{\partial x_i}\right) \tag{3.4}$$

3.2.3 Energy Conservation

The energy equation solved in fluid domain is given by

$$\frac{\partial}{\partial x_j}\left(\rho u_j h - k\frac{\partial T}{\partial x_j}\right) = u_j \frac{\partial p}{\partial x_j} + \tau_{ij}\frac{\partial u_i}{\partial x_j} \tag{3.5}$$

and the energy equation solved in solid domain is given by

$$\frac{\partial}{\partial x_j}(\lambda \frac{\partial T}{\partial x_j}) = 0 \tag{3.6}$$

3.3 Turbulent Model

The Reynolds number studied for the heat exchanger flow in this project range from 400 to 4000, the flows can be laminar or turbulent at the different flow velocities. Because these flow regimes behave differently, it can be necessary to model the flow in different ways. In this research,

turbulence models *k –epsilon* with Enhanced Wall Treatment is utilized in order to investigate which is best to use for the different types of flow. This section describes some of the commonly used turbulence models, and then presents relevant details regarding the specific turbulence models used in this project. A laminar flow model is also used for comparison with the turbulence models.

3.3.1 RNG k–ε Turbulentodel

The effect of turbulence on the flow field is included through the application of RNG k–ε turbulence model

Kinetic Energy

$$\frac{\partial}{\partial x_i}(\rho k)+\frac{\partial}{\partial x_i}(\rho k u_i)=\frac{\partial}{\partial x_j}\left(\alpha_k \mu_{eff}\frac{\partial k}{\partial x_j}\right)+G_k+G_b-\rho\varepsilon-Y_M+S_k \tag{3.7}$$

Dissipation rate

$$\frac{\partial}{\partial x_i}(\rho \varepsilon)+\frac{\partial}{\partial x_i}(\rho \varepsilon u_i)=\frac{\partial}{\partial x_j}\left(\alpha_p \mu_{eff}\frac{\partial \varepsilon}{\partial x_j}\right) + C_{1\varepsilon}\frac{\varepsilon}{k}(G_k+C_{3\varepsilon}G_b)-C_{2\varepsilon\rho}\frac{\varepsilon^2}{k}-R_\varepsilon+S_k \tag{3.8}$$

where, $\mu_{eff}=\mu+\mu_t$ and $\mu_t=\rho C_\mu \frac{k^2}{\varepsilon}$ in high Reynolds number range, C_μ = 0.0845. Turbulent kinetic energy generation term is $G_k=2\mu_t S^2_{ij}$. The rate of strain term R_ε is given by

$$R_\varepsilon=\frac{C_\mu \rho \eta^3(1-\eta/\eta_o)}{1+\beta\eta^3}\frac{\varepsilon^2}{k} \tag{3.9}$$

where $\eta=\frac{Sk}{\varepsilon}$ and η_o = 4.38 and β = 0.012 . The RNG theory provides values of the turbulence constants $C_{1\varepsilon}=1.42$ and $C_{2\varepsilon}=1.68$

3.4 Conjugate Heat transfer

The this project the three-dimensional geometrical models of air domain are constructed with the smallest cell size next to the wall being smaller than the fin's thickness as suggested by the previous worker. Conjugate heat transfer by Patankar, 1960

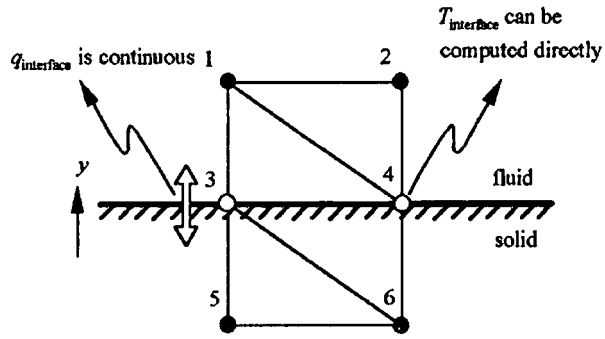

Figure 3.1 Elements across fluid-solid interface in finite element method [17]

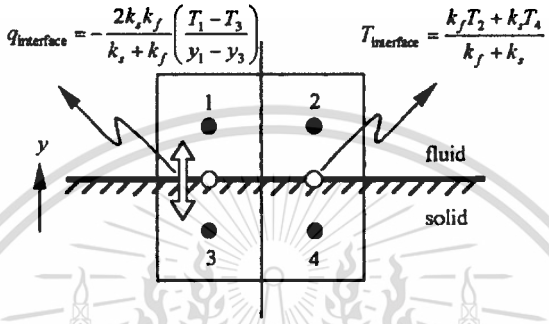

Figure 3.2 Control volumes across fluid-solid interface by the finite element method [17]

3.5 Modeling Turbulent Flow

They presented a mesh which was provided to accurate results at laminar flow conditions that may not be accepted for turbulent flow situations. As shown in the **Figure 3.3**, the turbulent boundary layer can be subdivided into several regions. Based on the region that needs to be resolved, the location of first cell adjacent to the wall is determined.

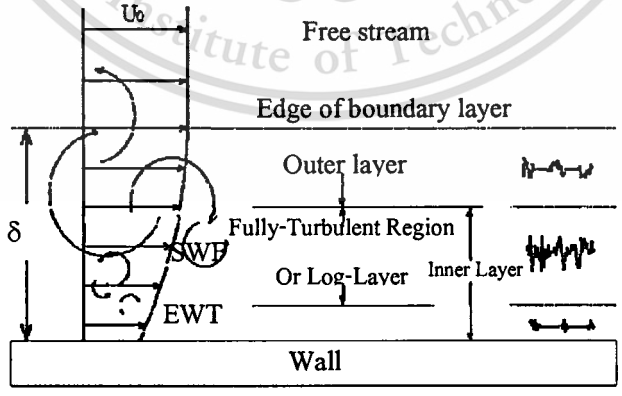

Figure 3.3 Modeling turbulent flows [8]

When flow characteristics in the viscous sub-layer need to be captured, Enhanced wall treatment should be used. Standard wall functions can be employed when the flow resolution starts from the log-layer region. Depending on the choice of near wall treatment, some constrains on the placement of the first cell from the wall are imposed, as presented in the **Table 3.1**.

Table 3.1 Mesh requirements of Turbulent Flows in Fluent.

Enhanced Wall Treatment (EWT)	Y^+ Can go up to $Y^+ \leq 5$ First cell in Laminar Sublayer	Low Re flows, better drag, pressure - drop prediction
Standard Wall Functions (SWF)	$Y^+ \geq$ 30 - 300 First cell in Log Layer	High Re flows, little gain by resolving sublayer
Non- Equilibrium Wall Functions	Limits same as SWF, Accounts for ∇p effects	For mildly separating, Reattaching flows

CHAPTER 4

NUMERICAL SIMULATION

4.1 Geometrical Parameter

The geometrical parameter for a plate-fin in this study is shown in **Table 4.1**. All samples in this analysis have the tube width (T_w) of 16 mm, depth (T_d) of 2 mm and fin thickness (F_t) of 0.05 mm. The length of the fins (F_l) in the airflow direction is 21.6 mm for single row and 41.6 mm associating with double-row tubes. Simulations were performed for different geometries with various fin pitches (F_p), louver pitches (L_p), tube pitches (T_p) and louver angle (α). Material properties parameter for a plate-fin in this study is shown in **Table 4.2**; all samples of the fin materials are made of copper and tube are made of brass.

Table 4.1 Dimension details of louver plate-fin geometry.

Number	F_p(mm)	L_p(mm)	α (deg)	T_p(mm)	n	d_h(mm)
1	2.02	1.4	25.5	11	2	3.43
2	3.25	1.4	25.5	11	2	5.16
3	1.65	1.4	25.5	11	2	2.86
4	2.09	1.4	21.5	11	2	3.54
5	2.03	1.4	28.5	11	2	3.45
6	2.15	1.4	25.5	11	1	3.65
7	1.70	1.4	25.5	11	1	2.97
8	2.11	0.81	29	11	2	3.57
9	1.72	0.81	29	11	2	2.97
10	3.33	0.81	29	11	2	5.27
11	2.18	1.1	30	11	2	3.67
12	2.16	0.81	20	11	2	3.64
13	2.16	1.1	28	8	2	3.41
14	2.17	1.1	22	14	2	3.79
15	2.17	1.1	22	8	2	3.43

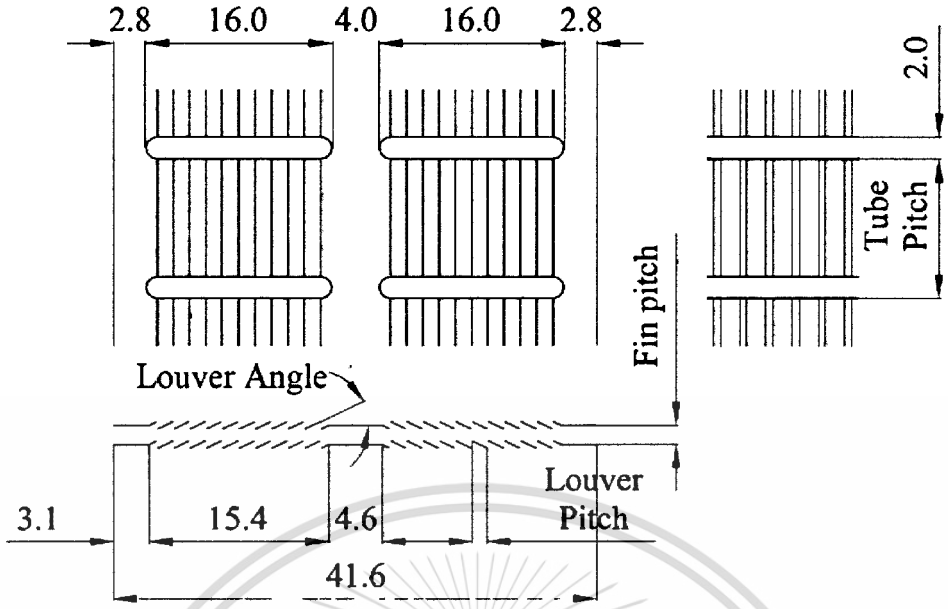

Figure 4.1 Geometrical parameter of the louvered plate fin geometry (mm)

Table 4.2 Material property

Property	Copper (Cu)
Density (ρ)	8930 (kg/m^3)
Specific Heat (C_p)	385 (J/kg.K)
Thermal Conductivity (k)	335 (W/m.K)

4.2 Computational domain and Boundary Conditions

The three-dimensional computational domain and boundary condition is shown in **Figure 4.2.** One-half of the tube pitch was considered with symmetry plane at one side and constant wall temperature at the other. The top and bottom surfaces of the domain are defined as periodic boundaries. Previous literature Malapure et al., [20] suggested that the 3D model was constructed with the smallest fluid cell size next to the wall being smaller than or equal to the fin's thickness. For simplicity of the computational mesh and modeling reason of heat transfer between solid and fluid interface, its thickness next to fin was assigned to be equal to the fin height with symmetrical geometry at upper and lower surface of the fin surface. The computation domain has contains boundary conditions as show in **Figure 4.2.**

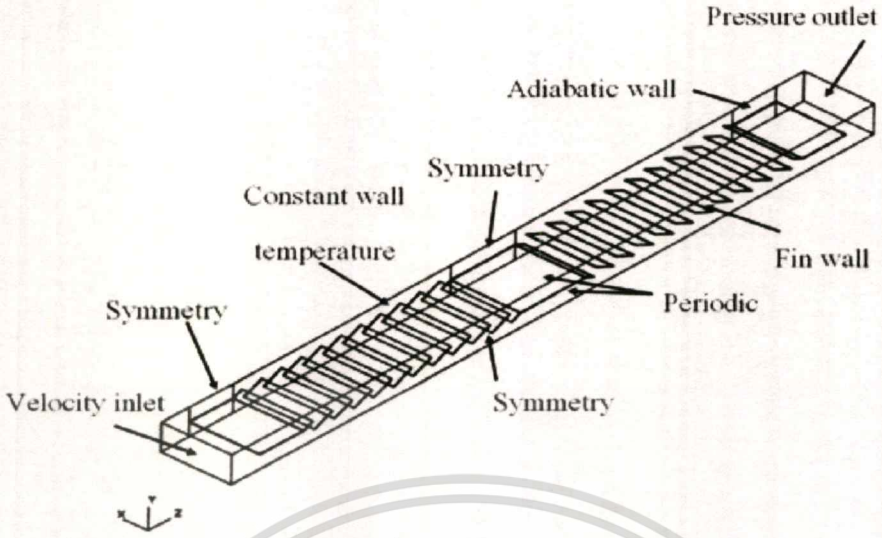

Figure 4.2 Three-dimensional computational domain and boundary condition

The numerical simulations are performed for different Reynolds number within the range from 100 to 4000. From experiment of T.A. Cowell and A. Achaichia [1988] the temperature variation of the tube surface is small, thus can be assumed constant at 358 K. The inlet air temperature of the louver fin is set at 288 K. All thermo-physical properties of the tube and fin surfaces are also assumed constant.

4.3 Computational Mesh

Three-dimensional geometrical models of air domain are constructed with the smallest cell size next to the wall being smaller than the fin's thickness as suggested by the previous worker, Conjugate heat transfer by Patanka[17]. The geometry, meshing and computational domain ware created using the Gambit 2.4 software. The Hexagonal mesh was used as mesh model; there was a range of meshes created for use in the grid independence study hexagonal meshes cell number ranged from approximately 100,000 to 2,300,000 cells. After the grid independence study the mesh of approximately 800,000 to 1,600,000 cells was chosen in this project.

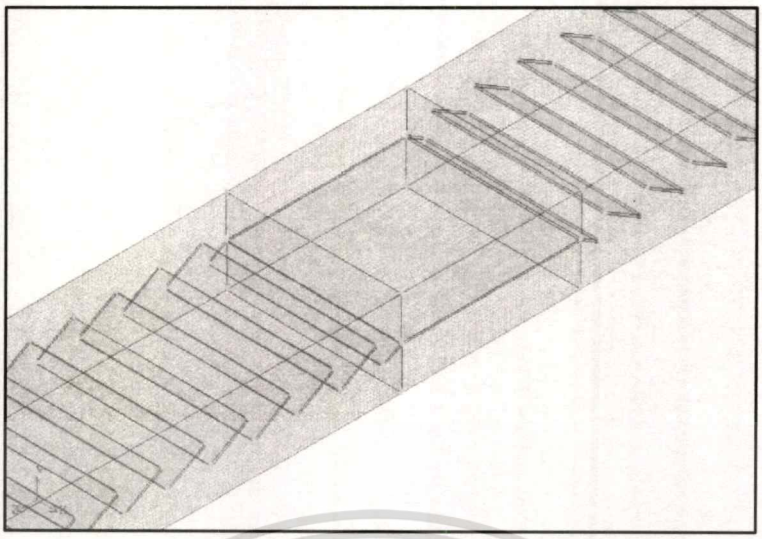

Figure 4.3 Three-dimensional meshes (Perspective view).

Figure 4.4 Three-dimensional meshes.

4.4 Numerical Technique

The numerical simulation model based on SIMLE algorithm were used steady-state solver for the numerical simulations. Flow diagram of this numerical algorithm was represented in **Figure 4.5**.

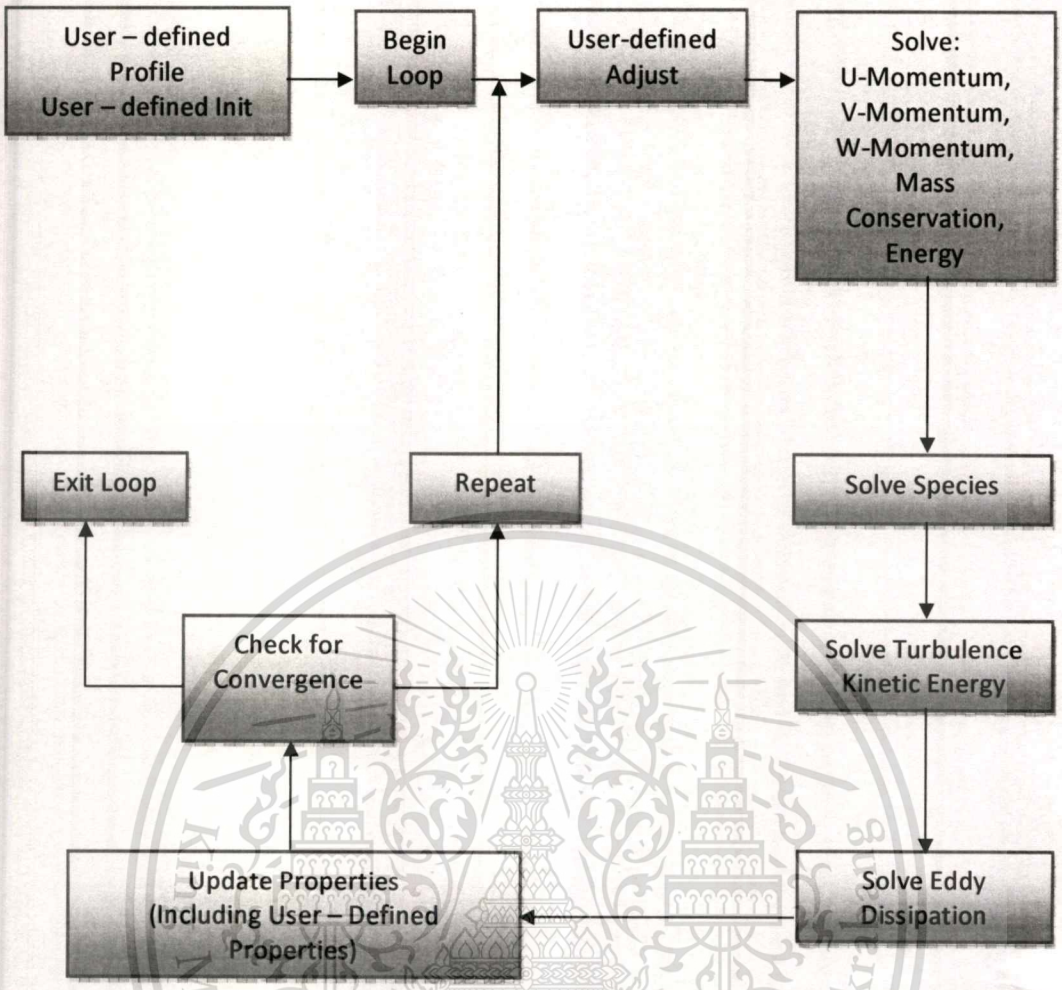

Figure 4.5 Computation Diagram.

A second-order upwind scheme was used for the space the discretizations of the momentum, turbulence kinetic energy, turbulence dissipation rate, and energy equations to set with second-order upwind. The under-relaxation factors for each iteration are, pressure = 0.3, momentum = 0.7, turbulence kinetic energy = 0.8, turbulence dissipation rate = 0.8 and energy = 1. The residuals were used the converged solution of the continuity, components of velocities, turbulent kinetic energy and turbulent dissipation rate are less than 10^{-5}, while for energy it is less than 10^{-7} for converged solution.

4.5 Empirical Value for Stanton Number and Friction Factor

Experimental value of Stanton Number (St) and Friction Factor (f) to validate the simulation result in this project was calculated from empirical equations (Equation 1.2, 1.3 and 1.5) , that mention were used to calculate compared with the simulation results determined results Achaichia and Cowell [1]. The values of Stanton Number and Friction Factor as read from the **Table 4.3-4.5.**

Table 4.3 Stanton Number (St_e) and friction factor (f_e) of empirical equations.

Re_d	Configuration number									
	1		2		3		4		5	
	St_e	f_e	St_e	f_e	St_e	f_e	St_e	f_e	St_e	f_e
400	0.054	0.262	0.062	0.346	0.051	0.234	0.053	0.253	0.055	0.272
600	0.044	0.187	0.051	0.235	0.041	0.171	0.043	0.180	0.044	0.194
800	0.037	0.151	0.044	0.184	0.035	0.140	0.037	0.145	0.038	0.157
1000	0.033	0.131	0.039	0.155	0.030	0.123	0.033	0.125	0.033	0.135
2000	0.022	0.091	0.026	0.099	0.020	0.089	0.022	0.087	0.022	0.094
3000	0.017	0.079	0.021	0.082	0.016	0.078	0.017	0.075	0.018	0.081
4000	0.015	0.073	0.018	0.074	0.014	0.074	0.015	0.069	0.015	0.076

Table 4.4 Stanton Number (St_e) and friction factor (f_e) of empirical equations. (Cont.)

Re_d	Configuration number									
	6		7		8		9		10	
	St_e	f_e	St_e	f_e	St_e	f_e	St_e	f_e	St_e	f_e
400	0.055	0.270	0.051	0.236	0.064	0.349	0.061	0.302	0.065	0.486
600	0.044	0.191	0.041	0.172	0.052	0.232	0.049	0.205	0.054	0.308
800	0.038	0.154	0.035	0.141	0.045	0.179	0.042	0.161	0.047	0.230
1000	0.033	0.133	0.031	0.123	0.040	0.149	0.037	0.135	0.042	0.186
2000	0.023	0.092	0.021	0.089	0.027	0.092	0.025	0.087	0.029	0.106
3000	0.018	0.079	0.016	0.078	0.021	0.074	0.020	0.071	0.023	0.082
4000	0.015	0.073	0.014	0.074	0.018	0.065	0.017	0.064	0.020	0.070

Table 4.5 Stanton Number (St_e) and friction factor (f_e) of empirical equations. (Cont.)

Re_d	Configuration number									
	11		12		13		14		15	
	St_e	f_e	St_e	f_e	St_e	f_e	St_e	f_e	St_e	f_e
400	0.061	0.314	0.056	0.316	0.059	0.263	0.056	0.315	0.056	0.245
600	0.049	0.216	0.047	0.210	0.048	0.183	0.046	0.215	0.046	0.170
800	0.042	0.170	0.041	0.161	0.041	0.145	0.040	0.170	0.039	0.135
1000	0.037	0.144	0.036	0.134	0.036	0.123	0.035	0.143	0.035	0.115
2000	0.025	0.094	0.025	0.082	0.024	0.082	0.024	0.093	0.024	0.076
3000	0.020	0.079	0.020	0.066	0.019	0.069	0.019	0.077	0.019	0.064
4000	0.017	0.071	0.017	0.058	0.016	0.063	0.016	0.070	0.016	0.058

During the comparisons, it was kept in the uncertainties of the Stanton Number values (St) (empirical determined values), the result can be uncertainty with in ± 10 % at Reynolds numbers Re_{Lp} > 75 and Friction Factor with in ± 10 % at Reynolds numbers Re_{Lp} 150 and 3000.

4.6 Computational Value for Stanton Number and Friction Factor

The computational values of Stanton Number (St) and Friction Factor (f) was compared with the validation in this research, the preciously simulation results to kept from Malapure et al., [20]. The values of the Reynolds Number and Stanton Number from preciously simulation were shown in **Table 4.6-4.8**.

Table 4.6 Stanton Number (St_m) and friction factor (f_m)

Re_d	Configuration number									
	1		2		3		4		5	
	St_m	f_m	St_m	f_m	St_m	f_m	St_m	f_m	St_m	f_m
400	0.066	0.222	0.073	0.228	0.058	0.220	0.067	0.205	0.068	0.231
600	0.049	0.169	0.057	0.178	0.043	0.167	0.051	0.161	0.051	0.176
800	0.041	0.141	0.048	0.153	0.036	0.137	0.042	0.133	0.042	0.148
1000	0.036	0.124	0.043	0.137	0.031	0.118	0.037	0.116	0.037	0.129
2000	0.025	0.093	0.029	0.095	0.020	0.081	0.023	0.078	0.024	0.092
3000	0.023	0.085	0.025	0.088	0.020	0.081	0.019	0.065	0.020	0.082
4000	0.019	0.073	0.024	0.083	0.014	0.082	0.020	0.066	0.018	0.074

Table 4.7 Stanton Number (St_m) and friction factor (f_m). (Cont.)

Re_d	Configuration number									
	6		7		8		9		10	
	St_m	f_m	St_m	f_m	St_m	f_m	St_m	f_m	St_m	f_m
400	0.068	0.290	0.062	0.206	0.085	0.277	0.084	0.280	0.049	0.176
600	0.052	0.210	0.046	0.155	0.065	0.220	0.062	0.210	0.062	0.193
800	0.043	0.180	0.037	0.126	0.055	0.180	0.052	0.180	0.051	0.180
1000	0.024	0.130	0.032	0.113	0.049	0.160	0.044	0.160	0.045	0.160
2000	0.024	0.087	0.019	0.077	0.032	0.119	0.029	0.110	0.031	0.120
3000	0.022	0.086	0.024	0.079	0.029	0.112	0.027	0.091	0.028	0.100
4000	0.019	0.078	0.020	0.068	0.024	0.097	0.021	0.080	0.023	0.100

Table 4.8 Stanton Number (St_m) and friction factor (f_m). (Cont.)

Re_d	Configuration number									
	11		12		13		14		15	
	St_m	f_m	St_m	f_m	St_m	f_m	St_m	f_m	St_m	f_m
400	0.078	0.264	0.066	0.198	0.071	0.230	0.074	0.233	0.070	0.208
600	0.060	0.200	0.055	0.179	0.055	0.180	0.060	0.189	0.055	0.165
800	0.050	0.170	0.049	0.160	0.046	0.153	0.050	0.159	0.045	0.141
1000	0.043	0.150	0.044	0.140	0.040	0.135	0.043	0.139	0.039	0.122
2000	0.028	0.107	0.031	0.100	0.035	0.110	0.027	0.098	0.025	0.083
3000	0.025	0.090	0.025	0.086	0.027	0.089	0.026	0.085	0.230	0.071
4000	0.020	0.087	0.021	0.076	0.022	0.076	0.079	0.079	0.210	0.067

The comparison was kept in the uncertainties of the Stanton Number values (St) (empirical determined values), It can be shown the uncertainty with in ± 10 % at Reynolds numbers $Re_{Lp} > 75$ and Friction Factor with in ± 10 % at Reynolds numbers Re_{Lp} 150 and 3000.

CHAPTER 5

RESULT AND DISCUSSION

5.1 Fin temperature Distribution

Figure 5.1 shows the result of static temperature contour on fin in configuration 9 at Reynolds number Re_d = 1000 and 4000, respectively. We can see temperature drop on louvers number 3, 4, 5 and 6 where the bulk of relatively colder air jet passes through them.

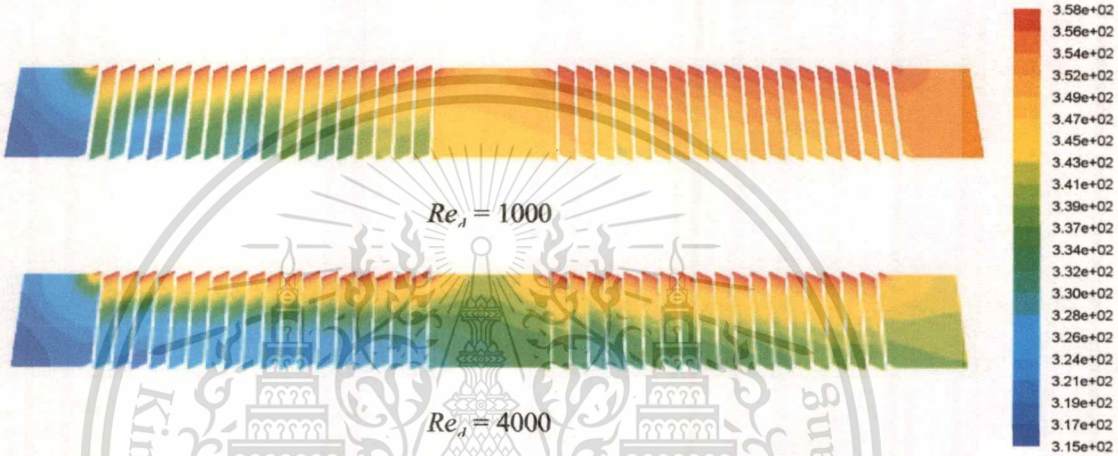

Figure 5.1 Static temperature (K) contour on louver fins of configuration 9 (Fp = 1.72 mm, Lp = 0.81 mm, α = 29°, T_p = 11 mm)

Recovery of temperature level can be seen further downstream in the louver number 7 as a result of less heat transfer with relatively warmer air jet coming from lower row of the fin. Vortex blocks to take place at fin number 1 and 2 where the bulk flow passes over and start to get into the lover channel from fin number 3 onwards.

5.2 Flow Aerodynamics

Figure 5.2 shows the results of velocity and temperature contours of two different Reynolds numbers; (a) and (b) at low Reynolds number (Re_d = 100), and for (c) and (d) at high Reynolds number (Re_d = 1000) on fins; Fp = 1.72 mm, Lp = 0.81 mm, α = 29°, T_p = 11 mm. For low Reynolds number, the boundary layers thickness around the lover is very thick as the air flows through the gap between the fins rather than flowing into the gap between the louvers. Generally speaking, the temperature difference between the fin surface and the air is not much. The result of heat transfer performance of the fin is poor.

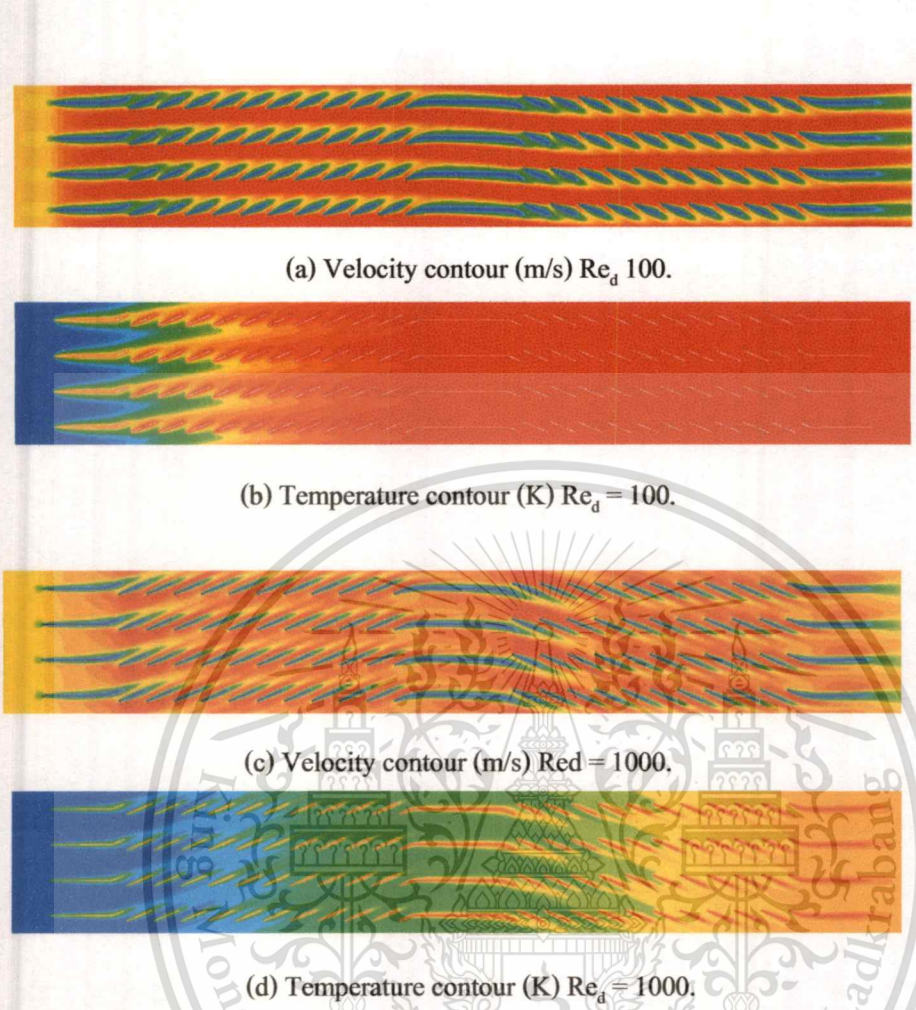

(a) Velocity contour (m/s) Re_d 100.

(b) Temperature contour (K) Re_d = 100.

(c) Velocity contour (m/s) Red = 1000.

(d) Temperature contour (K) Re_d = 1000.

Figure 5.2 Static temperature (K) and velocity contour on louver fins configuration 1.
(Fp = 2.02 mm, Lp = 1.4 mm, α = 25.5°, T_p = 11 mm)

For the high Reynolds numbers, the air flow was directed by the louvers. The boundary layer thickness around the louvers was very thin. In this case temperature of the air increases along the flow direction and a significant temperature difference was observed between air and fin. The result of the heat transfer is thus higher at high Reynolds number.

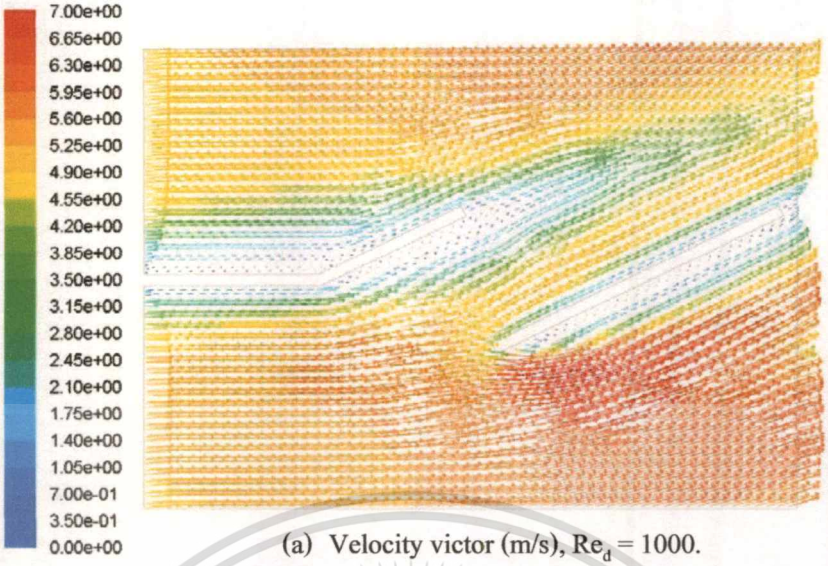

(a) Velocity victor (m/s), $Re_d = 1000$.

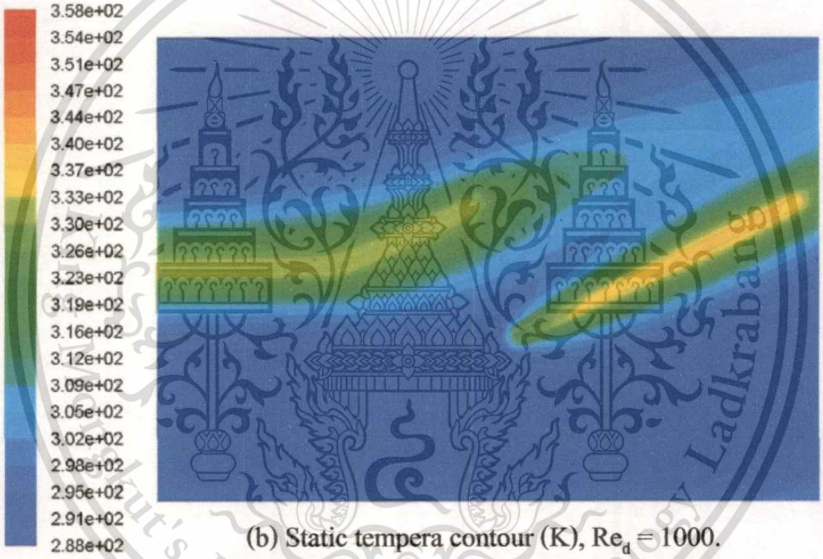

(b) Static tempera contour (K), $Re_d = 1000$.

Figure 5.3 Velocity vector and temperature contour (perspective view) on louver fin ($Fp = 2.02$ mm, $Lp = 1.4$ mm, $\alpha = 25.5°$, $T_p = 11$ mm)

Figure 5.3 shows the results of velocity vector and temperature contour on perspectives view between 1st and 2nd louvers fin, the vortexes block the air flow after transition region of the first louver. **Figure 5.3 (a),** In the this cause the boundary layers thickness at the bottom surface of lover was very thick and can't reduce the temperature **Figure 5.3 (b)**, the heat transfer performance was poor.

5.3 Comparison between Correlation and Computation

Heat transfer and friction loss of plate-fin radiator are expressed in terms of Stanton number (*St*) and friction factor (*f*). **Figures 5.3** to **5.17** show the result from this study compared with empirical results of Stanton number and friction factor as functions of Reynolds number from configuration number 1 to 15. Some cases suggest good prediction in **Figure 5.3, 5.5, 5.6, 5.8,** some cases the simulation underestimates the heat transfer rate, such as in **Figure 5.10, 5.11, 5.15, 5.16.** This may be attributed to k-Ɛ model.

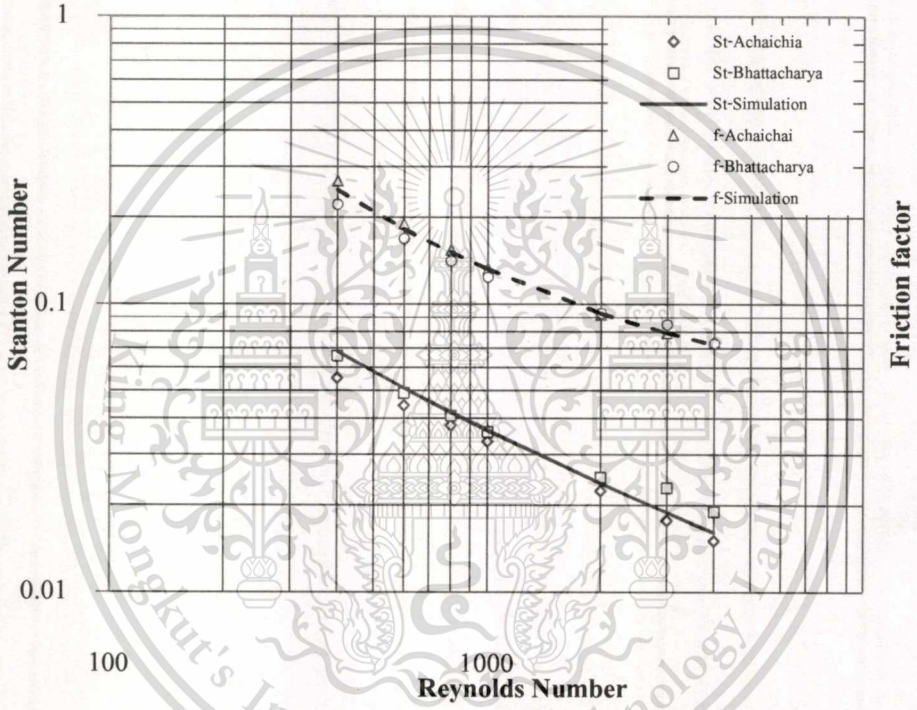

Figure 5.4 Stanton number and Friction factor of configuration number 1.

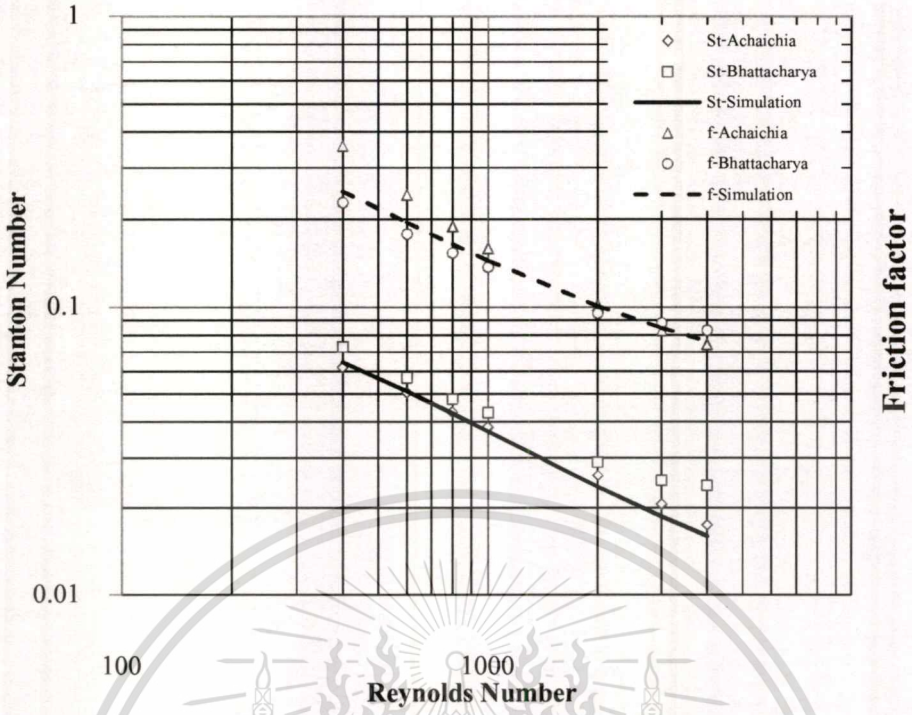

Figure 5.5 Stanton number and Friction factor of configuration number 2.

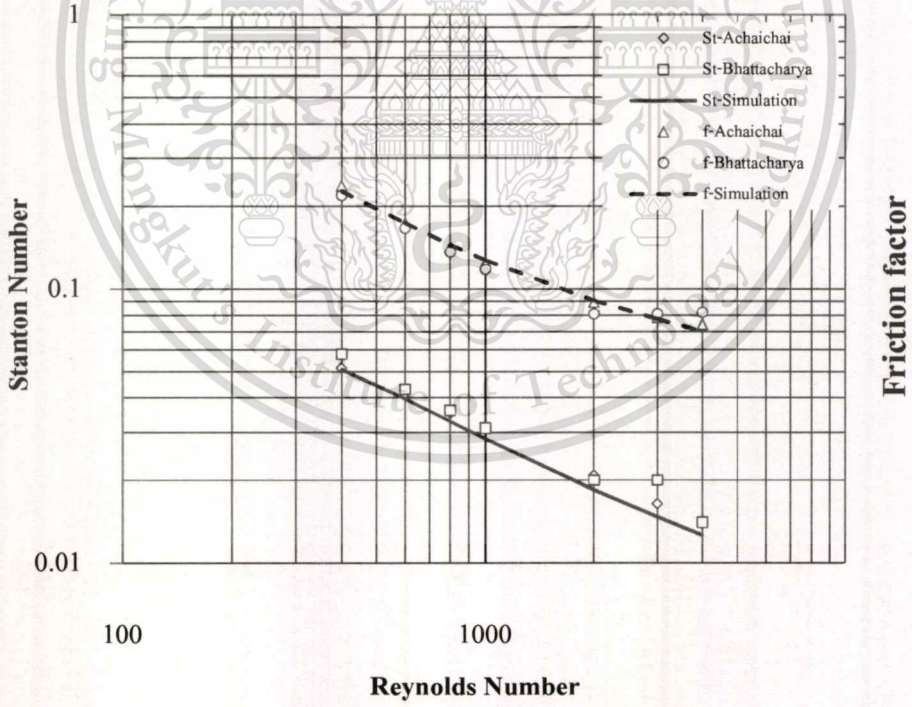

Figure 5.6 Stanton number and Friction factor of configuration number 3.

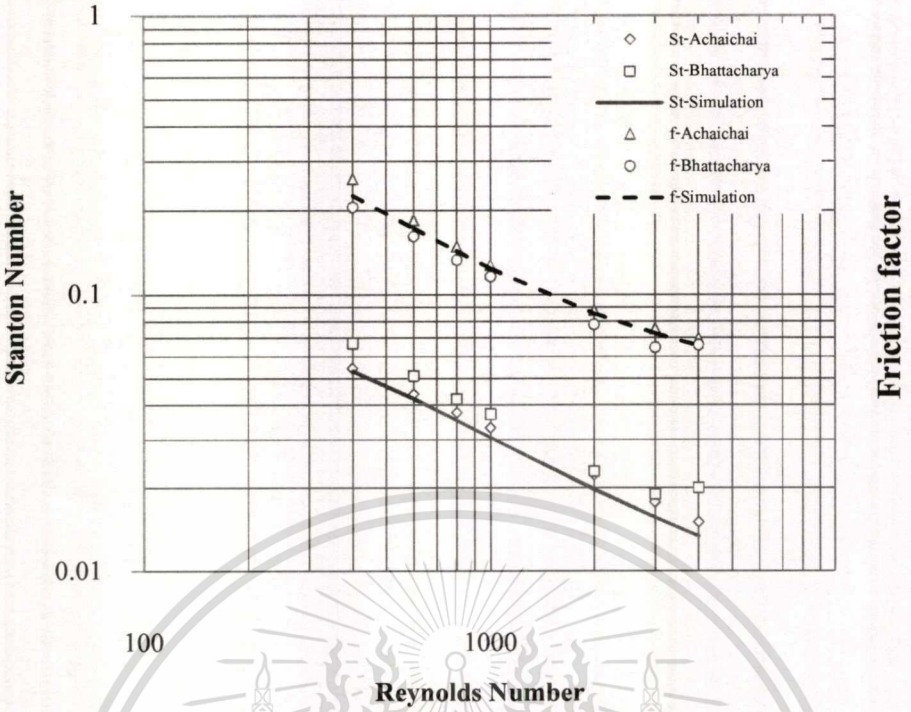

Figure 5.7 Number and Friction factor of configuration number 4.

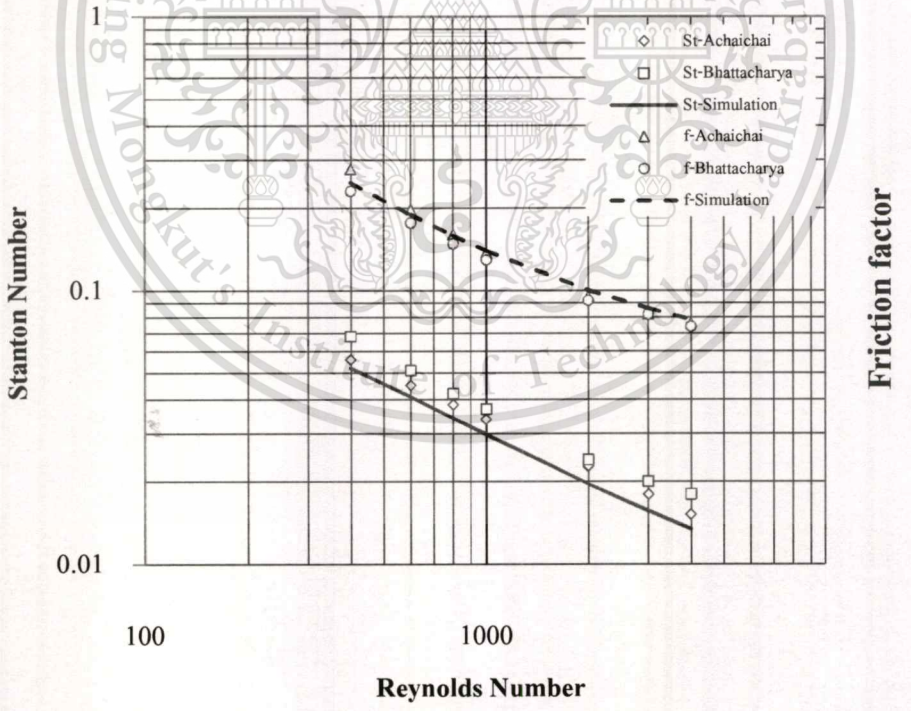

Figure 5.8 Stanton number and Friction factor of configuration number 5.

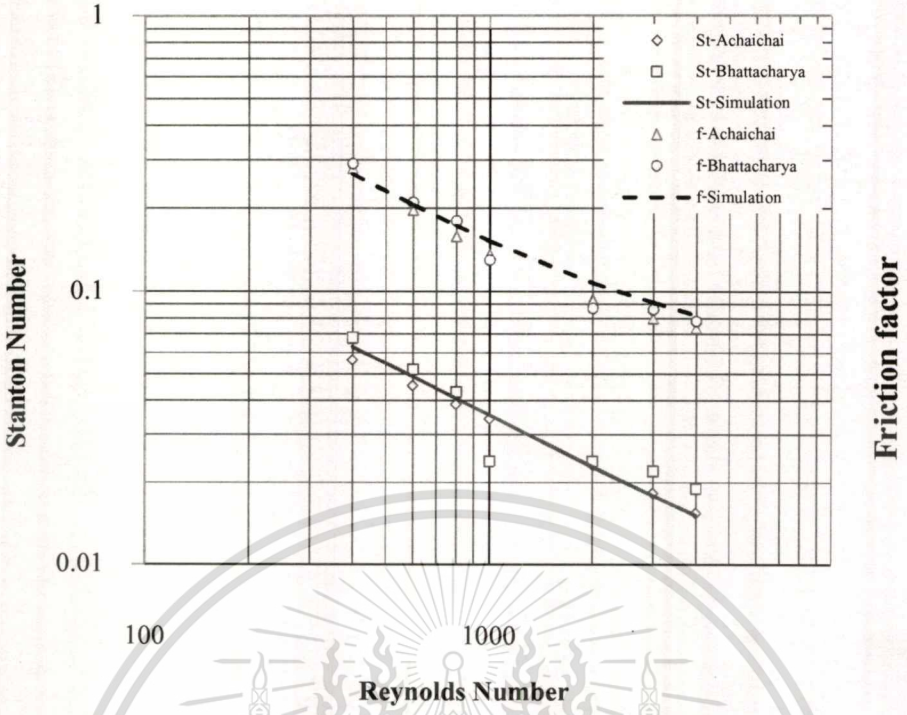

Figure 5.9 Stanton number and Friction factor of configuration number 6.

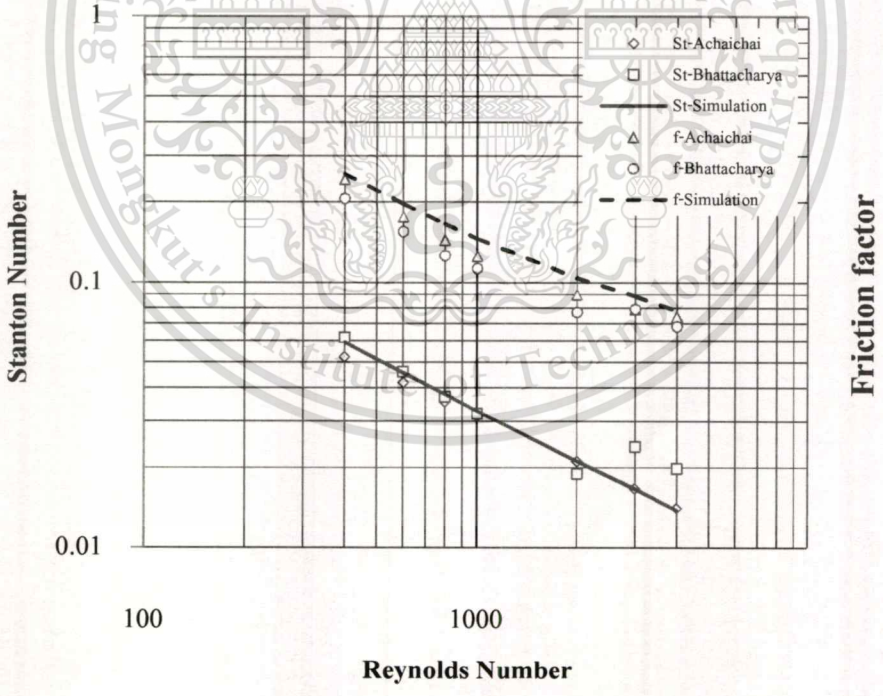

Figure 5.10 Number and Friction factor of configuration number 7.

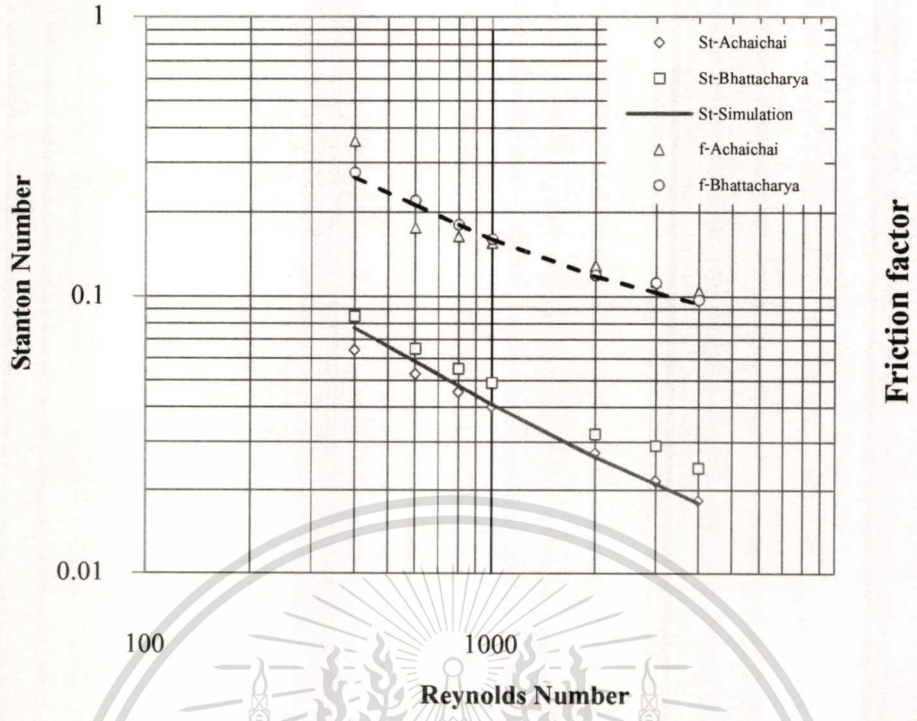

Figure 5.11 Number and Friction factor of configuration number 8.

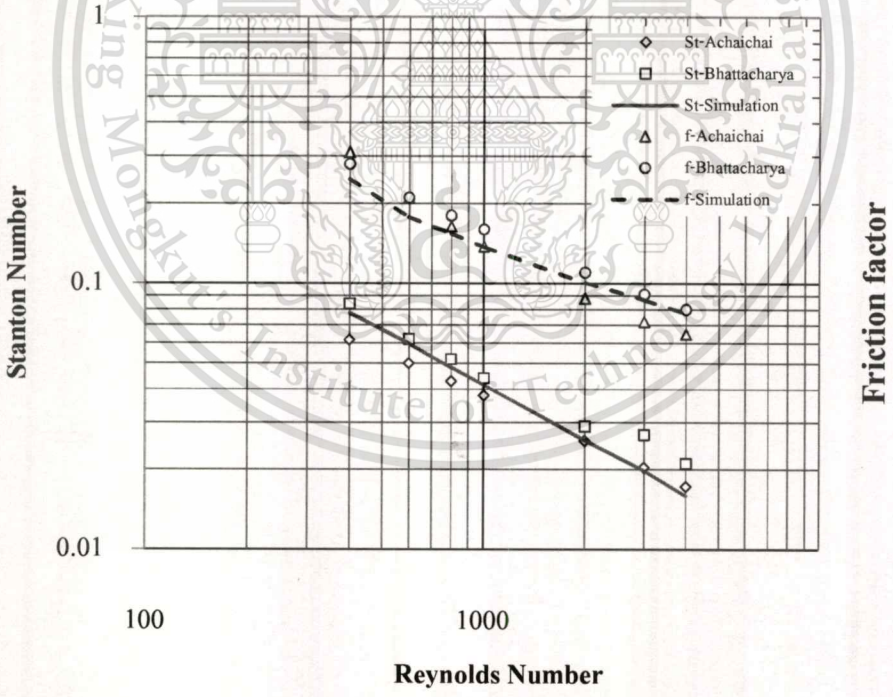

Figure 5.12 Number and Friction factor of configuration number 9.

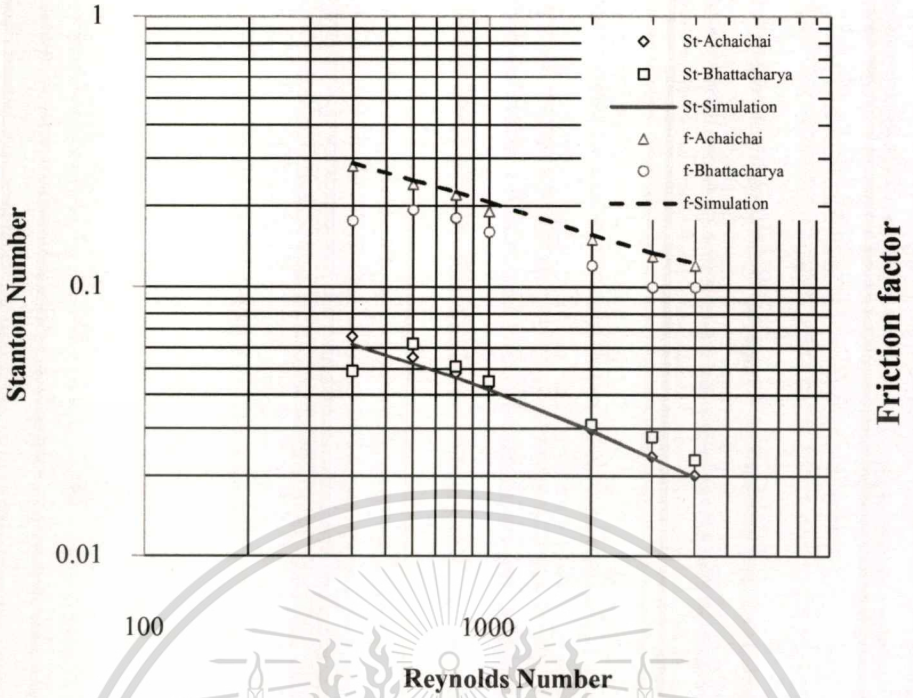

Figure 5.13 Number and Friction factor of configuration number 10.

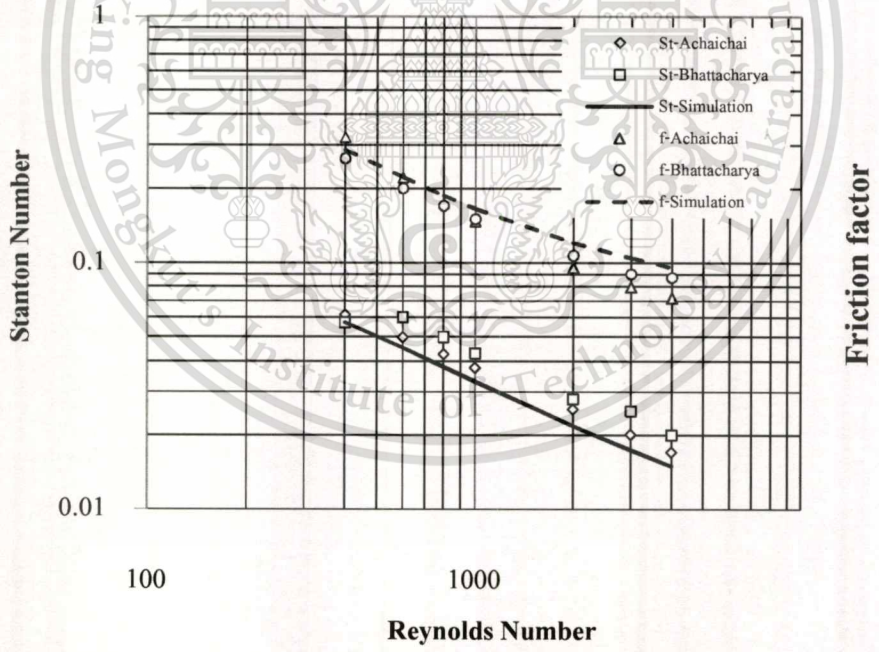

Figure 5.14 Number and Friction factor of configuration number 11.

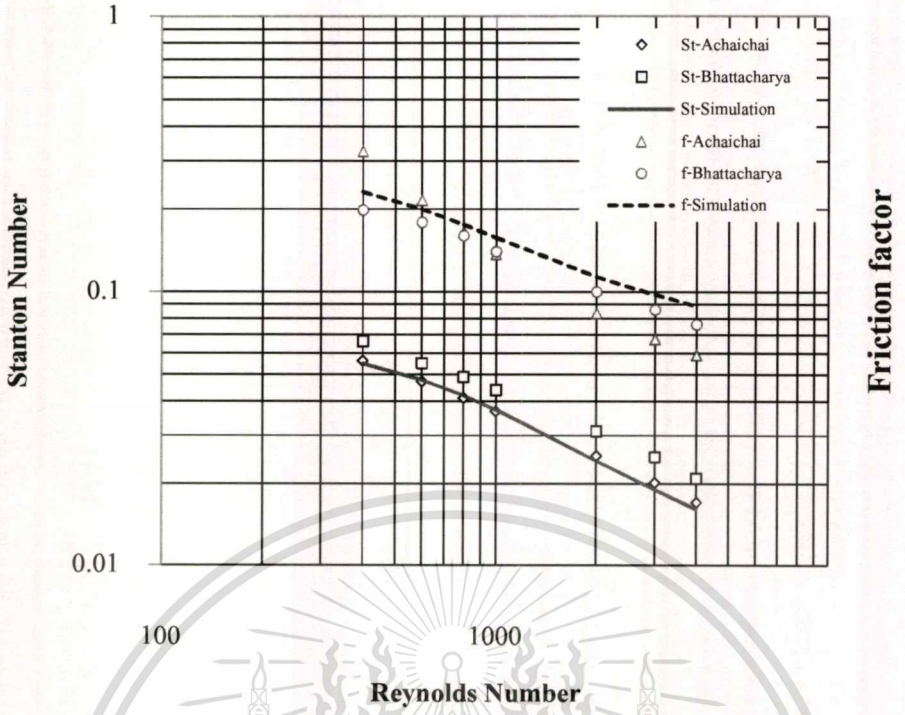

Figure 5.15 Number and Friction factor of configuration number 12.

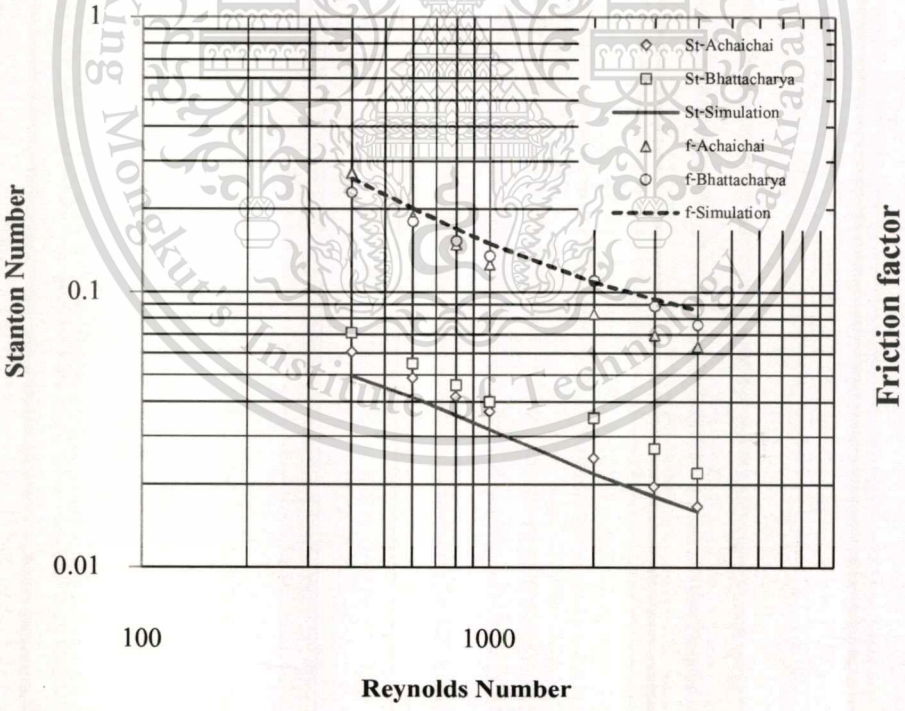

Figure 5.16 Number and Friction factor of configuration number 13.

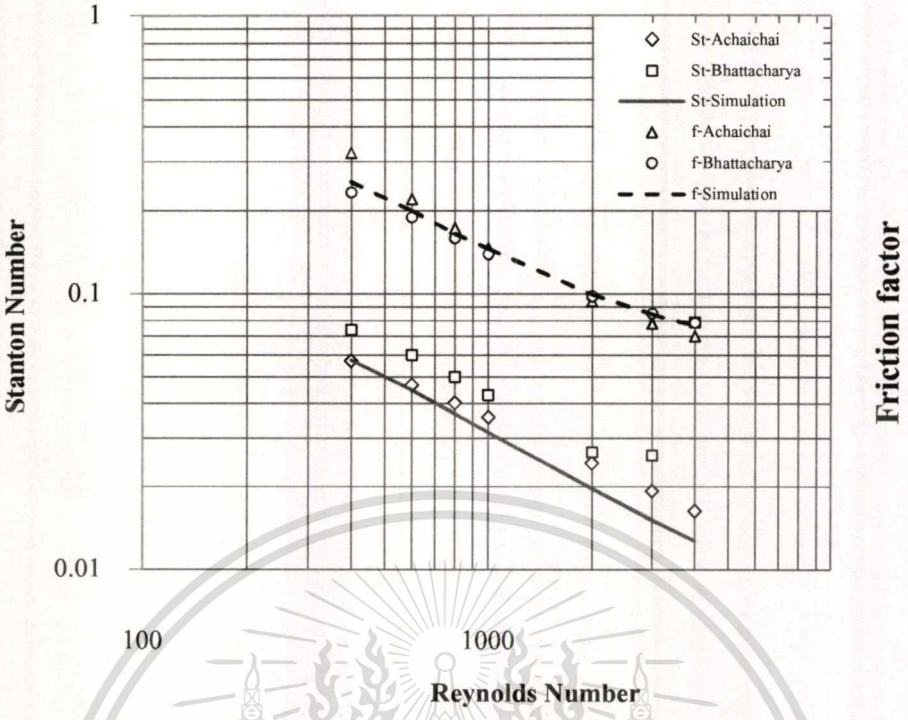

Figure 5.17 Number and Friction factor of configuration number 14.

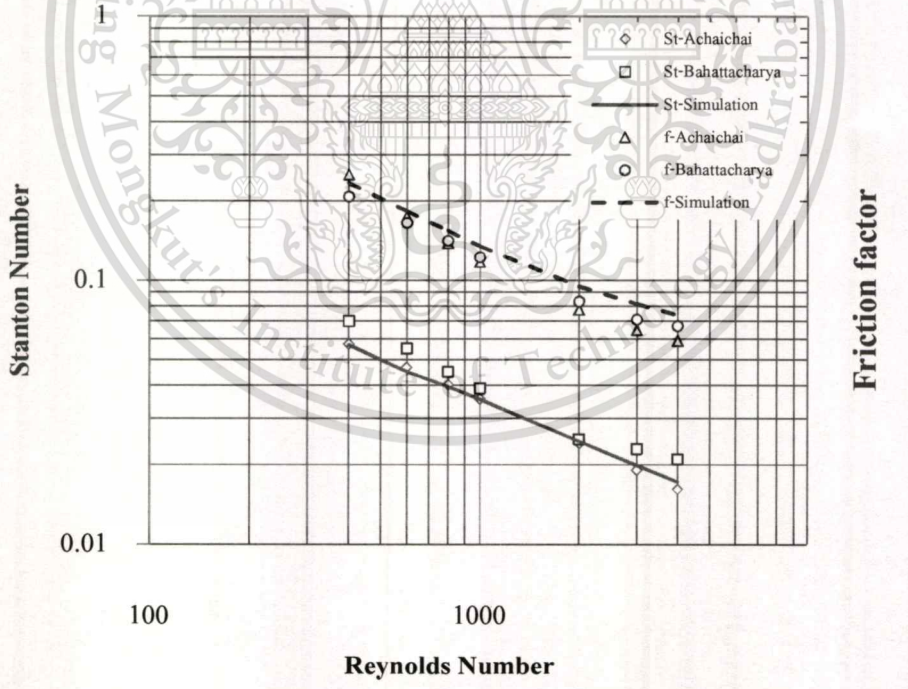

Figure 5.18 Number and Friction factor of configuration number 15.

Table 5.1 report the comparison between empirical and simulation of Stanton number. (St_e = Stanton nuber experimental, St_m = Stanton number by V.P. Malapure, St_s = Stanton number obtain from simulation)

Re_d	Configuration number											
	1			2			3			4		
	St_e	St_m	St_s	St_e	St_m	St_s	St_e	St_m	St_s	St_e	St_m	St_s
400	0.054	0.066	0.054	0.062	0.073	0.062	0.051	0.058	0.050	0.053	0.067	0.052
600	0.044	0.049	0.043	0.051	0.057	0.050	0.041	0.043	0.039	0.043	0.051	0.041
800	0.037	0.041	0.036	0.044	0.048	0.041	0.035	0.036	0.032	0.037	0.042	0.034
1000	0.033	0.036	0.032	0.039	0.043	0.036	0.030	0.031	0.028	0.033	0.037	0.030
2000	0.022	0.025	0.021	0.026	0.029	0.023	0.020	0.020	0.018	0.022	0.023	0.019
3000	0.017	0.023	0.016	0.021	0.025	0.018	0.016	0.020	0.014	0.017	0.019	0.015
4000	0.015	0.019	0.014	0.018	0.024	0.015	0.014	0.014	0.012	0.015	0.020	0.013

Table 5.2 Comparison between empirical and simulation of Stanton number. (Cont.)

Red	Configuration number											
	5			6			7			8		
	St_e	St_m	St_s	St_e	St_m	St_s	St_e	St_m	St_s	St_e	St_m	St_s
400	0.055	0.068	0.051	0.055	0.068	0.061	0.051	0.062	0.057	0.064	0.085	0.060
600	0.044	0.051	0.040	0.044	0.052	0.047	0.041	0.046	0.044	0.052	0.065	0.049
800	0.038	0.042	0.033	0.038	0.043	0.039	0.035	0.037	0.037	0.045	0.055	0.041
1000	0.033	0.037	0.029	0.033	0.024	0.034	0.031	0.032	0.032	0.040	0.049	0.036
2000	0.022	0.024	0.019	0.023	0.024	0.022	0.021	0.019	0.020	0.027	0.032	0.023
3000	0.018	0.020	0.015	0.018	0.022	0.017	0.016	0.024	0.016	0.021	0.029	0.018
4000	0.015	0.018	0.013	0.015	0.019	0.015	0.014	0.020	0.013	0.018	0.024	0.016

Table 5.3 Comparison between empirical and simulation of Stanton number. (Cont.)

Red	Configuration number											
	9			10			11			12		
	St_e	St_m	St_s	St_e	St_m	St_s	St_e	St_m	St_s	St_e	St_m	St_s
400	0.061	0.084	0.076	0.065	0.049	0.056	0.061	0.078	0.056	0.056	0.066	0.058
600	0.049	0.062	0.058	0.054	0.062	0.051	0.049	0.060	0.044	0.047	0.055	0.047
800	0.042	0.052	0.047	0.047	0.051	0.045	0.042	0.050	0.037	0.041	0.049	0.041
1000	0.037	0.044	0.040	0.042	0.045	0.041	0.037	0.043	0.032	0.036	0.044	0.036
2000	0.025	0.029	0.025	0.029	0.031	0.029	0.025	0.028	0.021	0.025	0.031	0.024
3000	0.020	0.027	0.019	0.023	0.028	0.023	0.020	0.025	0.017	0.020	0.025	0.019
4000	0.017	0.021	0.015	0.020	0.023	0.019	0.017	0.020	0.015	0.017	0.021	0.016

Table 5.4 Comparison between empirical and simulation of Stanton number. (Cont.)

Red	Configuration number								
	13			14			15		
	St_e	St_m	St_s	St_e	St_m	St_s	St_e	St_m	St_s
400	0.059	0.071	0.048	0.056	0.074	0.056	0.056	0.070	0.056
600	0.048	0.055	0.040	0.046	0.060	0.044	0.046	0.055	0.045
800	0.041	0.046	0.035	0.040	0.050	0.036	0.039	0.045	0.038
1000	0.036	0.040	0.031	0.035	0.043	0.031	0.035	0.039	0.034
2000	0.024	0.035	0.021	0.024	0.027	0.019	0.024	0.025	0.024
3000	0.019	0.027	0.018	0.019	0.026	0.015	0.019	0.230	0.019
4000	0.016	0.022	0.015	0.016	0.079	0.012	0.016	0.210	0.017

Table 5.5 Comparison between experimental and simulation of Fiction factor. (f_e = Fiction factor experimental, f_m = Fiction factor by V.P. Malapure, f_s = Fiction factor obtain from simulation)

Red	Configuration number											
	1			2			3			4		
	f_e	f_m	f_s	f_e	f_m	f_s	f_e	f_m	f_s	f_e	f_m	f_s
400	0.262	0.222	0.212	0.346	0.228	0.224	0.234	0.220	0.185	0.253	0.205	0.183
600	0.187	0.169	0.148	0.235	0.178	0.177	0.171	0.167	0.143	0.180	0.161	0.141
800	0.151	0.141	0.124	0.184	0.153	0.150	0.140	0.137	0.120	0.145	0.133	0.118
1000	0.131	0.124	0.109	0.155	0.137	0.133	0.123	0.118	0.106	0.125	0.116	0.103
2000	0.091	0.093	0.078	0.099	0.095	0.095	0.089	0.081	0.077	0.087	0.078	0.072
3000	0.079	0.085	0.068	0.082	0.088	0.081	0.078	0.081	0.067	0.075	0.065	0.062
4000	0.073	0.073	0.062	0.074	0.083	0.073	0.074	0.082	0.061	0.069	0.066	0.057

Table 5.6 Comparison between experimental and simulation of Fiction factor. (Cont.)

Red	Configuration number											
	5			6			7			8		
	f_e	f_m	f_s	f_e	f_m	f_s	f_e	f_m	f_s	f_e	f_m	f_s
400	0.272	0.231	0.201	0.270	0.290	0.213	0.236	0.206	0.204	0.349	0.277	0.250
600	0.194	0.176	0.155	0.191	0.210	0.167	0.172	0.155	0.160	0.232	0.220	0.200
800	0.157	0.148	0.131	0.154	0.180	0.142	0.141	0.126	0.136	0.179	0.180	0.171
1000	0.135	0.129	0.116	0.133	0.130	0.126	0.123	0.113	0.120	0.149	0.160	0.153
2000	0.094	0.092	0.085	0.092	0.087	0.090	0.089	0.077	0.088	0.092	0.119	0.115
3000	0.081	0.082	0.074	0.079	0.086	0.078	0.078	0.079	0.076	0.074	0.112	0.102
4000	0.076	0.074	0.068	0.073	0.078	0.070	0.074	0.068	0.067	0.065	0.097	0.094

Table 5.7 Comparison between experimental and simulation of Fiction factor. (Cont.)

Red	Configuration number											
	9			10			11			12		
	f_e	f_m	f_s	f_e	f_m	f_s	f_e	f_m	f_s	f_e	f_m	f_s
400	0.302	0.280	0.282	0.486	0.176	0.215	0.314	0.264	0.232	0.316	0.198	0.187
600	0.205	0.210	0.228	0.308	0.193	0.201	0.216	0.200	0.181	0.210	0.179	0.163
800	0.161	0.180	0.196	0.230	0.180	0.183	0.170	0.170	0.153	0.161	0.160	0.144
1000	0.135	0.160	0.176	0.186	0.160	0.169	0.144	0.150	0.137	0.134	0.140	0.130
2000	0.087	0.110	0.131	0.106	0.120	0.130	0.094	0.107	0.102	0.082	0.100	0.097
3000	0.071	0.091	0.112	0.082	0.100	0.113	0.079	0.090	0.089	0.066	0.086	0.083
4000	0.064	0.080	0.099	0.070	0.100	0.104	0.071	0.087	0.082	0.058	0.076	0.076

Table 5.8 Comparison between experimental and simulation of Fiction factor. (Cont.)

Red	Configuration number								
	13			14			15		
	f_e	f_m	f_s	f_e	f_m	f_s	f_e	f_m	f_s
400	0.263	0.230	0.207	0.315	0.233	0.207	0.245	0.208	0.187
600	0.183	0.180	0.162	0.215	0.189	0.164	0.170	0.165	0.147
800	0.145	0.153	0.137	0.170	0.159	0.137	0.135	0.141	0.124
1000	0.123	0.135	0.122	0.143	0.139	0.122	0.115	0.122	0.109
2000	0.082	0.110	0.090	0.093	0.098	0.085	0.076	0.083	0.078
3000	0.069	0.089	0.079	0.077	0.085	0.073	0.064	0.071	0.068
4000	0.063	0.076	0.073	0.070	0.079	0.067	0.058	0.067	0.062

Figure 5.19 and **Figure 5.20** shows a comparison of empirical and simulation result of Stanton number of each 105 data. The predictive quality of the selected all models are well in general with 87.62% of the test data being correlated with in ±15% compared with the empirical data of Stanton number (**Figure 5.19**) correlation had a mean deviation of 8.98% and average deviation was -0.13%, according to **Equation (5.1)**, [11].

$$\text{Average deviation} = \frac{1}{N}\left(\sum \frac{\phi_{pred} - \phi_{emp}}{\phi_{emp}}\right) \times 100\%,$$

$$\text{Mean deviation} = \frac{1}{N}\left(\sum \frac{\left|\phi_{pred} - \phi_{emp}\right|}{\phi_{emp}}\right) \times 100\%, \quad (5.1)$$

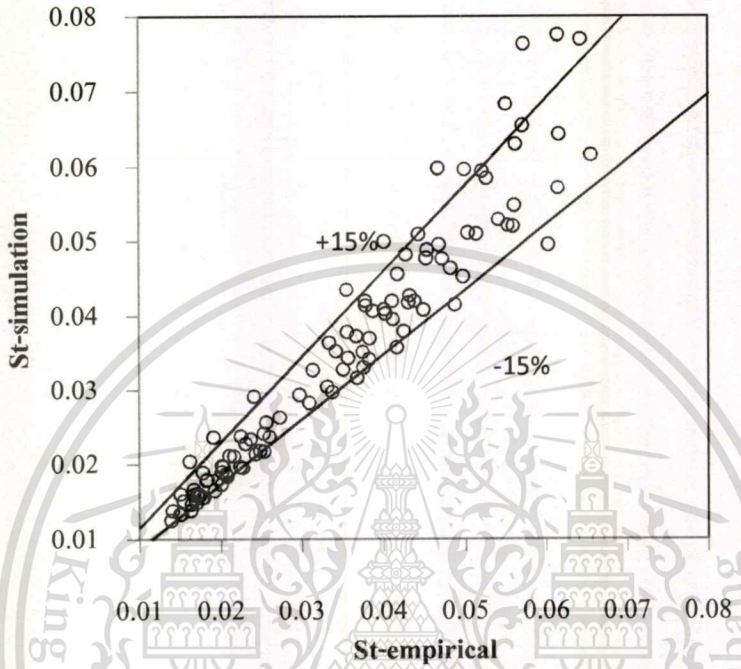

Figure 5.19 Comparisons of empirical and simulation of Stanton number

Figure 5.20 shows a comparison of empirical and simulation result of Friction factor with 86.67% of the test data being correlated with in ±15%, compared with the empirical data of Friction factor correlation had a mean deviation of 10.43% and average deviation was 3.42%, according to **Equation (5.1)**.

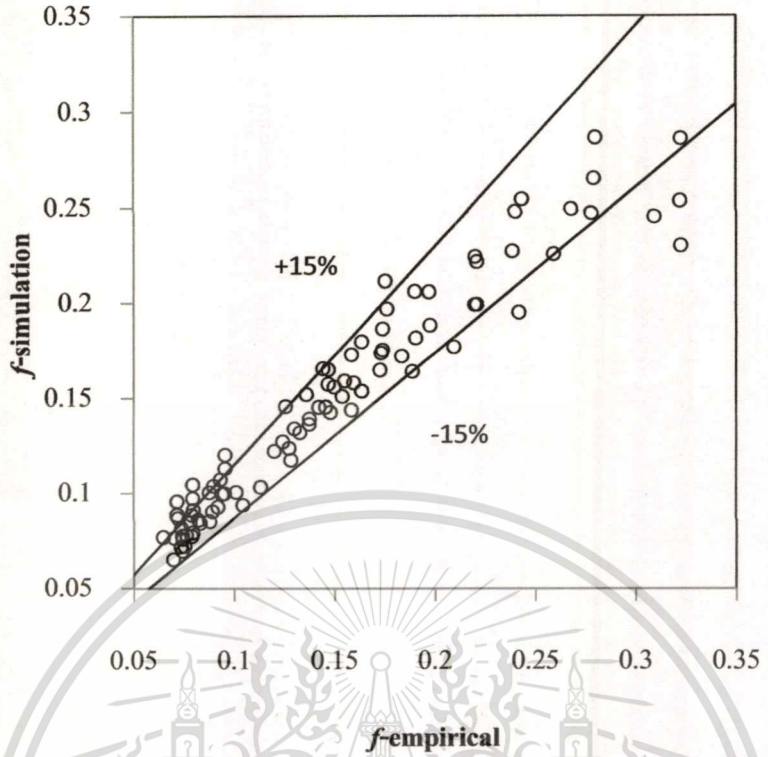

Figure 5.20 Comparisons of computation and correlation of Fiction factor

5.4 3D Local Nusselt number

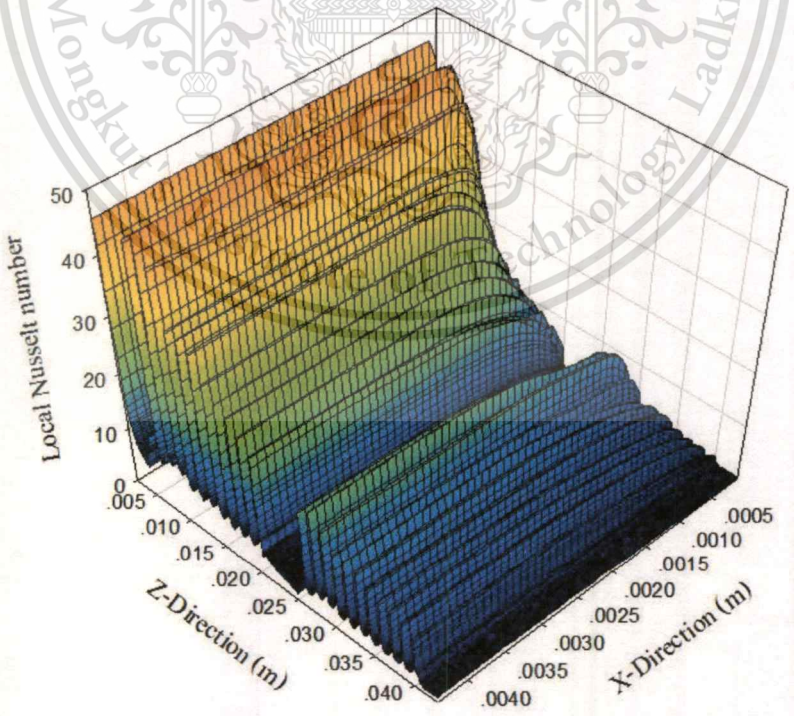

Figure 5.21 3D Local Nusselt number on the top surface

The 3D local Nusselt number (*Nu*) on the top surface of each louver in the flow direction was calculated and plotted along the length of fin for Reynolds number *Red* = 1000 as shown in **Figure 5.21**. It was observed that a high Nusselt number was obtained at the tip of the fin and after that falls rapidly over each louver before increasing slightly at the end of each louver. The Nusselt number was also high at the first half of fin and gradually decrease. Because the temperature of the air saturation, it was impossible to transfer heat from the fins into the air. Therefore the heat transfer at the second half of the fin was less than the half first of the fin.

5.5 Heat Transfer and Pressure Drop Characteristics

From this research we can see the tendency as follow; **Figures 5.22** and **5.23** shows the effects of fin length (21.6 and 41.6 mm) and fin pitch (1.70 and 2.15 mm) of single row and (1.65and 2.02 mm) double row tube on the performance of the louvered plate fin, in which the louvered pitch of 1.4 mm, tube pitch 11 mm, louver angle of 25.5°. From the figure, the heat transfer coefficient (**Figure 5.22**) were not more different at the same Reynolds number in while the pressure drop increase (**Figure 5.23**) with decreasing fin pitch and increasing fin length as a result of flow channel decreasing and fin surface area increasing. In the this cause the fiction loss of louvered fin was increase.

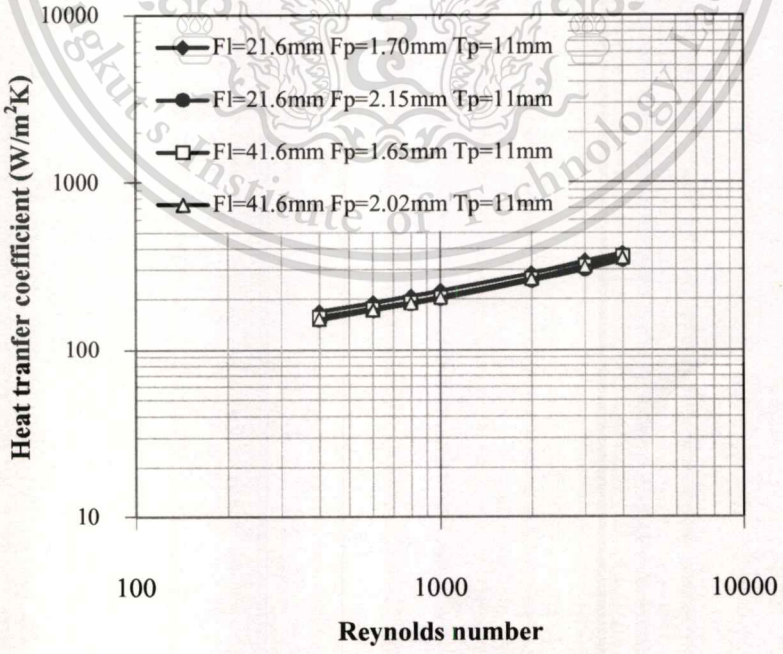

Figure 5.22 Effect of fin lengths (F_l) and fin pitch (F_p) on heat transfer coefficient

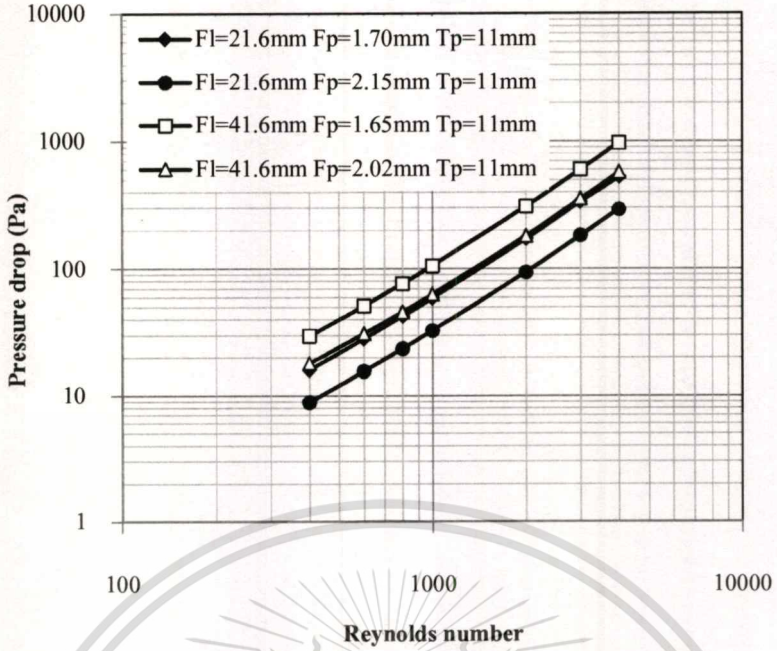

Figure 5.23 Effect of fin lengths (F_l) and fin pitch (F_p) on pressure drop

Figures 5.24 and **5.25** show the effects of tube pitch (8.0, 11 and 14 mm) on the performance of the louvered plate fin, in which the louvered pitch of 1.1 mm, louver angle of 22°, fin pitch 2.17 mm and fin length 41.6 mm of double row tube. Considering at the same Reynolds number, the heat transfer coefficient (**Figure 5.24**) increase with decreasing tube pitch but pressure drop was not more difference because the reduced flow has little effect on pressure drop in the channel.

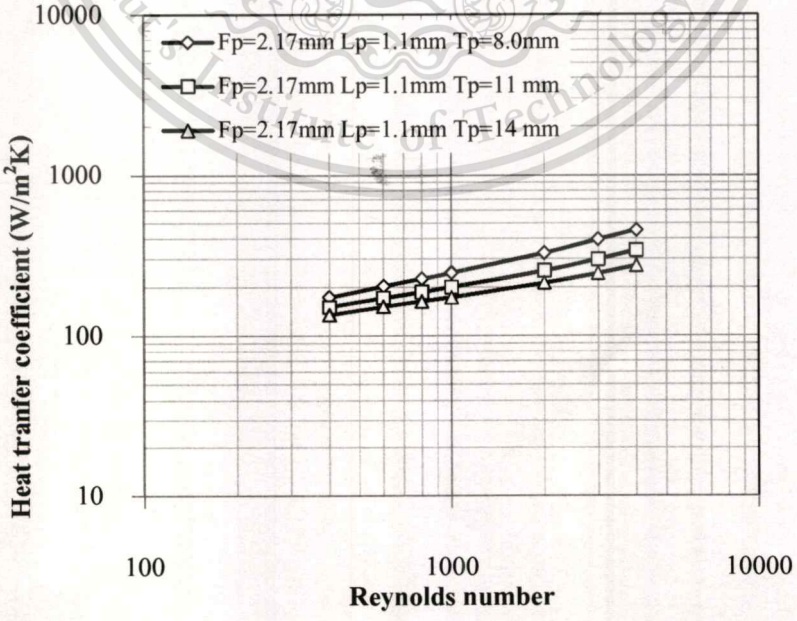

Figure 5.24 Effect of tube pitch (T_p) on heat transfer coefficient

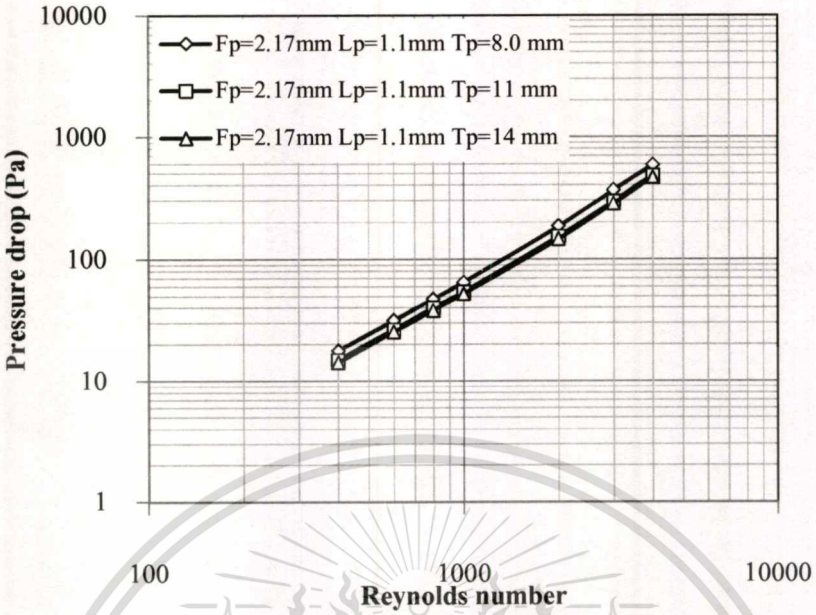

Figure 5.25 Effect of tube pitch (T_p) on pressure drop

The result of heat transfer coefficients and pressure drop were significant for design heat exchanger. In this study, this work was found that the heat transfer characteristic of louvered plate fin was besides related to flow aerodynamic and the distribution of pressure and temperature, it also depends on the heat transfer area of louvered plate fin as well. The result of heat transfer rate was increased or decreased as a function of fin length and tube pitch (longitudinal length and width) of louvered plate fin.

CHAPTER 6

CONCLUSION

6.1 Conclusion

The effects of geometric parameters have been investigated by considering heat transfer and friction loss of louver plate fins in terms of Stanton number and friction factor using 15 difference of louvered plate-fin, similar to Malapure et al. [20]. The study was performed within the range of Reynolds number from 100 to 4000. The comparison study with empirical equation of Achaichia and Cowell [1] was made to evaluate the predictive quality of the technique within the specified range of operating conditions and geometries. The best agreement was observed as far as Stanton number was concerned but the relatively larger deviation was found for friction factors. The predictive quality of the selected model was good in general with the deviation in heat transfer between ±15% where 8.98% of data was with out of this range. As far as friction factor was concerned, the deviation was +15% to -15% with 10.43 % of data with out of this range. The heat transfer characteristic of louvered plate fin was discussed in relation with flow aerodynamic and the distribution of pressure and temperature. The heat transfer coefficient and pressure drop increase with decreasing in fin pitch. The research was progressed to investigate the underlying mechanism of flow aerodynamic on heat transfer and pressure drop as they were very important to design characteristics of radiators and heat exchangers.

REFERENCES

[1] A. Achaichia, T.A. Cowell, **"Heat Transfer and Pressure Drop Characteristics of Flat Tube and Louver Plate Fin Surfaces,"** Experimental Thermal and Fluid Science, pp. 147-157, 1988.

[2] A.A. Antoniou, M.R. Heikal, T.A. Cowell, **"Measurements of Local Velocity and Turbulence Levels in Arrays of Louvered Plate Fins,"** Proceedings of the Ninth International Heat Transfer Conference, Jerusalem, pp. 105-110, 1990.

[3] A.C. Lyman **"Spatially Resolved Heat Transfer Studies in Louvered Fins for Compact Heat Exchangers,"** Master of Science Thesis, Mechanical Engineering, Virginia Polytechnic Institute and State University, Blacksburg, Virginia, 2000.

[4] A.M. Hansen, **"CFD Simulation of a Fin-and-Tube Heat Exchanger,"** Master of Science Thesis, Computational Chemical Engineering, Aalborg University, Denmark 2008.

[5] C.J. Davenport, **"Correlations for heat transfer and flow friction characteristics of louvered fin Heat Transfer,"** Seattle 1983, AICHE Symp, Vol. 79, No. 225, pp. 19-27, 1983.

[6] C.T. Hsieh, J.Y. Jang, **"3D Thermal-Hydraulic Analysis for Louver Fin Heat Exchangers with Variable Louver Angle,"** Applied Thermal Engineering, Vol. 26, pp. 1629-1639, 2006.

[7] D.K. Tafti and X. Zhang, **"Geometry Effects on Flow Transition in Multi Louvered Fins Onset, Propagation, and Characteristic Frequencies,"** International Journal of Heat Mass Transfer, Vol. 44, No.22, pp. 4195-4210, 2001.

[8] FLUENT, **User's Guide**, Release 6.3, Fluent Inc., Lebanon, New Hampshire.

[10] J. Cui, D.K. Tafti, **"Computations of flow and heat transfer in a three dimensional multi louvered fin geometry"**, International Journal of Heat Mass Transfer, Vol. 45, pp. 5007-5023, 2002.

[11] J. Dong, J. Chen, Z. Chen, W. Zhang, Y. Zhou, **"Heat Transfer and Pressure Drop Correlation for the Mulit-Louvered Fin Compact Heat Exchangers,"** Energy Conversion and Management, No.48, pp. 1506-1515. 2007.

REFERENCES (CONT.)

[12] J.P. Rugh, J. T. Pearson and S. Ramadhyani, **"A Study of a Very Compact Heat Exchanger Used for Passenger Compartment Heating in Automobiles,"** in Compact Heat Exchangers for Power and Process Industries, ASME Symp. Ser., HTD, Vol. 201, pp. 15-24, 1992.

[13] J.S. Leu, M.S. Liu, J.S. Liaw, C.C Wang, **"A Numerical Investigation of Louvered Fin-and-Tube Heat Exchangers Having Circular and Oval Tube Configurations,"** International Journal of Heat Mass Transfer, Vol. 44, pp. 4235-4243, 2001.

[14] R. L. Webb, **Principle of Enhanced Heat Transfer,** John Wiley & Son, 1993.

[15] R.K. Shah, D.P. Sekulic, **"Fundamentals of Heat Exchanger Design,"** John Wiley & Sons, Inc., Hoboken, New Jersey, 2003.

[16] R.L. Webb and S. H. Jung, **"Air-side performance of enhanced brazed aluminum heat exchangers,"** ASHRAE Trans. Vol. 98, pp. 391-401, 1992.

[17] S.V. Patankar, **"Numerical Heat Transfer and Fluid Flow,"** Hemisphere McGraw-Hill, Washington DC, pp. 41-77, 1998.

[18] T. Perrotin, D. Clodic, **"Thermal-hydraulic CFD study in louvered fin-andflat-tube heat exchangers,"** International Journal of Refrigeration, Vol. 27, pp. 422-432, 2004.

[19] T.A. Cowell, M.R. Heikal and A.A chaichia, **"Flow and Heat transfer in Compact Louvered Fin Surfaces,"** Experimental Thermal and Fluid Science, No.10, pp. 192-199, 1995.

[20] V.P. Malapure, Sushanta K. Mitra , A. Bhattacharya, **"Numerical Investigation of Fluid Flow and Heat Transfer Over Louvered Fins in Compact Heat Exchanger,"** International Journal of Thermal Sciences, No. 46, pp. 199-211, 2007.

[21] W.M. Kays, A.L. London, **Compact Heat Exchangers,** third ed., McGraw-Hill, New York, 1984.

[22] X. Zhang, D.K. Tafti, **"Flow Efficiency in Multi-Louvered Fins,"** International Journal of Heat Mass Transfer, Vol. 46, pp. 1737-1750, 2003.

[23] X. Zhang X, D.K. Tafti, **"Classification and Effects of Thermal Wakes on Heat Transfer in Multi Louvered Fins,"** International Journal of Heat Mass Transfer, Vol. 44, pp. 2461-2473, 2001.

REFERENCES (CONT.)

[24] Y.J. Chang, C.C. Wang, **"A generalized heat transfer correlation for louvered fin geometry"** International Journal of Heat Mass Transfer, Vol. 40, No. 3, pp. 533–544, 1997.

APPENDIX

A: Stanton Number and Friction Factor

A-1: Result of literature values from experiments

Stanton Number and friction factor determined from empirical equation of Achaichia and Cowell (1988) are used to calculate compared with the simulation results, the Stanton Number using Equation1.2 as follows:

$$St = 1.554\frac{\left(0.936 - \frac{243}{\mathrm{Re}_{L_p}} - 1.76\frac{F_p}{L_p} + 0.995\theta\right)}{\theta} \times \mathrm{Re}_{L_p}^{-0.59}\left(\frac{T_p}{L_p}\right)^{-0.09}\left(\frac{F_p}{L_p}\right)^{-0.04}$$

Friction factor can be calculated Equation1.3 as follows:

$$f_e = 0.895 f_A^{1.07} F_p^{-0.22} L_p^{0.25} T_p^{0.26} H^{0.33}$$

where Louver height is $H = L_p \sin\theta$, the value of f_A can be calculated from Equation 1.4 the as follow:

$$f_A = 596\mathrm{Re}_{L_p}^{(0.3181\log \mathrm{Re}_{L_p} - 2.25)}$$

Reynolds number on louver pitch can be defined from Equation 2.27 as follow:

$$\mathrm{Re}_{L_p} = \frac{\rho U L_p}{\mu}$$

The geometrical parameter for a plate-fin in this study is shown in Table 4.1. All samples in this analysis have the tube width 16 mm, depth 2 mm and fin thickness is 0.05mm. The length of the fins in the airflow direction is 41.6 mm associating with double-row tubes. All samples the fin materials are made of copper and tube are made of brass. In this Table as presented the calculation result of Stanton Number and friction factor determined from empirical equation of Achaichia and Cowell [1988], fifteen configurations.

Table A1.1 Stanton Number (St_e) and friction factor (f_e) of empirical equations.

Configuration number 1										
Re_d	Re_{Lp}	U [m/s]	$T_{a,o}$ [K]	T_{avg} [°C]	ρ [kg/m^3]	C_p [J/kg.K]	μ [N.s/m^2]	f_A	St_e	f_e
400	163	2.12	355	322	1.0610	1006	1.932E-05	0.226	0.055	0.268
600	245	3.15	352	320	1.0682	1006	1.924E-05	0.164	0.044	0.190
800	326	4.15	349	318	1.0751	1006	1.917E-05	0.135	0.038	0.154
1000	408	5.15	346	317	1.0813	1006	1.911E-05	0.117	0.033	0.133
2000	815	9.97	336	312	1.1035	1006	1.888E-05	0.083	0.022	0.092
3000	1223	14.67	330	309	1.1167	1005	1.875E-05	0.072	0.018	0.079
4000	1631	19.30	326	307	1.1260	1005	1.866E-05	0.067	0.015	0.074

Table A1.2 Stanton Number (St_e) and friction factor (f_e) of empirical equations (Continued)

Configuration number 2										
Re_d	Re_{Lp}	U [m/s]	$T_{a,o}$ [K]	T_{avg} [°C]	ρ [kg/m^3]	C_p [J/kg.K]	μ [N.s/m^2]	f_A	St_e	f_e
400	108	1.38	349	319	1.0744	1006	1.918E-05	0.326	0.062	0.357
600	163	2.04	345	316	1.0846	1006	1.907E-05	0.226	0.050	0.242
800	217	2.69	340	314	1.0937	1006	1.898E-05	0.180	0.043	0.189
1000	271	3.32	337	312	1.1017	1006	1.890E-05	0.153	0.038	0.159
2000	542	6.41	325	307	1.1270	1005	1.865E-05	0.100	0.026	0.101
3000	813	9.44	320	304	1.1402	1005	1.852E-05	0.083	0.021	0.083
4000	1084	12.44	316	302	1.1485	1005	1.844E-05	0.075	0.017	0.074

Table A1.3 Stanton Number (St_e) and friction factor (f_e) of empirical equations (Continued)

Configuration number 3										
Re_d	Re_{Lp}	U [m/s]	$T_{a,o}$ [K]	T_{avg} [°C]	ρ [kg/m^3]	C_p [J/kg.K]	μ [N.s/m^2]	f_A	St_e	f_e
400	196	2.54	354	321	1.0632	1006	1.929E-05	0.194	0.051	0.239
600	294	3.77	351	320	1.0705	1006	1.922E-05	0.144	0.041	0.173
800	392	4.97	348	318	1.0778	1006	1.914E-05	0.120	0.035	0.142
1000	490	6.15	345	316	1.0845	1006	1.907E-05	0.106	0.031	0.124
2000	980	11.90	334	311	1.1077	1005	1.884E-05	0.078	0.021	0.089
3000	1470	17.53	328	308	1.1207	1005	1.871E-05	0.069	0.016	0.079
4000	1959	23.07	324	306	1.1297	1005	1.862E-05	0.065	0.014	0.074

Table A1.4 Stanton Number (St_e) and friction factor (f_e) of empirical equations (Continued)

Configuration number 4										
Re_d	Re_{L_p}	U [m/s]	$T_{a,o}$ [K]	T_{avg} [°C]	ρ [kg/m^3]	C_p [J/kg.K]	μ [N.s/m^2]	f_A	St_e	f_e
400	158	2.04	352	320	1.0680	1006	1.924E-05	0.232	0.054	0.259
600	237	3.02	348	318	1.0764	1006	1.916E-05	0.168	0.044	0.184
800	316	3.98	345	316	1.0844	1006	1.908E-05	0.137	0.037	0.148
1000	395	4.92	341	315	1.0916	1006	1.900E-05	0.119	0.033	0.127
2000	791	9.50	330	309	1.1161	1005	1.876E-05	0.084	0.022	0.088
3000	1186	13.97	324	306	1.1295	1005	1.863E-05	0.073	0.018	0.075
4000	1582	18.41	321	304	1.1381	1005	1.854E-05	0.068	0.015	0.070

Table A1.5 Stanton Number (St_e) and friction factor (f_e) of empirical equations (Continued)

Configuration number 5										
Re_d	Re_{L_p}	U [m/s]	$T_{a,o}$ [K]	T_{avg} [°C]	ρ [kg/m^3]	C_p [J/kg.K]	μ [N.s/m^2]	f_A	St_e	f_e
400	162	2.09	352	320	1.0677	1006	1.925E-05	0.227	0.056	0.278
600	244	3.10	348	318	1.0765	1006	1.916E-05	0.165	0.045	0.197
800	325	4.08	345	316	1.0845	1006	1.907E-05	0.135	0.038	0.160
1000	406	5.05	341	315	1.0915	1006	1.900E-05	0.117	0.034	0.138
2000	812	9.76	331	309	1.1151	1005	1.877E-05	0.083	0.023	0.095
3000	1218	14.37	325	307	1.1279	1005	1.864E-05	0.072	0.018	0.082
4000	1624	18.94	321	305	1.1364	1005	1.856E-05	0.068	0.015	0.076

Table A1.6 Stanton Number (St_e) and friction factor (f_e) of empirical equations (Continued)

Configuration number 6										
Re_d	Re_{L_p}	U [m/s]	$T_{a,o}$ [K]	T_{avg} [°C]	ρ [kg/m^3]	C_p [J/kg.K]	μ [N.s/m^2]	f_A	St_e	f_e
400	153	1.91	342	315	1.0895	1006	1.902E-05	0.238	0.056	0.279
600	230	2.81	336	312	1.1033	1006	1.888E-05	0.172	0.045	0.197
800	307	3.70	331	310	1.1139	1005	1.878E-05	0.140	0.039	0.158
1000	384	4.57	328	308	1.1221	1005	1.870E-05	0.121	0.034	0.136
2000	767	8.83	317	303	1.1460	1005	1.847E-05	0.085	0.023	0.093
3000	1151	13.04	312	300	1.1576	1005	1.835E-05	0.074	0.018	0.080
4000	1535	17.21	309	299	1.1648	1005	1.829E-05	0.068	0.015	0.074

Table A1.7 Stanton Number (St_e) and friction factor (f_e) of empirical equations (Continued)

Configuration number 7										
Re_d	Re_{Lp}	U [m/s]	$T_{a,o}$ [K]	T_{avg} [°C]	ρ [kg/m^3]	C_p [J/kg.K]	μ [N.s/m^2]	f_A	St_e	f_e
400	190	2.39	346	317	1.0819	1006	1.910E-05	0.199	0.052	0.243
600	285	3.52	340	314	1.0953	1006	1.896E-05	0.147	0.042	0.176
800	380	4.63	335	311	1.1058	1005	1.886E-05	0.122	0.036	0.144
1000	475	5.71	331	310	1.1141	1005	1.878E-05	0.107	0.031	0.126
2000	949	11.04	320	304	1.1387	1005	1.854E-05	0.079	0.021	0.090
3000	1424	16.28	315	302	1.1510	1005	1.842E-05	0.070	0.017	0.079
4000	1899	21.44	311	300	1.1596	1005	1.833E-05	0.066	0.014	0.074

Table A1.8 Stanton Number (St_e) and friction factor (f_e) of empirical equations (Continued)

Configuration number 8										
Re_d	Re_{Lp}	U [m/s]	$T_{a,o}$ [K]	T_{avg} [°C]	ρ [kg/m^3]	C_p [J/kg.K]	μ [N.s/m^2]	f_A	St_e	f_e
400	91	2.04	356	322	1.0597	1006	1.933E-05	0.388	0.064	0.359
600	136	3.04	353	321	1.0653	1006	1.927E-05	0.199	0.053	0.175
800	182	4.02	350	319	1.0717	1006	1.921E-05	0.186	0.045	0.164
1000	227	4.97	348	318	1.0779	1006	1.914E-05	0.177	0.040	0.155
2000	454	9.64	338	313	1.0999	1006	1.892E-05	0.149	0.027	0.128
3000	681	14.19	332	310	1.1127	1005	1.879E-05	0.132	0.022	0.113
4000	908	18.67	328	308	1.1219	1005	1.870E-05	0.123	0.018	0.104

Table A1.9 Stanton Number (St_e) and friction factor (f_e) of empirical equations (Continued)

Configuration number 9										
Re_d	Re_{Lp}	U [m/s]	$T_{a,o}$ [K]	T_{avg} [°C]	ρ [kg/m^3]	C_p [J/kg.K]	μ [N.s/m^2]	f_A	St_e	f_e
400	109	2.46	356	322	1.0597	1006	1.933E-05	0.324	0.061	0.309
600	164	3.67	355	321	1.0629	1006	1.930E-05	0.225	0.050	0.209
800	218	4.85	352	320	1.0681	1006	1.924E-05	0.179	0.043	0.164
1000	273	6.02	350	319	1.0736	1006	1.919E-05	0.152	0.038	0.137
2000	546	11.73	341	315	1.0913	1006	1.901E-05	0.100	0.026	0.088
3000	818	17.19	334	311	1.1074	1005	1.884E-05	0.083	0.020	0.072
4000	1091	22.58	329	309	1.1180	1005	1.874E-05	0.075	0.017	0.065

Table A1.10 Stanton Number (St_e) and friction factor (f_e) of empirical equations (Continued)

Configuration number 10										
Re_d	Re_{Lp}	U [m/s]	$T_{a,o}$ [K]	T_{avg} [°C]	ρ [kg/m^3]	C_p [J/kg.K]	μ [N.s/m^2]	f_A	St_e	f_e
400	62	1.35	348	318	1.0770	1006	1.915E-05	0.586	0.066	0.504
600	92	2.00	345	316	1.0846	1006	1.907E-05	0.382	0.055	0.319
800	123	2.65	342	315	1.0904	1006	1.901E-05	0.290	0.048	0.237
1000	154	3.28	339	314	1.0960	1006	1.896E-05	0.237	0.043	0.192
2000	308	6.38	330	309	1.1160	1005	1.876E-05	0.140	0.030	0.109
3000	461	9.40	325	306	1.1290	1005	1.863E-05	0.109	0.024	0.083
4000	615	12.37	321	304	1.1382	1005	1.854E-05	0.094	0.020	0.071

Table A1.11 Stanton Number (St_e) and friction factor (f_e) of empirical equations (Continued)

Configuration number 11										
Re_d	Re_{Lp}	U [m/s]	$T_{a,o}$ [K]	T_{avg} [°C]	ρ [kg/m^3]	C_p [J/kg.K]	μ [N.s/m^2]	f_A	St_e	f_e
400	120	1.96	353	320	1.0668	1006	1.926E-05	0.297	0.061	0.323
600	180	2.91	349	319	1.0748	1006	1.917E-05	0.208	0.050	0.221
800	239	3.84	345	317	1.0826	1006	1.909E-05	0.167	0.042	0.174
1000	299	4.75	342	315	1.0893	1006	1.903E-05	0.142	0.038	0.147
2000	599	9.19	332	310	1.1125	1005	1.879E-05	0.095	0.025	0.096
3000	898	13.54	326	307	1.1256	1005	1.866E-05	0.080	0.020	0.079
4000	1197	17.84	322	305	1.1340	1005	1.858E-05	0.073	0.017	0.072

Table A1.12 Stanton Number (St_e) and friction factor (f_e) of empirical equations (Continued)

Configuration number 12										
Re_d	Re_{Lp}	U [m/s]	$T_{a,o}$ [K]	T_{avg} [°C]	ρ [kg/m^3]	C_p [J/kg.K]	μ [N.s/m^2]	f_A	St_e	f_e
400	89	1.98	352	320	1.0678	1006	1.925E-05	0.396	0.056	0.325
600	133	2.95	350	319	1.0725	1006	1.920E-05	0.269	0.047	0.215
800	178	3.90	348	318	1.0776	1006	1.915E-05	0.210	0.041	0.165
1000	222	4.84	345	317	1.0830	1006	1.909E-05	0.176	0.037	0.137
2000	444	9.36	335	311	1.1060	1005	1.886E-05	0.111	0.025	0.084
3000	667	13.76	329	308	1.1199	1005	1.872E-05	0.091	0.020	0.067
4000	889	18.10	324	306	1.1292	1005	1.863E-05	0.080	0.017	0.059

Table A1.13 Stanton Number (St_e) and friction factor (f_e) of empirical equations (Continued)

Configuration number 13										
Re_d	Re_{Lp}	U [m/s]	$T_{a,o}$ [K]	T_{avg} [°C]	ρ [kg/m^3]	C_p [J/kg.K]	μ [N.s/m^2]	f_A	St_e	f_e
400	129	2.11	352	320	1.0689	1006	1.923E-05	0.277	0.060	0.271
600	193	3.13	349	318	1.0753	1006	1.917E-05	0.196	0.049	0.187
800	258	4.14	346	317	1.0818	1006	1.910E-05	0.158	0.042	0.148
1000	322	5.13	343	316	1.0877	1006	1.904E-05	0.136	0.037	0.126
2000	645	9.96	334	311	1.1080	1005	1.884E-05	0.092	0.025	0.083
3000	967	14.71	329	308	1.1190	1005	1.873E-05	0.078	0.020	0.070
4000	1289	19.42	326	307	1.1261	1005	1.866E-05	0.071	0.017	0.063

Table A1.14 Stanton Number (St_e) and friction factor (f_e) of empirical equations (Continued)

Configuration number 14										
Re_d	Re_{Lp}	U [m/s]	$T_{a,o}$ [K]	T_{avg} [°C]	ρ [kg/m^3]	C_p [J/kg.K]	μ [N.s/m^2]	f_A	St_e	f_e
400	116	1.90	352	320	1.0675	1006	1.925E-05	0.306	0.057	0.322
600	174	2.82	348	318	1.0766	1006	1.916E-05	0.214	0.047	0.220
800	232	3.71	344	316	1.0855	1006	1.906E-05	0.171	0.040	0.173
1000	290	4.58	340	314	1.0935	1006	1.898E-05	0.145	0.036	0.146
2000	581	8.82	328	308	1.1202	1005	1.872E-05	0.097	0.024	0.094
3000	871	12.96	322	305	1.1349	1005	1.857E-05	0.081	0.019	0.078
4000	1161	17.05	318	303	1.1443	1005	1.848E-05	0.074	0.016	0.070

Table A1.15 Stanton Number (St_e) and friction factor (f_e) of empirical equations. (Continued)

Configuration number 15										
Re_d	Re_{Lp}	U [m/s]	$T_{a,o}$ [K]	T_{avg} [°C]	ρ [kg/m^3]	C_p [J/kg.K]	μ [N.s/m^2]	f_A	St_e	f_e
400	128	2.10	352	320	1.0678	1006	1.925E-05	0.278	0.057	0.252
600	193	3.14	350	319	1.0724	1006	1.920E-05	0.197	0.047	0.174
800	257	4.15	348	318	1.0775	1006	1.915E-05	0.158	0.040	0.138
1000	321	5.15	346	317	1.0824	1006	1.910E-05	0.136	0.035	0.117
2000	642	10.02	337	312	1.1017	1006	1.890E-05	0.092	0.024	0.077
3000	963	14.77	331	310	1.1136	1005	1.878E-05	0.078	0.019	0.065
4000	1285	19.46	328	308	1.1219	1005	1.870E-05	0.071	0.016	0.059

A-2: Result from CFD simulation by Malapure et al.

The simulation result of Stanton Number (*St*) and Friction Factor (*f*) is compared validate in this project, the simulation results determined results of Malapure et al. [20], in "**Numerical Investigation of Fluid Flow and Heat Transfer Over Louvered Fins in Compact Heat Exchanger,**" International Journal of Thermal Sciences, No. 46, 2007, p 199–211.

Table A2.1 Stanton Number (St_m) and friction factor (f_m) of simulation.

Re_d	Configuration number									
	1		2		3		4		5	
	St_m	f_m	St_m	f_m	St_m	f_m	St_m	f_m	St_m	f_m
400	0.066	0.222	0.073	0.228	0.058	0.220	0.067	0.205	0.068	0.231
600	0.049	0.169	0.057	0.178	0.043	0.167	0.051	0.161	0.051	0.176
800	0.041	0.141	0.048	0.153	0.036	0.137	0.042	0.133	0.042	0.148
1000	0.036	0.124	0.043	0.137	0.031	0.118	0.037	0.116	0.037	0.129
2000	0.025	0.093	0.029	0.095	0.020	0.081	0.023	0.078	0.024	0.092
3000	0.023	0.085	0.025	0.088	0.020	0.081	0.019	0.065	0.020	0.082
4000	0.019	0.073	0.024	0.083	0.014	0.082	0.020	0.066	0.018	0.074

Table A2.2 Stanton Number (St_m) and friction factor (f_m) of simulation (Continued).

Re_d	Configuration number									
	6		7		8		9		10	
	St_m	f_m	St_m	f_m	St_m	f_m	St_m	f_m	St_m	f_m
400	0.068	0.290	0.062	0.206	0.085	0.277	0.084	0.280	0.049	0.176
600	0.052	0.210	0.046	0.155	0.065	0.220	0.062	0.210	0.062	0.193
800	0.043	0.180	0.037	0.126	0.055	0.180	0.052	0.180	0.051	0.180
1000	0.024	0.130	0.032	0.113	0.049	0.160	0.044	0.160	0.045	0.160
2000	0.024	0.087	0.019	0.077	0.032	0.119	0.029	0.110	0.031	0.120
3000	0.022	0.086	0.024	0.079	0.029	0.112	0.027	0.091	0.028	0.100
4000	0.019	0.078	0.020	0.068	0.024	0.097	0.021	0.080	0.023	0.100

Table A2.3 Stanton Number (St_m) and friction factor (f_m) of simulation (Continued).

Re_d	Configuration number									
	11		12		13		14		15	
	St_m	f_m	St_m	f_m	St_m	f_m	St_m	f_m	St_m	f_m
400	0.078	0.264	0.066	0.198	0.071	0.230	0.074	0.233	0.070	0.208
600	0.060	0.200	0.055	0.179	0.055	0.180	0.060	0.189	0.055	0.165
800	0.050	0.170	0.049	0.160	0.046	0.153	0.050	0.159	0.045	0.141
1000	0.043	0.150	0.044	0.140	0.040	0.135	0.043	0.139	0.039	0.122
2000	0.028	0.107	0.031	0.100	0.035	0.110	0.027	0.098	0.025	0.083
3000	0.025	0.090	0.025	0.086	0.027	0.089	0.026	0.085	0.230	0.071
4000	0.020	0.087	0.021	0.076	0.022	0.076	0.079	0.079	0.210	0.067

A-3: Result from CFD simulation of this research

This project concentrate on the heat transfer rate calculation is based on the heat transfer balance at the inlet and outlet on the air side.

Reynolds number on hydraulic diameter can be defined from equation 2.26 as follow:

$$\mathrm{Re}_d = \frac{\rho U d_h}{\mu}$$

Hydraulic diameter in consideration to internal flow of *non-circular tube* cross section can be defined from equation 2.27 as follow:

$$d_h = \frac{4 A_c L_s}{A}$$

where A_c is the minimum flow area, A is the total heat transfer area and L_s is the fin length of heat exchanger.

Friction Factor defined from equation 2.30 as follow:

$$f = \frac{\Delta P}{\frac{\rho U^2}{2}\frac{A_c}{A}}$$

Stanton number is dimensionless representation of the heat transfer coefficient can be defined from equation 2.34 as follow:

$$St = \frac{A_c}{A}\frac{(T_{a,o} - T_{a,i})}{LMTD}$$

Table A3.1 Stanton Number (St_s) and friction factor (f_s) of this research

Configuration number1											
Re_d	U [m/s]	$T_{a,o}$ [K]	T_{avg} [K]	ρ [kg/m^3]	C_p [J/kg.K]	μ [N.s/m^2]	$P_{a,i}$ [Pa]	$P_{a,o}$ [Pa]	*LMTD*	St_s	f_s
400	1.71	355	322	1.0610	1006	1.932E-05	21.69	1.98	20.37	0.068	0.263
600	2.56	352	320	1.0682	1006	1.924E-05	35.25	4.36	25.95	0.051	0.182
800	3.42	349	318	1.0751	1006	1.917E-05	53.57	7.64	29.86	0.042	0.151
1000	4.27	346	317	1.0813	1006	1.911E-05	74.98	11.87	32.87	0.036	0.132
2000	8.54	336	312	1.1035	1006	1.888E-05	228.13	47.09	41.51	0.024	0.093
3000	12.81	330	309	1.1167	1005	1.875E-05	458.55	105.78	45.82	0.019	0.079
4000	17.08	326	307	1.1260	1005	1.866E-05	761.48	187.94	48.61	0.016	0.072

Table A3.2 Stanton Number (St_s) and friction factor (f_s) of this research (Continued).

Configuration number 2											
Re_d	U [m/s]	$T_{a,o}$ [K]	T_{avg} [K]	ρ [kg/m^3]	C_p [J/kg.K]	μ [N.s/m^2]	$P_{a,i}$ [Pa]	$P_{a,o}$ [Pa]	*LMTD*	St_s	f_s
400	1.14	349	319	1.0744	1006	1.918E-05	6.46	0.91	29.53	0.064	0.249
600	1.70	345	316	1.0846	1006	1.907E-05	11.90	2.00	34.31	0.051	0.195
800	2.27	340	314	1.0937	1006	1.898E-05	18.41	3.48	37.99	0.043	0.164
1000	2.84	337	312	1.1017	1006	1.890E-05	25.99	5.38	40.88	0.037	0.144
2000	5.68	325	307	1.1270	1005	1.865E-05	80.14	21.19	48.90	0.024	0.101
3000	8.52	320	304	1.1402	1005	1.852E-05	160.10	47.46	52.57	0.019	0.085
4000	11.36	316	302	1.1485	1005	1.844E-05	266.20	84.27	54.76	0.016	0.076

Table A3.3 Stanton Number (St_s) and friction factor (f_s) of this research (Continued).

Configuration number 3											
Re_d	U [m/s]	$T_{a,o}$ [K]	T_{avg} [K]	ρ [kg/m^3]	C_p [J/kg.K]	μ [N.s/m^2]	$P_{a,i}$ [Pa]	$P_{a,o}$ [Pa]	*LMTD*	St_s	f_s
400	2.05	354	321	1.0632	1006	1.929E-05	32.46	2.83	22.37	0.051	0.227
600	3.08	351	320	1.0705	1006	1.922E-05	57.58	6.20	27.34	0.040	0.174
800	4.10	348	318	1.0778	1006	1.914E-05	87.80	10.93	31.22	0.033	0.145
1000	5.13	345	316	1.0845	1006	1.907E-05	122.89	17.02	34.27	0.028	0.127
2000	10.26	334	311	1.1077	1005	1.884E-05	374.99	67.73	42.94	0.018	0.091
3000	15.39	328	308	1.1207	1005	1.871E-05	751.74	152.25	47.04	0.015	0.078
4000	20.52	324	306	1.1297	1005	1.862E-05	1238.67	270.61	49.66	0.013	0.070

Table A3.4 Stanton Number (St_s) and friction factor (f_s) of this research (Continued)

Configuration number 4											
Re_d	U [m/s]	$T_{a,o}$ [K]	T_{avg} [K]	ρ [kg/m^3]	C_p [J/kg.K]	μ [N.s/m^2]	$P_{a,i}$ [Pa]	$P_{a,o}$ [Pa]	$LMTD$	St_s	f_s
400	1.66	352	320	1.0680	1006	1.924E-05	17.44	1.88	25.79	0.053	0.226
600	2.48	348	318	1.0764	1006	1.916E-05	31.08	4.15	30.52	0.042	0.172
800	3.31	345	316	1.0844	1006	1.908E-05	47.20	7.26	34.23	0.035	0.143
1000	4.14	341	315	1.0916	1006	1.900E-05	65.84	11.24	37.16	0.031	0.124
2000	8.28	330	309	1.1161	1005	1.876E-05	197.91	44.38	45.62	0.020	0.085
3000	12.42	324	306	1.1295	1005	1.863E-05	396.10	99.66	49.62	0.016	0.072
4000	16.57	321	304	1.1381	1005	1.854E-05	657.79	177.19	51.99	0.013	0.065

Table A3.5 Stanton Number (St_m) and friction factor (f_m) of simulation (Continued)

Configuration number 5											
Re_d	U [m/s]	$T_{a,o}$ [K]	T_{avg} [K]	ρ [kg/m^3]	C_p [J/kg.K]	μ [N.s/m^2]	$P_{a,i}$ [Pa]	$P_{a,o}$ [Pa]	$LMTD$	St_s	f_s
400	1.70	352	320	1.0677	1006	1.925E-05	20.40	1.97	25.63	0.052	0.247
600	2.55	348	318	1.0765	1006	1.916E-05	36.17	4.31	30.58	0.041	0.189
800	3.40	345	316	1.0845	1006	1.907E-05	55.47	7.58	34.28	0.034	0.158
1000	4.25	341	315	1.0915	1006	1.900E-05	78.15	11.79	37.14	0.030	0.140
2000	8.50	331	309	1.1151	1005	1.877E-05	241.11	46.81	45.30	0.020	0.100
3000	12.75	325	307	1.1279	1005	1.864E-05	486.09	105.18	49.16	0.016	0.086
4000	17.00	321	305	1.1364	1005	1.856E-05	807.40	186.91	51.53	0.013	0.078

Table A3.6 Stanton Number (St_s) and friction factor (f_s) of this research (Continued).

Configuration number 6											
Re_d	U [m/s]	$T_{a,o}$ [K]	T_{avg} [K]	ρ [kg/m^3]	C_p [J/kg.K]	μ [N.s/m^2]	$P_{a,i}$ [Pa]	$P_{a,o}$ [Pa]	$LMTD$	St_s	f_s
400	1.61	342	315	1.0895	1006	1.902E-05	10.65	1.79	36.36	0.063	0.266
600	2.41	336	312	1.1033	1006	1.888E-05	19.62	3.97	41.46	0.049	0.206
800	3.21	331	310	1.1139	1005	1.878E-05	30.57	6.98	44.94	0.041	0.173
1000	4.02	328	308	1.1221	1005	1.870E-05	43.49	10.82	47.46	0.035	0.152
2000	8.04	317	303	1.1460	1005	1.847E-05	136.75	42.72	54.09	0.023	0.107
3000	12.06	312	300	1.1576	1005	1.835E-05	277.65	95.87	57.06	0.018	0.091
4000	16.07	309	299	1.1648	1005	1.829E-05	462.17	170.32	58.82	0.015	0.082

Table A3.7 Stanton Number (St_s) and friction factor (f_s) of this research (Continued)

Configuration number 7											
Re_d	U [m/s]	$T_{a,o}$ [K]	T_{avg} [K]	ρ [kg/m^3]	C_p [J/kg.K]	μ [N.s/m^2]	$P_{a,i}$ [Pa]	$P_{a,o}$ [Pa]	$LMTD$	St_s	f_s
400	1.99	346	317	1.0819	1006	1.910E-05	18.68	2.71	33.15	0.059	0.255
600	2.98	340	314	1.0953	1006	1.896E-05	34.12	6.00	38.59	0.046	0.197
800	3.98	335	311	1.1058	1005	1.886E-05	52.98	10.55	42.30	0.038	0.166
1000	4.97	331	310	1.1141	1005	1.878E-05	75.21	16.39	45.01	0.033	0.146
2000	9.94	320	304	1.1387	1005	1.854E-05	236.16	64.91	52.17	0.021	0.104
3000	14.91	315	302	1.1510	1005	1.842E-05	478.06	145.86	55.39	0.017	0.089
4000	19.88	311	300	1.1596	1005	1.833E-05	781.29	259.28	57.56	0.014	0.078

Table BA.8 Stanton Number (St_m) and friction factor (f_m) of simulation (Continued)

Configuration number 8											
Re_d	U [m/s]	$T_{a,o}$ [K]	T_{avg} [K]	ρ [kg/m^3]	C_p [J/kg.K]	μ [N.s/m^2]	$P_{a,i}$ [Pa]	$P_{a,o}$ [Pa]	$LMTD$	St_s	f_s
400	1.64	356	322	1.0597	1006	1.933E-05	22.53	1.85	18.97	0.077	0.310
600	2.46	353	321	1.0653	1006	1.927E-05	41.35	4.06	24.00	0.058	0.247
800	3.29	350	319	1.0717	1006	1.921E-05	63.78	7.13	28.05	0.048	0.210
1000	4.11	348	318	1.0779	1006	1.914E-05	89.91	11.05	31.26	0.041	0.186
2000	8.21	338	313	1.0999	1006	1.892E-05	281.64	43.70	40.28	0.026	0.138
3000	12.32	332	310	1.1127	1005	1.879E-05	573.76	98.17	44.55	0.021	0.121
4000	16.43	328	308	1.1219	1005	1.870E-05	948.41	174.45	47.41	0.018	0.110

Table A3.9 Stanton Number (St_s) and friction factor (f_s) of this research (Continued)

Configuration number 9											
Re_d	U [m/s]	$T_{a,o}$ [K]	T_{avg} [K]	ρ [kg/m^3]	C_p [J/kg.K]	μ [N.s/m^2]	$P_{a,i}$ [Pa]	$P_{a,o}$ [Pa]	$LMTD$	St_s	f_s
400	1.98	356	322	1.0597	1006	1.933E-05	42.94	2.71	18.99	0.064	0.347
600	2.96	355	321	1.0629	1006	1.930E-05	71.44	5.94	22.08	0.054	0.251
800	3.95	352	320	1.0681	1006	1.924E-05	112.41	10.84	25.90	0.044	0.217
1000	4.94	350	319	1.0736	1006	1.919E-05	158.43	16.95	29.06	0.038	0.193
2000	9.88	341	315	1.0913	1006	1.901E-05	488.85	64.32	37.06	0.026	0.142
3000	14.81	334	311	1.1074	1005	1.884E-05	981.56	144.75	42.83	0.019	0.123
4000	19.75	329	309	1.1180	1005	1.874E-05	1594.12	257.47	46.20	0.016	0.109

Table A3.10 Stanton Number (St_s) and friction factor (f_s) of this research (Continued)

Configuration number 10											
Re_d	U [m/s]	$T_{a,o}$ [K]	T_{avg} [K]	ρ [kg/m^3]	C_p [J/kg.K]	μ [N.s/m^2]	$P_{a,i}$ [Pa]	$P_{a,o}$ [Pa]	$LMTD$	St_s	f_s
400	1.11	348	318	1.0770	1006	1.915E-05	6.93	0.89	30.84	0.062	0.287
600	1.67	345	316	1.0846	1006	1.907E-05	13.81	1.95	34.30	0.052	0.248
800	2.23	342	315	1.0904	1006	1.901E-05	22.62	3.45	36.71	0.046	0.225
1000	2.78	339	314	1.0960	1006	1.896E-05	33.05	5.39	38.85	0.042	0.206
2000	5.57	330	309	1.1160	1005	1.876E-05	106.02	20.77	45.59	0.029	0.156
3000	8.35	325	306	1.1290	1005	1.863E-05	212.73	45.91	49.48	0.023	0.134
4000	11.13	321	304	1.1382	1005	1.854E-05	354.47	81.40	52.03	0.020	0.123

Table A3.11 Stanton Number (St_s) and friction factor (f_s) of this research (Continued).

Configuration number 11											
Re_d	U [m/s]	$T_{a,o}$ [K]	T_{avg} [K]	ρ [kg/m^3]	C_p [J/kg.K]	μ [N.s/m^2]	$P_{a,i}$ [Pa]	$P_{a,o}$ [Pa]	$LMTD$	St_s	f_s
400	1.60	353	320	1.0668	1006	1.926E-05	19.37	1.75	25.01	0.057	0.286
600	2.39	349	319	1.0748	1006	1.917E-05	34.79	3.86	29.73	0.045	0.222
800	3.19	345	317	1.0826	1006	1.909E-05	53.36	6.74	33.43	0.038	0.187
1000	3.99	342	315	1.0893	1006	1.903E-05	75.27	10.44	36.27	0.033	0.165
2000	7.98	332	310	1.1125	1005	1.879E-05	234.48	41.24	44.51	0.022	0.120
3000	11.97	326	307	1.1256	1005	1.866E-05	474.51	92.78	48.48	0.017	0.105
4000	15.96	322	305	1.1340	1005	1.858E-05	790.46	164.88	50.89	0.015	0.096

Table A3.12 Stanton Number (St_s) and friction factor (f_s) of this research (Continued).

Configuration number 12											
Re_d	U [m/s]	$T_{a,o}$ [K]	T_{avg} [K]	ρ [kg/m^3]	C_p [J/kg.K]	μ [N.s/m^2]	$P_{a,i}$ [Pa]	$P_{a,o}$ [Pa]	$LMTD$	St_s	f_s
400	1.61	352	320	1.0678	1006	1.925E-05	16.34	1.81	25.69	0.055	0.230
600	2.39	350	319	1.0725	1006	1.920E-05	32.44	3.97	28.50	0.048	0.203
800	3.19	348	318	1.0776	1006	1.915E-05	51.64	6.92	31.12	0.042	0.179
1000	3.99	345	317	1.0830	1006	1.909E-05	73.71	10.68	33.61	0.037	0.161
2000	7.97	335	311	1.1060	1005	1.886E-05	226.90	41.96	42.36	0.024	0.115
3000	11.96	329	308	1.1199	1005	1.872E-05	456.76	94.12	46.80	0.019	0.099
4000	15.94	324	306	1.1292	1005	1.863E-05	758.41	167.19	49.53	0.016	0.090

Table A3.13 Stanton Number (St_s) and friction factor (f_s) of this research (Continued).

Configuration number 13											
Re_d	U [m/s]	$T_{a,o}$ [K]	T_{avg} [K]	ρ [kg/m^3]	C_p [J/kg.K]	μ [N.s/m^2]	$P_{a,i}$ [Pa]	$P_{a,o}$ [Pa]	$LMTD$	St_s	f_s
400	1.72	352	320	1.0689	1006	1.923E-05	21.97	2.04	26.38	0.050	0.259
600	2.58	349	318	1.0753	1006	1.917E-05	39.46	4.49	29.99	0.042	0.201
800	3.44	346	317	1.0818	1006	1.910E-05	60.54	7.87	33.11	0.036	0.169
1000	4.30	343	316	1.0877	1006	1.904E-05	85.27	12.20	35.63	0.032	0.149
2000	8.59	334	311	1.1080	1005	1.884E-05	264.39	48.32	43.05	0.022	0.108
3000	12.89	329	308	1.1190	1005	1.873E-05	535.01	108.56	46.53	0.018	0.094
4000	17.19	326	307	1.1261	1005	1.866E-05	890.38	192.89	48.64	0.016	0.086

Table A3.14 Stanton Number (St_s) and friction factor (f_s) of this research (Continued).

Configuration number 14											
Re_d	U [m/s]	$T_{a,o}$ [K]	T_{avg} [K]	ρ [kg/m^3]	C_p [J/kg.K]	μ [N.s/m^2]	$P_{a,i}$ [Pa]	$P_{a,o}$ [Pa]	$LMTD$	St_s	f_s
400	1.55	352	320	1.0675	1006	1.925E-05	15.89	1.64	25.51	0.057	0.254
600	2.32	348	318	1.0766	1006	1.916E-05	29.03	3.62	30.61	0.045	0.199
800	3.10	344	316	1.0855	1006	1.906E-05	44.41	6.74	34.72	0.037	0.165
1000	3.87	340	314	1.0935	1006	1.898E-05	62.14	9.80	37.91	0.032	0.146
2000	7.74	328	308	1.1202	1005	1.872E-05	185.35	38.63	46.88	0.020	0.100
3000	11.61	322	305	1.1349	1005	1.857E-05	370.39	86.67	51.13	0.015	0.085
4000	15.48	318	303	1.1443	1005	1.848E-05	615.71	153.96	53.67	0.013	0.077

Table A3.15 Stanton Number (St_s) and friction factor (f_s) of this research (Continued).

Configuration number 15											
Re_d	U [m/s]	$T_{a,o}$ [K]	T_{avg} [K]	ρ [kg/m^3]	C_p [J/kg.K]	μ [N.s/m^2]	$P_{a,i}$ [Pa]	$P_{a,o}$ [Pa]	$LMTD$	St_s	f_s
400	1.71	352	320	1.0678	1006	1.925E-05	19.79	2.04	25.66	0.052	0.234
600	2.57	350	319	1.0724	1006	1.920E-05	35.92	4.50	28.41	0.045	0.183
800	3.42	348	318	1.0775	1006	1.915E-05	55.05	7.88	31.07	0.040	0.154
1000	4.28	346	317	1.0824	1006	1.910E-05	76.92	12.20	33.37	0.035	0.134
2000	8.56	337	312	1.1017	1006	1.890E-05	233.73	48.10	40.89	0.025	0.095
3000	12.84	331	310	1.1136	1005	1.878E-05	470.38	107.91	44.85	0.020	0.081
4000	17.12	328	308	1.1219	1005	1.870E-05	781.37	191.65	47.40	0.017	0.074

B: Heat transfer coefficient calculation

B-1: Result of heat transfer coefficient values from this research

Heat transfer rate can be defined from equation 2.5 as follow:

$$Q = h_c A \Delta T_m = \rho U A_c c_p (T_{a,o} - T_{a,i})$$

Log mean temperatures difference (*LMTD*) ΔT_m can be defined from equation 2.4 as follow:

$$LMTD = \Delta T_m = \frac{\Delta T_o - \Delta T_i}{\ln(\Delta T_o / \Delta T_i)} \quad , \Delta T_i = T_w - T_{a,i}, \quad \Delta T_o = T_w - T_{a,o}$$

Heat transfer coefficient for design of heat exchangers h_c can be defined from equation 2.6 as follow:

$$h_c = \rho U c_p \frac{A_c}{A} \frac{(T_{a,o} - T_{a,i})}{LMTD}$$

To find Heat transfer rate Q from simulated result, the geometry for calculation heat transfer coefficient of h found using Table 7.1.

Table B1.1 Heat transfer coefficient (h_c) of this research

Configuration number 1										
Re_d	$T_{a,o}$ [K]	T_{avg} [K]	ρ [kg/m^3]	C_p [J/kg.K]	μ [N.s/m^2]	*LMTD*	A_c [mm]	A [mm]	Q [W]	h_c [W/m^2.K]
400	355	322	1.0610	1006	1.932E-05	20.37	859.12	17.73	2.71	154.71
600	352	320	1.0682	1006	1.924E-05	25.95	859.12	17.73	3.84	172.31
800	349	318	1.0751	1006	1.917E-05	29.86	859.12	17.73	4.85	189.03
1000	346	317	1.0813	1006	1.911E-05	32.87	859.12	17.73	5.76	203.86
2000	336	312	1.1035	1006	1.888E-05	41.51	859.12	17.73	9.40	263.64
3000	330	309	1.1167	1005	1.875E-05	45.82	859.12	17.73	12.27	311.72
4000	326	307	1.1260	1005	1.866E-05	48.61	859.12	17.73	14.68	351.51

Table B1.2 Heat transfer coefficient (h_c) of this research (Continued)

Configuration number 2										
Re_d	$T_{a,o}$ [K]	T_{avg} [K]	ρ [kg/m^3]	C_p [J/kg.K]	μ [N.s/m^2]	*LMTD*	A_c [mm]	A [mm]	Q [W]	h_c [W/m^2.K]
400	349	319	1.0744	1006	1.918E-05	29.53	928.00	28.80	2.63	96.103
600	345	316	1.0846	1006	1.907E-05	34.31	928.00	28.80	3.63	113.954
800	340	314	1.0937	1006	1.898E-05	37.99	928.00	28.80	4.46	126.481
1000	337	312	1.1017	1006	1.890E-05	40.88	928.00	28.80	5.17	136.239
2000	325	307	1.1270	1005	1.865E-05	48.90	928.00	28.80	7.83	172.585
3000	320	304	1.1402	1005	1.852E-05	52.57	928.00	28.80	9.87	202.279
4000	316	302	1.1485	1005	1.844E-05	54.76	928.00	28.80	11.61	228.445

Table B1.3 Heat transfer coefficient (h_c) of this research (Continued)

Configuration number 3										
Re_d	$T_{a,o}$ [K]	T_{avg} [K]	ρ [kg/m^3]	C_p [J/kg.K]	μ [N.s/m^2]	*LMTD*	A_c [mm]	A [mm]	Q [W]	h_c [W/m^2.K]
400	354	321	1.0632	1006	1.929E-05	22.37	838.40	14.40	2.60	138.480
600	351	320	1.0705	1006	1.922E-05	27.34	838.40	14.40	3.68	160.673
800	348	318	1.0778	1006	1.914E-05	31.22	838.40	14.40	4.63	176.875
1000	345	316	1.0845	1006	1.907E-05	34.27	838.40	14.40	5.47	190.338
2000	334	311	1.1077	1005	1.884E-05	42.94	838.40	14.40	8.79	244.160
3000	328	308	1.1207	1005	1.871E-05	47.04	838.40	14.40	11.45	290.255
4000	324	306	1.1297	1005	1.862E-05	49.66	838.40	14.40	13.69	328.893

Table B1.4 Heat transfer coefficient (h_c) of this research (Continued)

Configuration number 4										
Re_d	$T_{a,o}$ [K]	T_{avg} [K]	ρ [kg/m^3]	C_p [J/kg.K]	μ [N.s/m^2]	*LMTD*	A_c [mm]	A [mm]	Q [W]	h_c [W/m^2.K]
400	352	320	1.0680	1006	1.924E-05	25.79	863.04	18.36	2.58	115.817
600	348	318	1.0764	1006	1.916E-05	30.52	863.04	18.36	3.62	137.274
800	345	316	1.0844	1006	1.908E-05	34.23	863.04	18.36	4.51	152.514
1000	341	315	1.0916	1006	1.900E-05	37.16	863.04	18.36	5.29	164.820
2000	330	309	1.1161	1005	1.876E-05	45.62	863.04	18.36	8.28	210.164
3000	324	306	1.1295	1005	1.863E-05	49.62	863.04	18.36	10.59	247.387
4000	321	304	1.1381	1005	1.854E-05	51.99	863.04	18.36	12.61	281.123

Table B1.5 Heat transfer coefficient (h_c) of this research (Continued)

Configuration number 2										
Re_d	$T_{a,o}$ [K]	T_{avg} [K]	ρ [kg/m^3]	C_p [J/kg.K]	μ [N.s/m^2]	*LMTD*	A_c [mm]	A [mm]	Q [W]	h_c [W/m^2.K]
400	352	320	1.0677	1006	1.925E-05	25.63	859.68	17.82	2.57	116.812
600	348	318	1.0765	1006	1.916E-05	30.58	859.68	17.82	3.60	136.895
800	345	316	1.0845	1006	1.907E-05	34.28	859.68	17.82	4.48	152.189
1000	341	315	1.0915	1006	1.900E-05	37.14	859.68	17.82	5.27	165.023
2000	331	309	1.1151	1005	1.877E-05	45.30	859.68	17.82	8.34	214.119
3000	325	307	1.1279	1005	1.864E-05	49.16	859.68	17.82	10.76	254.655
4000	321	305	1.1364	1005	1.856E-05	51.53	859.68	17.82	12.86	290.295

Table B1.6 Heat transfer rate (Q) and heat transfer coefficient (h_c) of this research (Continued)

Configuration number 6										
Re_d	$T_{a,o}$ [K]	T_{avg} [K]	ρ [kg/m^3]	C_p [J/kg.K]	μ [N.s/m^2]	*LMTD*	A_c [mm]	A [mm]	Q [W]	h_c [W/m^2.K]
400	342	315	1.0895	1006	1.902E-05	36.36	447.60	18.90	2.15	132.175
600	336	312	1.1033	1006	1.888E-05	41.46	447.60	18.90	2.83	152.681
800	331	310	1.1139	1005	1.878E-05	44.94	447.60	18.90	3.39	168.373
1000	328	308	1.1221	1005	1.870E-05	47.46	447.60	18.90	3.86	181.689
2000	317	303	1.1460	1005	1.847E-05	54.09	447.60	18.90	5.61	231.854
3000	312	300	1.1576	1005	1.835E-05	57.06	447.60	18.90	6.93	271.243
4000	309	299	1.1648	1005	1.829E-05	58.82	447.60	18.90	8.04	305.262

Table B1.7 Heat transfer rate (Q) and heat transfer coefficient (h_c) of this research (Continued)

Configuration number 7										
Re_d	$T_{a,o}$ [K]	T_{avg} [K]	ρ [kg/m^3]	C_p [J/kg.K]	μ [N.s/m^2]	*LMTD*	A_c [mm]	A [mm]	Q [W]	h_c [W/m^2.K]
400	346	317	1.0819	1006	1.910E-05	33.15	435.00	14.85	2.23	154.919
600	340	314	1.0953	1006	1.896E-05	38.59	435.00	14.85	2.97	177.185
800	335	311	1.1058	1005	1.886E-05	42.30	435.00	14.85	3.58	194.682
1000	331	310	1.1141	1005	1.878E-05	45.01	435.00	14.85	4.10	209.644
2000	320	304	1.1387	1005	1.854E-05	52.17	435.00	14.85	6.07	267.325
3000	315	302	1.1510	1005	1.842E-05	55.39	435.00	14.85	7.55	313.534
4000	311	300	1.1596	1005	1.833E-05	57.56	435.00	14.85	8.65	345.295

Table B1.8 Heat transfer rate (Q) and heat transfer coefficient (h_c) of this research (Continued)

Configuration number 8										
Re_d	$T_{a,o}$ [K]	T_{avg} [K]	ρ [kg/m^3]	C_p [J/kg.K]	μ [N.s/m^2]	$LMTD$	A_c [mm]	A [mm]	Q [W]	h_c [W/m^2.K]
400	356	322	1.0597	1006	1.933E-05	18.97	864.16	18.54	2.75	167.721
600	353	321	1.0653	1006	1.927E-05	24.00	864.16	18.54	3.95	190.527
800	350	319	1.0717	1006	1.921E-05	28.05	864.16	18.54	5.01	206.750
1000	348	318	1.0779	1006	1.914E-05	31.26	864.16	18.54	5.96	220.575
2000	338	313	1.0999	1006	1.892E-05	40.28	864.16	18.54	9.79	281.223
3000	332	310	1.1127	1005	1.879E-05	44.55	864.16	18.54	12.90	335.021
4000	328	308	1.1219	1005	1.870E-05	47.41	864.16	18.54	15.51	378.502

Table B1.9 Heat transfer rate (Q) and heat transfer coefficient (h_c) of this research (Continued)

Configuration number 9										
Re_d	$T_{a,o}$ [K]	T_{avg} [K]	ρ [kg/m^3]	C_p [J/kg.K]	μ [N.s/m^2]	$LMTD$	A_c [mm]	A [mm]	Q [W]	h_c [W/m^2.K]
400	356	322	1.0597	1006	1.933E-05	18.99	842.32	15.03	2.68	167.567
600	355	321	1.0629	1006	1.930E-05	22.08	842.32	15.03	3.93	211.033
800	352	320	1.0681	1006	1.924E-05	25.90	842.32	15.03	5.03	230.373
1000	350	319	1.0736	1006	1.919E-05	29.06	842.32	15.03	6.02	245.795
2000	341	315	1.0913	1006	1.901E-05	37.06	842.32	15.03	10.34	331.301
3000	334	311	1.1074	1005	1.884E-05	42.83	842.32	15.03	13.29	368.371
4000	329	309	1.1180	1005	1.874E-05	46.20	842.32	15.03	15.82	406.597

Table B1.10 Heat transfer rate (Q) and heat transfer coefficient (h_c) of this research (Continued)

Configuration number 10										
Re_d	$T_{a,o}$ [K]	T_{avg} [K]	ρ [kg/m^3]	C_p [J/kg.K]	μ [N.s/m^2]	$LMTD$	A_c [mm]	A [mm]	Q [W]	h_c [W/m^2.K]
400	348	318	1.0770	1006	1.915E-05	30.84	932.48	29.52	2.59	90.092
600	345	316	1.0846	1006	1.907E-05	34.30	932.48	29.52	3.65	114.001
800	342	315	1.0904	1006	1.901E-05	36.71	932.48	29.52	4.62	134.906
1000	339	314	1.0960	1006	1.896E-05	38.85	932.48	29.52	5.48	151.358
2000	330	309	1.1160	1005	1.876E-05	45.59	932.48	29.52	8.95	210.576
3000	325	306	1.1290	1005	1.863E-05	49.48	932.48	29.52	11.52	249.634
4000	321	304	1.1382	1005	1.854E-05	52.03	932.48	29.52	13.60	280.381

Table B1.11 Heat transfer rate (Q) and heat transfer coefficient (h_c) of this research (Continued)

Configuration number 11										
Re_d	$T_{a,o}$ [K]	T_{avg} [K]	ρ [kg/m^3]	C_p [J/kg.K]	μ [N.s/m^2]	LMT D	A_c [mm]	A [mm]	Q [W]	h_c [W/m^2.K]
400	353	320	1.0668	1006	1.926E-05	25.01	868.08	19.17	2.62	120.577
600	349	319	1.0748	1006	1.917E-05	29.73	868.08	19.17	3.68	142.697
800	345	317	1.0826	1006	1.909E-05	33.43	868.08	19.17	4.60	158.675
1000	342	315	1.0893	1006	1.903E-05	36.27	868.08	19.17	5.43	172.324
2000	332	310	1.1125	1005	1.879E-05	44.51	868.08	19.17	8.65	223.921
3000	326	307	1.1256	1005	1.866E-05	48.48	868.08	19.17	11.19	265.882
4000	322	305	1.1340	1005	1.858E-05	50.89	868.08	19.17	13.40	303.363

Table B1.12 Heat transfer rate (Q) and heat transfer coefficient (h_c) of this research (Continued)

Configuration number 12										
Re_d	$T_{a,o}$ [K]	T_{avg} [K]	ρ [kg/m^3]	C_p [J/kg.K]	μ [N.s/m^2]	LMT D	A_c [mm]	A [mm]	Q [W]	h_c [W/m^2.K]
400	352	320	1.0678	1006	1.925E-05	25.69	866.96	18.99	2.59	116.429
600	350	319	1.0725	1006	1.920E-05	28.50	866.96	18.99	3.75	151.654
800	348	318	1.0776	1006	1.915E-05	31.12	866.96	18.99	4.79	177.718
1000	345	317	1.0830	1006	1.909E-05	33.61	866.96	18.99	5.73	196.561
2000	335	311	1.1060	1005	1.886E-05	42.36	866.96	18.99	9.25	251.918
3000	329	308	1.1199	1005	1.872E-05	46.80	866.96	18.99	11.94	294.310
4000	324	306	1.1292	1005	1.863E-05	49.53	866.96	18.99	14.24	331.614

Table B1.13 Heat transfer rate (Q) and heat transfer coefficient (h_c) of this research (Continued)

Configuration number 13										
Re_d	$T_{a,o}$ [K]	T_{avg} [K]	ρ [kg/m^3]	C_p [J/kg.K]	μ [N.s/m^2]	LMT D	A_c [mm]	A [mm]	Q [W]	h_c [W/m^2.K]
400	352	320	1.0689	1006	1.923E-05	26.38	617.36	12.66	1.83	112.398
600	349	318	1.0753	1006	1.917E-05	29.99	617.36	12.66	2.61	140.897
800	346	317	1.0818	1006	1.910E-05	33.11	617.36	12.66	3.29	161.191
1000	343	316	1.0877	1006	1.904E-05	35.63	617.36	12.66	3.91	177.963
2000	334	311	1.1080	1005	1.884E-05	43.05	617.36	12.66	6.45	242.739
3000	329	308	1.1190	1005	1.873E-05	46.53	617.36	12.66	8.59	299.032
4000	326	307	1.1261	1005	1.866E-05	48.64	617.36	12.66	10.54	350.886

Table B1.14 Heat transfer rate (Q) and heat transfer coefficient (h_c) of this research (Continued)

Configuration number 14										
Re_d	$T_{a,o}$ [K]	T_{avg} [K]	ρ [kg/m^3]	C_p [J/kg.K]	μ [N.s/m^2]	LMT D	A_c [mm]	A [mm]	Q [W]	h_c [W/m^2.K]
400	352	320	1.0675	1006	1.925E-05	25.51	1117.12	25.44	3.35	117.501
600	348	318	1.0766	1006	1.916E-05	30.61	1117.12	25.44	4.67	136.668
800	344	316	1.0855	1006	1.906E-05	34.72	1117.12	25.44	5.78	148.892
1000	340	314	1.0935	1006	1.898E-05	37.91	1117.12	25.44	6.72	158.729
2000	328	308	1.1202	1005	1.872E-05	46.88	1117.12	25.44	10.23	195.291
3000	322	305	1.1349	1005	1.857E-05	51.13	1117.12	25.44	12.78	223.768
4000	318	303	1.1443	1005	1.848E-05	53.67	1117.12	25.44	14.91	248.693

Table B1.15 Heat transfer rate (Q) and heat transfer coefficient (h_c) of this research (Continued)

Configuration number 15										
Re_d	$T_{a,o}$ [K]	T_{avg} [K]	ρ [kg/m^3]	C_p [J/kg.K]	μ [N.s/m^2]	LMT D	A_c [mm]	A [mm]	Q [W]	h_c [W/m^2.K]
400	352	320	1.0678	1006	1.925E-05	25.66	617.92	12.72	1.85	116.587
600	350	319	1.0724	1006	1.920E-05	28.41	617.92	12.72	2.67	152.303
800	348	318	1.0775	1006	1.915E-05	31.07	617.92	12.72	3.42	178.185
1000	346	317	1.0824	1006	1.910E-05	33.37	617.92	12.72	4.10	198.884
2000	337	312	1.1017	1006	1.890E-05	40.89	617.92	12.72	6.88	272.324
3000	331	310	1.1136	1005	1.878E-05	44.85	617.92	12.72	9.13	329.546
4000	328	308	1.1219	1005	1.870E-05	47.40	617.92	12.72	11.09	378.727

C: Fin efficiency calculation

C-1: Result of heat transfer coefficient from this research

Fin efficiency (η_f) can be defined from equation 2.25 as follow:

$$\eta_f = \frac{\tanh ml}{ml}, \quad m = \sqrt{\frac{2h_c}{kF_t}}$$

Heat conductivity of plate fin $k = 335\,(\mathrm{w/m.K})$

The fin surface effectiveness η_o is the ratio of actual heat transfer can be from equation 2.26 as follow:

$$\eta_o = 1 - \frac{A_f}{A}(1 - \eta_f)$$

Table C1.1 Fin efficiency calculations

Configuration number 1													
Re_d	h_c [W/m^2.K]	Fp [mm]	Lp [mm]	a [°]	Tp [mm]	n	A [mm^2]	A_c [mm^2]	A_f [mm^2]	A_t [mm^2]	m	η_f	η_o
400	154.71	2.02	1.4	25.5	11	2	859.12	17.73	748.80	110.32	4.298	0.0517	0.1735
600	172.31	2.02	1.4	25.5	11	2	859.12	17.73	748.80	110.32	4.536	0.0490	0.1711
800	189.03	2.02	1.4	25.5	11	2	859.12	17.73	748.80	110.32	4.751	0.0468	0.1692
1000	203.86	2.02	1.4	25.5	11	2	859.12	17.73	748.80	110.32	4.934	0.0450	0.1677
2000	263.64	2.02	1.4	25.5	11	2	859.12	17.73	748.80	110.32	5.611	0.0396	0.1629
3000	311.72	2.02	1.4	25.5	11	2	859.12	17.73	748.80	110.32	6.101	0.0364	0.1602
4000	351.51	2.02	1.4	25.5	11	2	859.12	17.73	748.80	110.32	6.479	0.0343	0.1583

Table C1.2 Fin efficiency calculations (Continued)

Configuration number 2													
Re_d	h_c [W/m^2.K]	Fp [mm]	Lp [mm]	a [°]	Tp [mm]	n	A [mm^2]	A_c [mm^2]	A_f [mm^2]	A_t [mm^2]	m	η_f	η_o
400	96.103	3.25	1.4	25.5	11	2	928.00	28.80	748.80	179.20	3.387	0.0656	0.2460
600	113.954	3.25	1.4	25.5	11	2	928.00	28.80	748.80	179.20	3.689	0.0602	0.2417
800	126.481	3.25	1.4	25.5	11	2	928.00	28.80	748.80	179.20	3.886	0.0572	0.2392
1000	136.239	3.25	1.4	25.5	11	2	928.00	28.80	748.80	179.20	4.033	0.0551	0.2376
2000	172.585	3.25	1.4	25.5	11	2	928.00	28.80	748.80	179.20	4.540	0.0490	0.2326
3000	202.279	3.25	1.4	25.5	11	2	928.00	28.80	748.80	179.20	4.915	0.0452	0.2296
4000	228.445	3.25	1.4	25.5	11	2	928.00	28.80	748.80	179.20	5.223	0.0425	0.2274

Table C1.3 Fin efficiency calculations (Continued)

Configuration number 3													
Re_d	h_c [W/m^2.K]	Fp [mm]	Lp [mm]	a [°]	Tp [mm]	n	A [mm^2]	A_c [mm^2]	A_f [mm^2]	A_t [mm^2]	m	η_f	η_o
400	138.480	1.65	1.4	25.5	11	2	838.40	14.40	748.80	89.60	4.066	0.0546	0.1557
600	160.673	1.65	1.4	25.5	11	2	838.40	14.40	748.80	89.60	4.380	0.0507	0.1522
800	176.875	1.65	1.4	25.5	11	2	838.40	14.40	748.80	89.60	4.596	0.0484	0.1501
1000	190.338	1.65	1.4	25.5	11	2	838.40	14.40	748.80	89.60	4.767	0.0466	0.1485
2000	244.160	1.65	1.4	25.5	11	2	838.40	14.40	748.80	89.60	5.399	0.0412	0.1436
3000	290.255	1.65	1.4	25.5	11	2	838.40	14.40	748.80	89.60	5.887	0.0377	0.1406
4000	328.893	1.65	1.4	25.5	11	2	838.40	14.40	748.80	89.60	6.267	0.0355	0.1385

Table C1.4 Fin efficiency calculations (Continued)

Configuration number 4													
Re_d	h_c [W/m^2.K]	Fp [mm]	Lp [mm]	a [°]	Tp [mm]	n	A [mm^2]	A_c [mm^2]	A_f [mm^2]	A_t [mm^2]	m	η_f	η_o
400	115.817	2.09	1.4	21.5	11	2	863.04	18.36	748.80	114.24	3.719	0.0598	0.1842
600	137.274	2.09	1.4	21.5	11	2	863.04	18.36	748.80	114.24	4.049	0.0549	0.1800
800	152.514	2.09	1.4	21.5	11	2	863.04	18.36	748.80	114.24	4.267	0.0521	0.1776
1000	164.820	2.09	1.4	21.5	11	2	863.04	18.36	748.80	114.24	4.436	0.0501	0.1758
2000	210.164	2.09	1.4	21.5	11	2	863.04	18.36	748.80	114.24	5.009	0.0444	0.1709
3000	247.387	2.09	1.4	21.5	11	2	863.04	18.36	748.80	114.24	5.435	0.0409	0.1678
4000	281.123	2.09	1.4	21.5	11	2	863.04	18.36	748.80	114.24	5.794	0.0384	0.1656

Table C1.5 Fin efficiency calculations (Continued)

Configuration number 5													
Re_d	h_c [W/m^2.K]	Fp [mm]	Lp [mm]	a [°]	Tp [mm]	n	A [mm^2]	A_c [mm^2]	A_f [mm^2]	A_t [mm^2]	m	η_f	η_o
400	116.812	2.03	1.4	28.5	11	2	859.68	17.82	748.80	110.88	3.735	0.0595	0.1808
600	136.895	2.03	1.4	28.5	11	2	859.68	17.82	748.80	110.88	4.043	0.0550	0.1769
800	152.189	2.03	1.4	28.5	11	2	859.68	17.82	748.80	110.88	4.263	0.0521	0.1744
1000	165.023	2.03	1.4	28.5	11	2	859.68	17.82	748.80	110.88	4.439	0.0501	0.1726
2000	214.119	2.03	1.4	28.5	11	2	859.68	17.82	748.80	110.88	5.056	0.0439	0.1673
3000	254.655	2.03	1.4	28.5	11	2	859.68	17.82	748.80	110.88	5.514	0.0403	0.1641
4000	290.295	2.03	1.4	28.5	11	2	859.68	17.82	748.80	110.88	5.887	0.0377	0.1619

Table C1.6 Fin efficiency calculations (Continued)

Configuration number 6													
Re_d	h_c [W/m^2.K]	Fp [mm]	Lp [mm]	a [o]	Tp [mm]	n	A [mm^2]	A_c [mm^2]	A_f [mm^2]	A_t [mm^2]	m	η_f	η_o
400	132.175	2.15	1.4	25.5	11	1	447.60	18.90	388.80	58.80	3.973	0.0559	0.1800
600	152.681	2.15	1.4	25.5	11	1	447.60	18.90	388.80	58.80	4.270	0.0520	0.1766
800	168.373	2.15	1.4	25.5	11	1	447.60	18.90	388.80	58.80	4.484	0.0496	0.1744
1000	181.689	2.15	1.4	25.5	11	1	447.60	18.90	388.80	58.80	4.658	0.0477	0.1728
2000	231.854	2.15	1.4	25.5	11	1	447.60	18.90	388.80	58.80	5.262	0.0422	0.1681
3000	271.243	2.15	1.4	25.5	11	1	447.60	18.90	388.80	58.80	5.691	0.0390	0.1653
4000	305.262	2.15	1.4	25.5	11	1	447.60	18.90	388.80	58.80	6.037	0.0368	0.1633

Table C1.7 Fin efficiency calculations (Continued)

Configuration number 7													
Re_d	h_c [W/m^2.K]	Fp [mm]	Lp [mm]	a [o]	Tp [mm]	n	A [mm^2]	A_c [mm^2]	A_f [mm^2]	A_t [mm^2]	m	η_f	η_o
400	154.919	1.70	1.4	25.5	11	1	435.00	14.85	388.80	46.20	4.301	0.0517	0.1524
600	177.185	1.70	1.4	25.5	11	1	435.00	14.85	388.80	46.20	4.600	0.0483	0.1494
800	194.682	1.70	1.4	25.5	11	1	435.00	14.85	388.80	46.20	4.821	0.0461	0.1474
1000	209.644	1.70	1.4	25.5	11	1	435.00	14.85	388.80	46.20	5.003	0.0444	0.1459
2000	267.325	1.70	1.4	25.5	11	1	435.00	14.85	388.80	46.20	5.650	0.0393	0.1414
3000	313.534	1.70	1.4	25.5	11	1	435.00	14.85	388.80	46.20	6.119	0.0363	0.1387
4000	345.295	1.70	1.4	25.5	11	1	435.00	14.85	388.80	46.20	6.421	0.0346	0.1371

Table C1.8 Fin efficiency calculations (Continued)

Configuration number 8													
Re_d	h_c [W/m^2.K]	Fp [mm]	Lp [mm]	a [o]	Tp [mm]	n	A [mm^2]	A_c [mm^2]	A_f [mm^2]	A_t [mm^2]	m	η_f	η_o
400	167.721	2.11	0.81	29	11	2	864.16	18.54	748.80	115.36	4.475	0.0497	0.1765
600	190.527	2.11	0.81	29	11	2	864.16	18.54	748.80	115.36	4.770	0.0466	0.1739
800	206.750	2.11	0.81	29	11	2	864.16	18.54	748.80	115.36	4.969	0.0447	0.1722
1000	220.575	2.11	0.81	29	11	2	864.16	18.54	748.80	115.36	5.132	0.0433	0.1710
2000	281.223	2.11	0.81	29	11	2	864.16	18.54	748.80	115.36	5.795	0.0383	0.1667
3000	335.021	2.11	0.81	29	11	2	864.16	18.54	748.80	115.36	6.325	0.0351	0.1639
4000	378.502	2.11	0.81	29	11	2	864.16	18.54	748.80	115.36	6.723	0.0331	0.1621

Table C1.9 Fin efficiency calculations (Continued)

Configuration number 9													
Re_d	h_c [W/m^2.K]	Fp [mm]	Lp [mm]	a [°]	Tp [mm]	n	A [mm^2]	A_c [mm^2]	A_f [mm^2]	A_t [mm^2]	m	η_f	η_o
400	167.567	1.72	0.81	29	11	2	842.32	15.03	748.80	93.52	4.473	0.0497	0.1552
600	211.033	1.72	0.81	29	11	2	842.32	15.03	748.80	93.52	5.020	0.0443	0.1504
800	230.373	1.72	0.81	29	11	2	842.32	15.03	748.80	93.52	5.245	0.0424	0.1487
1000	245.795	1.72	0.81	29	11	2	842.32	15.03	748.80	93.52	5.417	0.0410	0.1475
2000	331.301	1.72	0.81	29	11	2	842.32	15.03	748.80	93.52	6.290	0.0353	0.1424
3000	368.371	1.72	0.81	29	11	2	842.32	15.03	748.80	93.52	6.632	0.0335	0.1408
4000	406.597	1.72	0.81	29	11	2	842.32	15.03	748.80	93.52	6.968	0.0319	0.1394

Table C1.10 Fin efficiency calculations (Continued)

Configuration number 10													
Re_d	h_c [W/m^2.K]	Fp [mm]	Lp [mm]	a [°]	Tp [mm]	n	A [mm^2]	A_c [mm^2]	A_f [mm^2]	A_t [mm^2]	m	η_f	η_o
400	90.092	3.33	0.81	29	11	2	932.48	29.52	748.80	183.68	3.280	0.0678	0.2514
600	114.001	3.33	0.81	29	11	2	932.48	29.52	748.80	183.68	3.689	0.0602	0.2453
800	134.906	3.33	0.81	29	11	2	932.48	29.52	748.80	183.68	4.013	0.0554	0.2414
1000	151.358	3.33	0.81	29	11	2	932.48	29.52	748.80	183.68	4.251	0.0523	0.2390
2000	210.576	3.33	0.81	29	11	2	932.48	29.52	748.80	183.68	5.014	0.0443	0.2326
3000	249.634	3.33	0.81	29	11	2	932.48	29.52	748.80	183.68	5.460	0.0407	0.2297
4000	280.381	3.33	0.81	29	11	2	932.48	29.52	748.80	183.68	5.786	0.0384	0.2278

Table C1.11 Fin efficiency calculations (Continued)

Configuration number 11													
Re_d	h_c [W/m^2.K]	Fp [mm]	Lp [mm]	a [°]	Tp [mm]	n	A [mm^2]	A_c [mm^2]	A_f [mm^2]	A_t [mm^2]	m	η_f	η_o
400	120.577	2.18	1.1	30	11	2	868.08	19.17	748.80	119.28	3.794	0.0586	0.1879
600	142.697	2.18	1.1	30	11	2	868.08	19.17	748.80	119.28	4.128	0.0538	0.1838
800	158.675	2.18	1.1	30	11	2	868.08	19.17	748.80	119.28	4.353	0.0511	0.1814
1000	172.324	2.18	1.1	30	11	2	868.08	19.17	748.80	119.28	4.536	0.0490	0.1797
2000	223.921	2.18	1.1	30	11	2	868.08	19.17	748.80	119.28	5.171	0.0430	0.1745
3000	265.882	2.18	1.1	30	11	2	868.08	19.17	748.80	119.28	5.634	0.0394	0.1714
4000	303.363	2.18	1.1	30	11	2	868.08	19.17	748.80	119.28	6.019	0.0369	0.1693

Table C1.12 Fin efficiency calculations (Continued)

Configuration number 12													
Re_d	h_c [W/m^2.K]	Fp [mm]	Lp [mm]	a [°]	Tp [mm]	n	A [mm^2]	A_c [mm^2]	A_f [mm^2]	A_t [mm^2]	m	η_f	η_o
400	116.429	2.16	0.81	20	11	2	866.96	18.99	748.80	118.16	3.729	0.0596	0.1878
600	151.654	2.16	0.81	20	11	2	866.96	18.99	748.80	118.16	4.255	0.0522	0.1814
800	177.718	2.16	0.81	20	11	2	866.96	18.99	748.80	118.16	4.607	0.0482	0.1780
1000	196.561	2.16	0.81	20	11	2	866.96	18.99	748.80	118.16	4.845	0.0459	0.1759
2000	251.918	2.16	0.81	20	11	2	866.96	18.99	748.80	118.16	5.484	0.0405	0.1713
3000	294.310	2.16	0.81	20	11	2	866.96	18.99	748.80	118.16	5.928	0.0375	0.1687
4000	331.614	2.16	0.81	20	11	2	866.96	18.99	748.80	118.16	6.293	0.0353	0.1668

Table C1.13 Fin efficiency calculations (Continued)

Configuration number 13													
Re_d	h_c [W/m^2.K]	Fp [mm]	Lp [mm]	a [°]	Tp [mm]	n	A [mm^2]	A_c [mm^2]	A_f [mm^2]	A_t [mm^2]	m	η_f	η_o
400	112.398	2.16	1.1	28	8	2	617.36	12.66	499.20	118.16	3.663	0.0910	0.2650
600	140.897	2.16	1.1	28	8	2	617.36	12.66	499.20	118.16	4.102	0.0813	0.2571
800	161.191	2.16	1.1	28	8	2	617.36	12.66	499.20	118.16	4.387	0.0760	0.2528
1000	177.963	2.16	1.1	28	8	2	617.36	12.66	499.20	118.16	4.610	0.0723	0.2499
2000	242.739	2.16	1.1	28	8	2	617.36	12.66	499.20	118.16	5.384	0.0619	0.2415
3000	299.032	2.16	1.1	28	8	2	617.36	12.66	499.20	118.16	5.975	0.0558	0.2365
4000	350.886	2.16	1.1	28	8	2	617.36	12.66	499.20	118.16	6.473	0.0515	0.2330

Table C1.14 Fin efficiency calculations (Continued)

Configuration number 14													
Re_d	h_c [W/m^2.K]	Fp [mm]	Lp [mm]	a [°]	Tp [mm]	n	A [mm^2]	A_c [mm^2]	A_f [mm^2]	A_t [mm^2]	m	η_f	η_o
400	117.501	2.17	1.1	22	14	2	1117.12	25.44	998.40	118.72	3.746	0.0445	0.1460
600	136.668	2.17	1.1	22	14	2	1117.12	25.44	998.40	118.72	4.040	0.0413	0.1431
800	148.892	2.17	1.1	22	14	2	1117.12	25.44	998.40	118.72	4.216	0.0395	0.1416
1000	158.729	2.17	1.1	22	14	2	1117.12	25.44	998.40	118.72	4.353	0.0383	0.1405
2000	195.291	2.17	1.1	22	14	2	1117.12	25.44	998.40	118.72	4.829	0.0345	0.1371
3000	223.768	2.17	1.1	22	14	2	1117.12	25.44	998.40	118.72	5.169	0.0322	0.1351
4000	248.693	2.17	1.1	22	14	2	1117.12	25.44	998.40	118.72	5.449	0.0306	0.1336

Table C1.15 Fin efficiency calculations (Continued)

Configuration number 15													
Re_d	h_c [W/m^2.K]	Fp [mm]	Lp [mm]	a [o]	Tp [mm]	n	A [mm^2]	A_c [mm^2]	A_f [mm^2]	A_t [mm^2]	m	η_f	η_o
400	116.587	2.17	1.1	22	8	2	617.92	12.72	499.20	118.72	3.731	0.0893	0.2643
600	152.303	2.17	1.1	22	8	2	617.92	12.72	499.20	118.72	4.264	0.0782	0.2553
800	178.185	2.17	1.1	22	8	2	617.92	12.72	499.20	118.72	4.613	0.0723	0.2505
1000	198.884	2.17	1.1	22	8	2	617.92	12.72	499.20	118.72	4.873	0.0684	0.2474
2000	272.324	2.17	1.1	22	8	2	617.92	12.72	499.20	118.72	5.702	0.0585	0.2394
3000	329.546	2.17	1.1	22	8	2	617.92	12.72	499.20	118.72	6.273	0.0531	0.2351
4000	378.727	2.17	1.1	22	8	2	617.92	12.72	499.20	118.72	6.725	0.0496	0.2322

BIOGRAPHY

Name:	Mr. Winit Jaiboon
Date of Birth:	September 25, 1981
Place of Birth:	Nakhon Pathom, Thailand
Education:	
2000-2005	B. Eng. in Mechanical Engineering, Faculty of Engineering, King Mongkut's Institute of Technology Ladkrabang (KMITL)
2007-2010	M. Eng. in Automotive Engineering (International program), International College, King Mongkut's Institute of Technology Ladkrabang (KMITL)

Publications:

1. Winit Jaiboon, Niwat Phoocharoen, Seiji Okawa, Jarruwat Charoensuk, "Simulation of Flow Aerodynamics and Heat Transfer in a Plate-Fin Radiator", 2009, **13th International Annual Symposium on Computational Science and Engineering (ANSCSE 13)**, Faculty of Engineering, Kasetsart University, Bangkok, Thailand, March 25 –27, 2009.

2. Winit Jaiboon, Niwat Phoocharoen, Seiji Okawa, Jarruwat Charoensuk, "Numerical Investigation of Fluid Flow and Heat Transfer in a Plate-Fin Radiator", **9th International Conference on Computational & Experimental Engineering and Sciences (ICCES'09)** , Phuket, Thailand, April 8 –13, 2009.